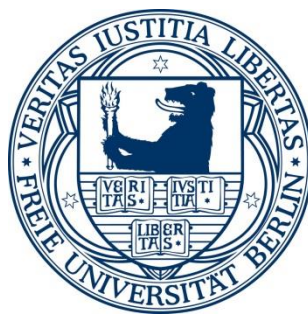


# Induction of Synapses by Agrin in Cultured Cortical Neurons

---

Inaugural Dissertation to obtain the academic degree  
Doctor rerum naturalium (Dr. rer. nat.)

Submitted to the Department of Biology, Chemistry and Pharmacy  
of the Freie Universität Berlin



by

**Hetsch, Florian Jan Alexander**

**2015**

This thesis was prepared between December 2010 and January 2015 at the Max-Delbrück-Center for Molecular Medicine at the Department of Developmental Neurobiology under the supervision of Prof. Dr. Fritz G. Rathjen.

Disputation on: 28.05.2015

1. Reviewer: Prof. Dr. Fritz G. Rathjen  
Department of Developmental Neurobiology, Max-Delbrück-Centrum für Molekulare Medizin Berlin-Buch
2. Reviewer: Prof. Dr. Gary Lewin  
Department of Molecular Physiology of Somatic Sensation, Max-Delbrück-Centrum für Molekulare Medizin Berlin-Buch

## Table of content

1. Introduction.....	7
1.1 The synapse - types and development.....	7
1.1.1 The neuromuscular junction .....	7
1.1.2 The chemical synapse and electrical synapse of the CNS .....	8
1.1.3 Synapse development in the CNS .....	11
1.2 Agrin – a synaptic organizer .....	14
1.2.1 Discovery and function at the NMJ .....	14
1.2.2 Agrin interacts with LRP4 at the NMJ.....	17
1.2.3 Agrin at the central synapse – its possible function .....	17
1.3 Aims of this study .....	20
2. Materials and methods .....	22
2.1 Materials .....	22
2.1.1 Animals.....	22
2.1.2 Antibodies .....	22
2.1.3 Agrin proteins.....	23
2.2 Methods .....	24
2.2.1 Cell culture .....	24
2.2.2 Genotyping of mutant mice by PCR and DNA electrophoresis.....	28
2.2.2.1 Preparation of genomic DNA .....	28
2.2.2.2 Genotyping of agrin mutant mice .....	28
2.2.2.3 Genotyping of LRP4 mutant mice .....	29
2.2.3 SDS-PAGE and western blot .....	30
2.2.4 ELISA for agrin-agrin interaction .....	33
2.2.5 Immunocytochemistry .....	34
2.2.5.1 Confocal imaging of immuno-stained cultures .....	35
2.2.5.2 Analysis of confocal images.....	35
2.2.6 Reverse transcription PCR & quantitative real-time PCR.....	36
2.2.7 Electrophysiology .....	39
2.2.7.1 Components of the electrophysiology set-up.....	39
2.2.7.2 Patching a cell.....	40
2.2.7.3 Determining the passive membrane properties of a cell.....	41
2.2.7.4 Determining the active membrane properties (voltage-gated sodium & potassium currents).....	42
2.2.7.5 Recordings of miniature postsynaptic currents (mPSCs).....	43

2.2.7.6 Determining the quantal size of miniature postsynaptic events .....	44
2.2.7.7 Analysis of voltage-gated calcium currents (VGCC) .....	44
2.2.7.8 Analysis of neurotransmitter release by extracellular stimulation with a monopolar electrode .....	44
2.2.7.9 Analysis of autaptic neurotransmitter release.....	45
2.2.7.10 Determining the quantal content of evoked postsynaptic currents.....	46
2.2.7.11 Analysis of the readily releasable pool by high osmolality sucrose stimulation.....	46
2.2.7.12 Solutions for electrophysiological experiments.....	47
2.2.7.13 List of inhibitors used in electrophysiological experiments.....	49
2.2.7.14 Offline analysis and statistics .....	49
2.2.8 List of chemicals and equipment.....	50
3. Results .....	53
3.1 Cortical microisland cultures.....	53
3.1.1 Characterization of single neurons in microisland cultures.....	53
3.1.2 Comparison of inhibitory and excitatory neurons shows distinct differences in their electrophysiological properties.....	56
3.1.3 Agrin increases the frequency of excitatory miniature postsynaptic currents in single cortical neurons.....	59
3.1.4 Agrin induces excitatory synapses in microisland cultures.....	60
3.1.5 Agrin treatment induces an increase in the number and size of synaptic AMPAR spots ....	61
3.1.6 Autaptic neurotransmitter release in single neurons seems unaffected by agrin application .....	62
3.1.7 Passive and active cell properties of single neurons are not affected by agrin incubation.	64
3.1.8 The agrin receptor LRP4 is expressed in cortical tissues and its expression is developmentally regulated .....	66
3.1.9 Agrin does not influence the mEPSC frequency of single excitatory neurons of LRP4 mutant cultures.....	68
3.1.10 Agrin does not influence mEPSC frequency of single agrin-deficient excitatory neurons.	70
3.1.11 Recombinant agrin does not interact with recombinant agrin in an ELISA-based binding assay.....	72
3.1.12 PI3K activation is involved in agrin-mediated signaling .....	74
3.1.13 Voltage-gated Ca <sup>2+</sup> currents of single neurons are not affected by agrin application.....	77
3.2 Monolayer cortical cultures .....	79
3.2.1 Characterization of conventional monolayer cultures of cortical neurons .....	79
3.2.2 Agrin increases inhibitory miniature postsynaptic currents of cortical neurons in monolayer cultures.....	80

3.2.3 The agrin-mediated effect on mIPSCs of cortical neurons is time and concentration dependent .....	83
3.2.4 The induction of inhibitory synapses in monolayer cultures is not affected by agrin incubation. ....	84
3.2.5 Presynaptic release of neurotransmitter of cortical neurons is not affected by agrin incubation.....	85
3.2.6 The readily releasable synaptic vesicle pool of cortical neurons in monolayer cultures is not influenced by agrin incubation.....	88
3.2.7 Passive and active cell properties of cortical neurons remain unchanged after agrin treatment .....	89
3.2.8 Agrin does not influence synaptic transmission of cortical neurons of agrin-deficient animals .....	91
3.2.9 PI3K is stimulated in cortical neurons by agrin incubation .....	93
3.2.10 LRP4 mRNA expression is increased in agrin-deficient cortical neurons .....	97
3.2.11 Incubation with a 95 kDa C-terminal agrin fragment does not change the mIPSC frequency of cortical neurons .....	97
4. Discussion.....	99
4.1 Comparison of neurons in monolayer or microisland culture shows similar maturation of their active and passive membrane properties as well as synaptic properties.....	99
4.2 Agrin induces excitatory synapses in microisland cultures of single neurons .....	100
4.2.1 Differences between GABAergic and glutamatergic neurons.....	100
4.2.2 mEPSC frequency in microisland cultures is increased by agrin treatment.....	101
4.2.3 Agrin incubation increases the number of excitatory synapses and clusters AMPAR at the synaptic site.....	101
4.2.4 Presynaptic release is unaffected by agrin-treatment in microisland cultures .....	102
4.2.5 LRP4 and endogenous agrin are essential for the agrin-mediated increase of mEPSCs....	103
4.2.6 Agrin induces PI3K signaling in single neurons .....	104
4.2.7 Agrin incubation does not influence voltage-gated Ca <sup>2+</sup> currents.....	106
4.2.8 A proposed model for agrin-mediated signaling in single excitatory neurons .....	106
4.3 Agrin increases the mIPSC frequency in monolayer cultures of cortical neurons .....	109
4.3.1 mIPSC frequency in monolayer cultures is increased by agrin treatment.....	109
4.3.2 The increase in mIPSC frequency is not caused by an increase in the number of inhibitory synapses .....	110
4.3.3 The presynaptic release is unaffected by treatment with neuronal agrin.....	110
4.3.4 The readily releasable pool (RRP) is unaffected by agrin treatment .....	110
4.3.5 Agrin-deficient neurons do not react to external agrin stimuli and express more LRP4 mRNA.....	111

4.3.6 Agrin induces PI3K signaling in neurons of monolayer cultures .....	111
4.4 Agrin incubation is not affecting input resistance, cell capacitance and voltage-gated K <sup>+</sup> currents .....	112
4.5 Differences between monolayer and microisland cultures of cortical neurons.....	112
4.6 Homophilic agrin interactions .....	113
4.7 Outlook.....	114
4.8 Conclusions.....	115
5. Summary .....	116
6. Zusammenfassung.....	118
7. Abbreviations list.....	120
8. Reference list.....	123
9. Acknowledgements.....	132
10. Curriculum vitae .....	133
11. Eidesstattliche Erklärung.....	135

# 1. Introduction

## 1.1 The synapse - types and development

An essential part of communications between neurons occurs via specialized structures called synapses. These intricate connections between nerve cells in the brain shape how we perceive our surroundings and give rise to higher cognitive functions. In this first chapter the different types of synapses found in vertebrates will be described and discussed to highlight the extraordinary mechanisms governing the development of synapses and enable the integration of a multitude of signals from one neuron to the other. Chapter 1.2 will in detail focus on one of the most important proteins for synaptic organization at the neuromuscular junction a proteoglycan called agrin and stress why it is of interest to investigate its role in the development of synapses in the central nervous system which was the aim of this study.

### 1.1.1 The neuromuscular junction

The neuromuscular junction (NMJ) has been the model of choice for the analysis of synapse formation for the past decades because of its simplicity and accessibility. Motor neurons with their respective somata lying in the grey matter of the dorsal horn of the spinal cord innervate skeletal muscle fibers and establish a synaptic connection. Initially multiple motor neuron axons contact an individual muscle fiber. During maturation only one axon terminal per fiber remains (Sanes and Lichtman, 1999). The NMJ is a complex structure (Figure 1) like any other synapse and is comprised of three distinct parts: the presynaptic site (the nerve terminal of a motor neuron), the synaptic basal lamina which is made up of extracellular matrix proteins and the postsynaptic site on the muscle fiber containing acetylcholine receptors (AChR), scaffolding proteins and the apparatus for maintaining the synapse structure (Punga and Ruegg, 2012). The formation of the NMJ is governed by intricate signaling mechanisms that have been extensively studied for the last couple of decades. The nerve terminal of the motor neurons secretes a neuronal agrin isoform and its binding to the low-density lipoprotein related receptor 4 (LRP4) (Kim et al., 2008; Zhang et al., 2008) are key steps for the subsequent activation of the muscle specific kinase (MuSK) (Glass et al., 1996), which in turn leads to the activation of rapsyn (Apel et al., 1997) and the clustering of AChR at the postsynaptic site (Figure 3). Agrin, secreted from motor neurons, has also been implicated to bind with its NtA-domain to laminin found in the basal lamina of the NMJ trapping it at synaptic sites (Denzer et al., 1997) as well as to  $\alpha$ -dystroglycan (Sugiyama et al.,

1994) helping to build and maintain the NMJ and its synaptic composition. The proteins agrin, LRP4, MuSK and rapsyn have been shown to be essential for normal NMJ development. A genetic knock out of only one of these components results in a disturbed appearance of the NMJ, leading to a loss of innervation and synaptic transmission that causes the newborn mutant mice to suffocate (DeChiara et al., 1996; Gautam et al., 1995, 1996; Weatherbee et al., 2006). Disruption of the interactions of agrin and LRP4 by autoimmune antibodies causes severe degeneration of the NMJ and has been linked to myasthenia gravis (MG) and amyotrophic lateral sclerosis (ALS) by disrupting agrin/LRP4/MuSK signaling. Immunization with ecto-domains of LRP4 causes MG-like effects in mice and autoantibodies against agrin and LRP4 have been found in patients affected with MG and ALS (Shen et al., 2013; Tzartos et al., 2014; Zhang et al., 2014). Also mutations to the third  $\beta$ -propeller domain of LRP4 have been linked to myasthenia by compromising agrin/LRP4/MuSK signaling (Ohkawara et al., 2014) further strengthening the importance of these molecules in maintaining the NMJ .

### **1.1.2 The chemical synapse and electrical synapse of the CNS**

Chemical synapses are the most common type of synapse found in the CNS of vertebrates. They are highly specialized structures that convey information from one nerve cell of the brain to another or even over large distances e.g. from sensory cells to areas of cerebral cortex. When axon terminals arrive at their target site (e.g. dendrites or the soma of a neuron) initial contact is made with the prospective postsynaptic cell. This leads to the formation of specialized protein complexes on the pre- and postsynaptic sites. Presynaptic sites contain synaptic vesicles filled with neurotransmitters, which can be of different variety (e.g. glutamate for excitatory cells or GABA ( $\gamma$ -aminobutyric acid) and glycine for inhibitory cells) and ion channels such as voltage-gated calcium channels (VGCC) which are important for neurotransmitter release. The excitatory synapse is characterized by relying on glutamate as the neurotransmitter and by the appearance of specific postsynaptic proteins e.g. the postsynaptic density protein PSD95 and glutamate receptors. Inhibitory synapses use GABA and glycine as neurotransmitters and use the postsynaptic scaffolding protein gephyrin to stabilize GABA and glycine receptors at the synaptic site.

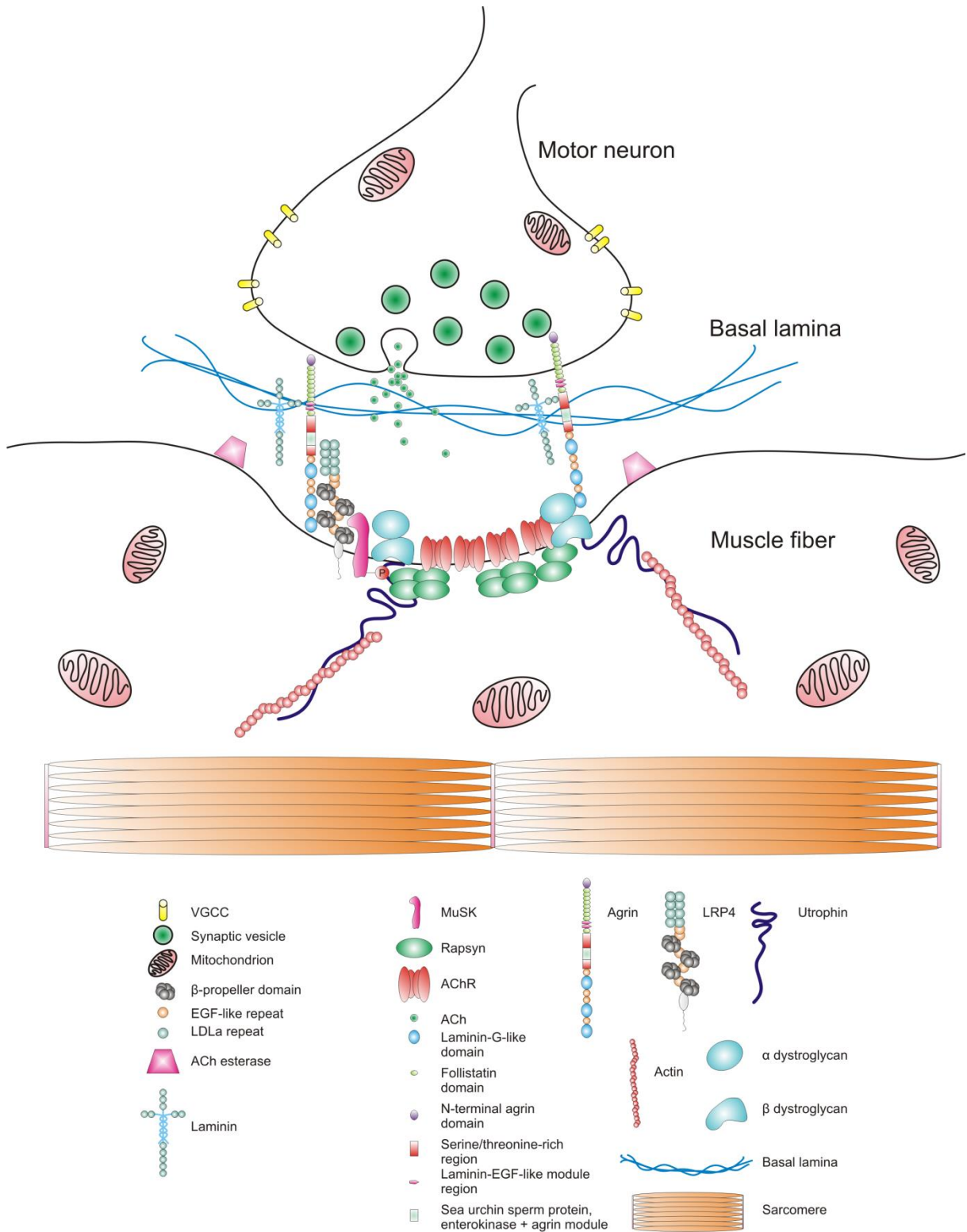


Figure 1: Schematic overview of a NMJ with associated proteins. The motor neuron releases stabilizing molecules like agrin and neurotransmitters into the synaptic cleft. On the postsynaptic site agrin associates with LRP4 and activates MuSK leading to a reorganization of the AChR and their recruitment to the synaptic site through interactions with rapsyn. Maintenance of the synapse is also dependent on agrin interaction with laminin and alpha dystroglycan. Further stabilization of the synapse is achieved by actin filaments and utrophin. Scheme modified from Punga and Ruegg, 2012.

The postsynaptic site undergoes dramatic changes during maturation. Neurotransmitter receptors are newly integrated into the membrane or transported from extrasynaptic sites to the newborn synapse. They are anchored by scaffolding proteins such as the postsynaptic density proteins for instance PSD95 for excitatory synapses or gephyrin for inhibitory synapses (Figure 2A and B). Remodeling of the actin cytoskeleton also takes place ensuring the correct morphology of a mature synapse and the formation of highly specialized structures like dendritic spines. Synaptic transmission, the means of communication in neurons, is elicited by action potentials arriving at the axon terminal. Here VGCC open upon receiving this stimulus and synaptic vesicle fusion is initiated by calcium influx. Neurotransmitters are released into the synaptic cleft, the space between the pre- and postsynaptic site, and drift to their respective binding site localized on the postsynaptic neurotransmitter receptors leading to a conformational change in these molecules and the opening of an aqueous pore selective to different kinds of ions. This induces ion fluxes across the membrane and leads to changes in the membrane potential of the postsynaptic cell. If the membrane potential of the postsynaptic cell is depolarized sufficiently by these ion currents, the postsynaptic neuron itself will fire action potentials relaying the information from the presynaptic cell to a different cell. Through interplay with other excitatory and inhibitory neurons this information can be further modified, amplified or attenuated.

The electrical synapse (or gap junction) is found in the vertebrate nervous system not relying on neurotransmitter release to propagate information but ions and small molecules that pass through an aqueous pore. This structure is completely different from other types of synapses. It is made up of two hexameric connexin hemichannels forming the aqueous pore or connexon (Caspar et al., 1977; Makowski et al., 1977). Two opposing connexon hemichannels make up the actual channel, also called gap junction (Perkins et al., 1998). Through such a channel currents can flow easily from one cell to the other as well as molecules with a molecular mass of up to 900 Da (Hu and Dahl, 1999). This kind of synapse is often found in connections between interneurons especially in the hippocampus (Fukuda and Kosaka, 2000; Hamzei-Sichani et al., 2007).

### 1.1.3 Synapse development in the CNS

The development of synapses in the central nervous system has always been of great interest to the scientific community for a long time. Camillo Golgi and Ramón y Cajal first stained neurons in the brain by using a special staining technique developed by Golgi. This sparse labeling of neurons, making even smallest arborizations visible led Cajal to postulate the neuron theory stating that the brain is not a continuous mesh but made up of single cells that may have distinct sites of contact. The term synapse was only later coined by Sir Charles Sherrington in the late 19<sup>th</sup> century describing the “special connection of one nerve cell with another” (López-Muñoz et al., 2006). What this connection looked like was only possible to resolve with the invention of electron microscopes. In the year 1954 Palade and Palay used this new technique to investigate neuromuscular junctions and could show distinct pre- and postsynaptic sites, synaptic vesicles and the synaptic cleft of a synapse. They were not the only ones to use this new technique to gain insight into the ultrastructure of synapses. Robertis and Bennett analyzed synaptic connections in earthworms and frogs (Robertis and Bennett, 1955) showing that Cajal’s initial observations and assumptions were correct. Only much later it was possible to unravel the processes that lead to the birth of a synapse and some remain still unknown today.

For the establishment of new synaptic contacts axonal guidance is of utmost importance. It is a complex process mediated by repulsion or attraction of axonal growth cones through diffusible guidance cues (chemoattraction/-repulsion) like NGF or semaphorin3A, extracellular matrix proteins, the establishment of contacts (contact-mediated attraction/repulsion) and stimulation of axon outgrowth by cell adhesion molecules (CAMs) like NCAM or L1 (Brümmendorf et al., 1998; Walsh and Doherty, 1997). Once the axon has found its target and contact is initiated with the aid of CAMs like the neuroligins on the presynaptic and neuroligins on the postsynaptic site synaptogenesis starts. For instance the interaction of neuroligin 1 and  $\beta$ -neurexin has been demonstrated (Nguyen and Sudhof, 1997) and the localization of these two proteins has been shown to be concentrated at excitatory synapses (Song et al., 1999). The expression of neuroligins in nonneuronal cells was sufficient to induce synaptic vesicle clusters of contacting axons (Scheiffele et al., 2000). Neuroligin 1 and another cell adhesion molecule, synCAM, can even form artificial synapses in HEK cells co-transfected with GluR2 subunits of glutamate receptors (Sara et al., 2005). These findings stress the importance of CAMs for the triggering of synaptic specializations.

The process of recruiting proteins to the synaptic sites has been shown to be faster than was initially expected. In hippocampal neuron cultures functional glutamatergic synapses were formed in one to two hours after the first initial contact showing immunoreactivity for bassoon after 45 min followed by AMPA receptor (AMPA) subunit GluR1, NMDA receptor (NMDAR) subunit NR1 and PSD95 after one to two hours (Friedman et al., 2000). Synaptic vesicles were highly mobile and could be recruited to new synapses very quickly. Using time-lapse microscopy Sabo and colleagues showed that synaptic vesicle protein transport vesicles stopped at predefined sites along axons from visual cortex neurons and initiated the formation of the presynaptic site (Sabo et al., 2006). These findings indicate that synaptogenesis in the brain is not a process of days or weeks but rather of hours.

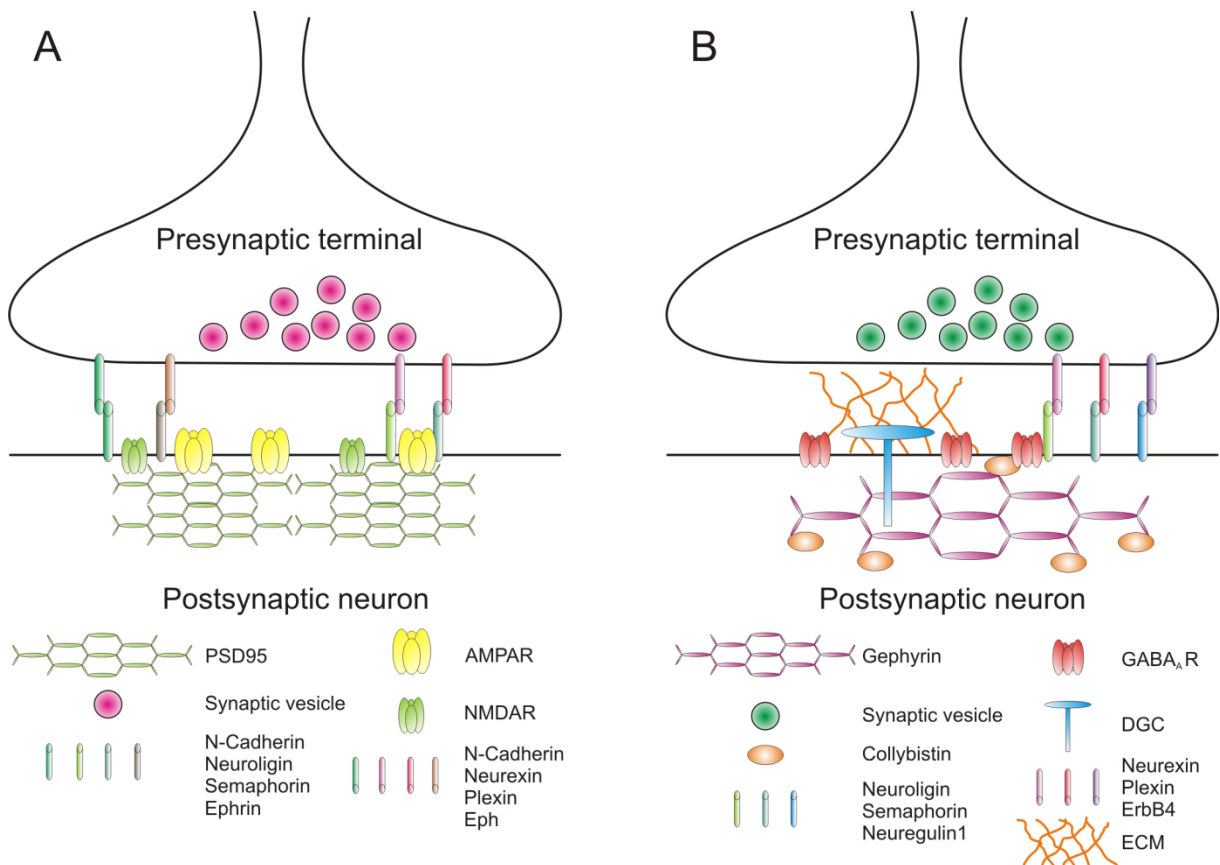


**Figure 2: Structure of glutamatergic and GABAergic synapses.** The presynaptic terminal harbors synaptic vesicles filled with neurotransmitter and is in contact with the postsynaptic site through different cell adhesion molecules. The postsynaptic site is made up of the neurotransmitter receptors and scaffolding proteins. A schematic overview of a glutamatergic synapse (A) and a GABAergic synapse respectively (B) highlights the differences between these two synapses. Modified from Kuzirian and Paradis, 2011.

The recruitment of the postsynaptic PSD95 and AMPAR in this process seems to be mediated by the PDZ domain of neuroligin 1, whereas its  $\beta$ -neurexin binding site is necessary for NMDAR recruitment (Chih et al., 2005) highlighting the importance of the molecules for the establishment of excitatory synapses.

Inhibitory synapse maturation is also dependent on CAMs. Neuroligin 2 for instance is an important component of inhibitory synapses. There it is highly concentrated as has been demonstrated by co-staining with the vesicular  $\gamma$ -aminobutyric acid transporter (VGAT) (Chih et al., 2005). The induction of the GABAergic postsynaptic specialization has been shown to be dependent on the neuroligin 2 binding partner  $\alpha$ -neurexin. For instance clustering of GABA<sub>A</sub> receptors and neuroligin 2 is induced in neurons when they make contact with  $\alpha$ -neurexin expressed in COS cells (Kang et al., 2008).

Neuroligin 2 also interacts with inhibitory synapse scaffolding proteins like gephyrin and collybistin. It is able to bind gephyrin with a highly conserved 15 amino acid containing motif at its C-terminal end and activates collybistin which triggers the tethering of the receptors to the membrane at the postsynaptic site (Poulopoulos et al., 2009). Collybistin and gephyrin are also important for the recruitment of GABA<sub>A</sub> receptors to the postsynaptic site of inhibitory synapses. Gephyrin has been shown to be required for the clustering of GABA<sub>A</sub> receptor subtypes in cultures of hippocampal neurons. Treatment with antisense oligonucleotides reduced GABA<sub>A</sub> clusters in cultured neurons (Essrich et al., 1998). Collybistin aggregates gephyrin after co-expression in HEK cells and knock-down of the protein in hippocampal neurons results in the loss of functional GABAergic synapses (Kins et al., 2000; Körber et al., 2012). The dystrophin glycoprotein complex (DGC) and most notably one of its components  $\alpha$ -dystroglycan are also implicated to be of importance at GABAergic synapses. Elevation of neuronal activity leads to an upregulated expression of  $\alpha$ -dystroglycan and homeostatic upscaling of GABAergic transmission (Pribiag et al., 2014).

The phosphatidylinositol 3-kinase (PI3K) also seems to take up a critical role in the developing nervous system. PI3K has been shown to be necessary for the elongation of neurites in human neuroblastoma cell lines (Sánchez et al., 2004). Pharmacological block of the enzyme with wortmannin or LY294002 stopped neurite outgrowth in *in vitro* assays (Sánchez et al., 2004). PI3K is also implicated in having effects on the dendritic morphology and soma size of hippocampal neurons. Expression of constitutively active forms of the enzyme resulted in enhanced dendritic arborization, increased soma size and higher spine density (Kumar et al., 2005). PI3K led in these experiments to phosphorylation of AKT which also seems to play a role in these processes (Kumar et al., 2005). Long-term potentiation (LTP) in hippocampal neurons is also dependent on PI3K signaling. Incubation with

wortmannin or LY294002 abolished LTP in these cultures (Man et al., 2003). Co-immune precipitation and immunocytochemistry revealed that PI3K is associated with AMPARs and seems to regulate their insertion in the membrane leading to the prominent effects of LTP (Man et al., 2003). These studies highlight the importance of PI3K signaling during development of the nervous system and synaptogenesis.

The synaptic organizer agrin is also expressed in the central nervous system (Kröger and Mann, 1996; Kröger et al., 1996; Li et al., 1997; O'Connor et al., 1994) and has been found to be enriched in synaptosomal preparations from rat hippocampus (Böse et al., 2000) implying an important function for agrin at the synapse of the central nervous system but it is still highly debated if it is as integral in the process of synaptogenesis in the CNS as it is at the NMJ. In chapter 1.2.3 a summary of the agrin-mediated actions at the CNS synapse will be presented to give some insight on what is known about agrin's function in the CNS.

This short and by no means complete introduction to some of the many processes that are necessary to engineer a functional synapse in the central nervous system highlights some of the many proteins that are of great importance in this process but also shows that synaptogenesis does not have to be necessarily a slow procedure. Instead some processes leading to functional synaptic connections need only a few hours of time.

## **1.2 Agrin – a synaptic organizer**

This chapter will focus on agrin's importance in the development of the neuromuscular junction and will also summarize what is known about its role in the establishment of synapses in the CNS.

### **1.2.1 Discovery and function at the NMJ**

Agrin is a heavily glycosylated proteoglycan. It was first isolated from the electric organ of the pacific electric ray *Torpedo californica* by the McMahan lab (Godfrey et al., 1984; Nitkin et al., 1987). Early studies from this lab showed that the insoluble fraction of the electric organ contained a molecule that was able to induce clustering of AChR in cultured myotubes. This protein was later further purified and called agrin from the Greek word "ageirein" which means to assemble because of its effect on AChR (Nitkin et al., 1987). In subsequent experiments the people from the McMahan lab were able to clone a cDNA that comprised the active form of neuronal agrin from chicken with a predicted mass molecular of around 207 kDa (Tsim et al., 1992). Expression studies and functional studies showed that

the protein encoded by this cDNA was able to induce AChR clusters on cultured myotubes similar to those seen when agrin purified from the electric organ was used. In the same year Markus Ruegg was able to isolate cDNAs encoding different agrin isoforms (Ruegg et al., 1992). These isoforms were characterized by two splicing sites that were termed A and B in chick or  $\gamma$  and  $\zeta$  in rodents. Isoforms that lack distinct amino acid inserts at the B site render these proteins unable to induce AChR clusters (Figure 4) (Ruegg et al., 1992). Another study confirmed that the B insert and the C-terminal laminin-G-like domain are indeed needed for the AChR clustering ability of agrin (Gesemann et al., 1995).

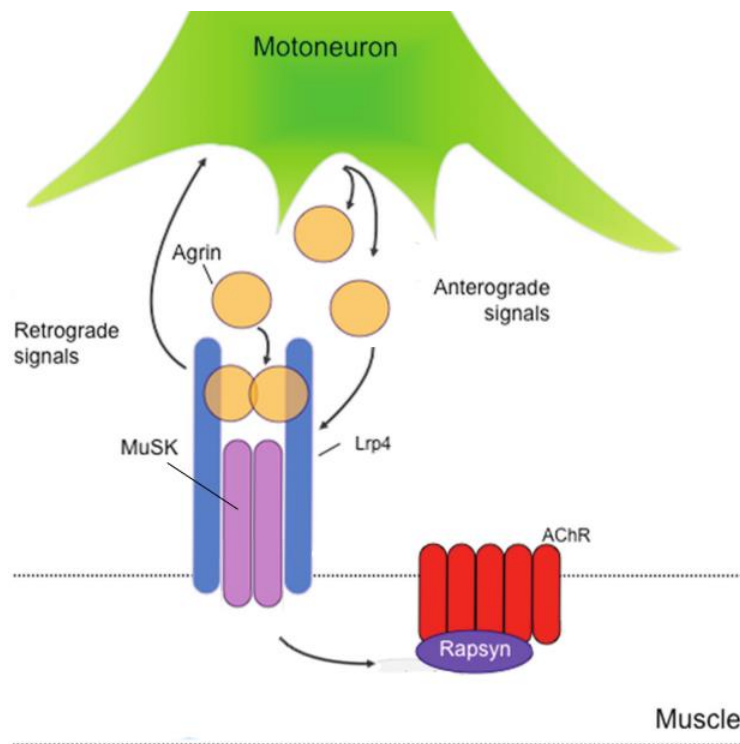
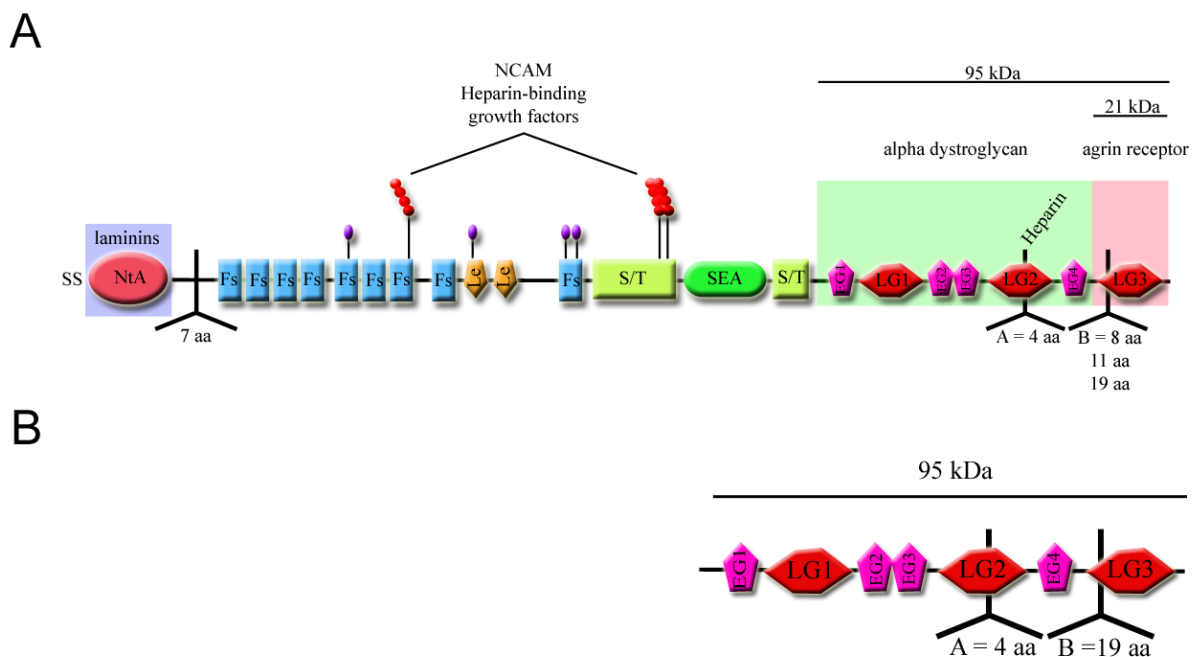


Figure 3: A simplified schematic overview of the agrin induced signaling at the NMJ. Agrin is secreted by the presynaptic motor neuron terminal and binds to LRP4. LRP4 in turn aggregates with MuSK and causes the assembly of AChR clusters with the aid of rapsyn. Modified from Barik et al., 2014.

With the development of transgenic mice agrin was once more becoming of major interest to scientists. The lab of Joshua Sanes created mice deficient in neuronal forms (lacking the B/ $\zeta$  insert) of agrin by replacing exons 32 and 33 with a neomycin resistance cassette (Gautam et al., 1996). Homozygous mutant mice were stillborn or died *in utero* caused by grave defects in the formation and maturation of a functional NMJ. While wild type animals showed normal clustering of AChR near the endplate band of diaphragm muscles mutant mice possessed smaller AChR clusters and longer axon branches of the phrenic nerve. Mutant mice suffered from a significant loss of pre- and postsynaptic specializations

(Gautam et al., 1996). Even though this study targeted neuronal forms of agrin mutant mice additionally appeared to be severe hypomorphs for all forms of agrin (Gautam et al., 1996). In 2001 Lin et al. developed a mouse mutant lacking most of the coding exons (6-33) for all agrin variants (Lin et al., 2001). These mice showed similar defects as the mice lacking only the neuronal form of agrin comprised of a lack of AChR clusters and larger axon terminals of the phrenic nerve. They also investigated MuSK mutant mice and mice lacking innervation by deletion of the motor neuron-specific transcription factor Hb9. AChR clusters were still seen in aneural Hb9  $-/-$  mutant mice but absent in MuSK  $-/-$  animals stressing the necessity of MuSK for the normal development of the NMJ.

Only recently it was shown that agrin induces microtubule networks that guide the insertion of AChR by activation of the phosphatidylinositol 3-kinase (PI3K) (Schmidt et al., 2012). Activation of PI3K led to the phosphorylation of AKT and GSK3 $\beta$  leading to the capture of microtubules at the synaptic membrane (Schmidt et al., 2012).



**Figure 4: Structure of secreted full-length neuronal chicken agrin (A) and the 95 kDa C-terminal fragment of agrin (B).** Note the three splice sites in the full-length agrin molecule. The A and B site are called  $\gamma$  and  $\zeta$  in rodents. Amino acid insert B and the third LG domain are sufficient for AChR clustering activity (Gesemann et al., 1995). The core protein has a molecular mass of around 200 kDa but due to heavy glycosylation the apparent mass is 400-600 kDa (Gesemann et al., 1995). LG – laminin-G-like; EG – EGF-like; S/T – serine/threonine rich; SEA – sea urchin enterokinase sperm protein agrin; Fs – follistatin-like; NtA – N-terminal agrin; SS – signal sequence. Modified from Ruegg and Bixby, 1998.

### **1.2.2 Agrin interacts with LRP4 at the NMJ**

For a long time it was not clear which molecule was bridging the gap between agrin and activation of MuSK because agrin itself is not able to bind MuSK (Glass et al., 1996). In 2008 two labs showed that the missing agrin receptor at the NMJ was LRP4, a low-density lipoprotein receptor-related protein (Kim et al., 2008; Zhang et al., 2008). Since LRP4 mutant mice had a very similar phenotype to agrin and MuSK knock out mice (Weatherbee et al., 2006), one group used LRP4 mutant myotubes and stimulated them with neural agrin. Normal agrin signaling should have led to robust MuSK phosphorylation but it was absent in these myotubes (Kim et al., 2008) signifying an important function of LRP4 in relaying the agrin signal to MuSK. They further investigated LRP4's mode of signal transduction by using chimeric constructs expressing the low-density lipoprotein receptor (LDLR) cytoplasmic domain together with the extracellular and transmembrane domain of LRP4. The chimeric vector was able to convey agrin stimulation whereas the LDLR expression constructs without the LRP4 domains were not (Kim et al., 2008). The necessity of the extracellular domains of LRP4 for agrin interaction was also shown by a different lab in 2008. Using secreted forms of neuronal agrin (C-terminal agrin with flag-tag) and LRP4 (extracellular domain with myc-tag) they performed immune precipitation experiments proving interaction of LRP4 with agrin but no interaction with MuSK or LRP6 (Zhang et al., 2008). These findings clearly provide evidence that agrin and LRP4 are binding partners at the NMJ.

Surprisingly not many experiments have been conducted on LRP4's role in synapse development in the CNS. One study showed that the expression of LRP4 in HEK293 cells led to the induction of presynaptic specializations in cortical neurons contacting these transfected cells suggesting a synaptic function for LRP4 (Wu et al., 2012). A second study demonstrated that rescued LRP4-deficient mice lacking LRP4 expression in the brain had severe cognitive defects affecting learning and memory as well as a reduction in spontaneous neurotransmitter release together with a reduction in spine density (Gomez et al., 2014). These findings highlight the importance of LRP4 at the CNS and not only at the NMJ synapse. Whether or not agrin signaling is important in these processes remains to be investigated.

### **1.2.3 Agrin at the central synapse – its possible function**

The role of agrin in the formation of synapses in the central nervous system is not well understood and different mechanisms have been proposed (for a review see: Daniels, 2012).

Seeing the dramatic effects of agrin depletion at the NMJ one wonders if it would affect neurons and their synapse development as well. Since agrin expression in the central nervous system is high as has been shown in adult rats, during development in mice (Li et al., 1997; O'Connor et al., 1994) and also in the chick retina (Kröger et al., 1996; Mann and Kröger, 1996), it was tempting to think agrin might also act as a key player in shaping the circuitry in the brain perhaps by taking up the same important role in synapse development in the CNS as in the NMJ.

Li et al. used agrin-deficient mice from the Sanes lab to make cortical cell cultures and investigated their synaptic properties. Immunocytochemistry revealed no differences in the distribution of the synaptic proteins synaptophysin and glutamate receptors in agrin mutant cultures (Li et al., 1999). Both proteins co-localized nicely and were evenly distributed on dendrites. To strengthen this result whole cell patch clamp experiments were conducted proving that indeed agrin mutant neurons behaved physiologically like wild type neurons. The recorded cells showed spontaneous miniature postsynaptic currents with long and short decay kinetics accounting for inhibitory (GABAergic) and excitatory (glutamatergic) postsynaptic events, respectively (Li et al., 1999). The frequency of these events was developmentally regulated and increased with longer culturing periods showing a normal development of these agrin-deficient neurons *in vitro* (Li et al., 1999).

Even though agrin-deficient neurons seemed to develop normally a different study done on cultured hippocampal rat neurons showed that agrin might be important in synapse development and maintenance. After a ten day treatment with antisense oligonucleotides directed against agrin, or treatment with agrin-specific antibodies the neurons showed a strong reduction of synapsin-I-immunoreactive puncta as well as a reduced mEPSC frequency (Böse et al., 2000). This phenotype could be rescued by additionally applying recombinant agrin to the culture medium. Only cultures incubated with the neural form of agrin showed the same synapsin-I distribution as untreated control cultures. The effect on synapsin-I-positive puncta could not be induced in agrin-deficient neurons after treatment with the antisense oligonucleotides leading the authors to highlight the possibility of compensatory effects in agrin-deficient cells (Böse et al., 2000). A second study using antisense oligonucleotides showed a reduction of glutamate receptor subunit GluR1 and an even stronger reduction of GABA<sub>A</sub>R after treatment of hippocampal neuron cultures using

western blot analysis (Ferreira, 1999). The expression of agrin in the hippocampus was also investigated and their results showed a decrease in agrin expression with longer days *in vitro* reaching a minimum at 30 days *in vitro* showing that agrin expression preceded synaptogenesis (Ferreira, 1999).

Further studies were conducted on agrin's role on the induction of filopodia-like structures. Filopodia are highly mobile protrusions of the cytoplasm of growth cones of axons and dendrites. They harbor a dense network of actin filaments and have been implicated to represent initial sites for synaptic contacts and precursors of mature synapses. In 2006 agrin was shown to play a crucial role in the induction of filopodia-like processes on neurons. In this study clustering of transmembrane proteins by incubation with polyclonal antibodies against transmembrane agrin was performed in chick retinal ganglion cells (RGC) to initiate downstream signaling which led to the induction of filopodia-like processes on the axons of cultured RGC (Annie et al., 2006). Labeling with phalloidin revealed a complex cytoskeletal structure in these protrusions (Annie et al., 2006). Knocking-down agrin by lentiviral introduction of RNAi further strengthened agrin's role in filopodia induction. Rat hippocampal neurons showed less filopodia-like structures per 100  $\mu\text{m}$  of dendrite, and a depletion of synapses after agrin knock-down with RNAi (McCroskery et al., 2009). The lab of Stephan Kröger tried to map the structures needed for the induction of these filopodia-like processes using overexpression constructs of transmembrane agrin in 2010. Their results indicated that the seventh follistatin-like domain of agrin (Figure 4) was needed for process formation (Porten et al., 2010). This clearly shows that the splice variants of neuronal agrin mediating the AChR clustering are dispensable for the induction of filopodia-like structures. These findings may provide evidence for the hypothesis that filopodia may be indeed precursors/initiators of synapses and that agrin seems to play a significant part in the process of their induction.

Agrin is also able to induce the expression of the immediate early gene c-Fos in cortical neurons which is a sign of neuronal activity (Hilgenberg et al., 1999). This upregulation of c-Fos expression could be attributed to a specific agrin receptor that relays the agrin signal to the nucleus. The stimulation of cortical neurons also led to an increase in intracellular calcium (Hilgenberg and Smith, 2004). By biochemical crosslinking agrin fragments (C-terminal 15, 20 & 90 kDa) to cultured cortical neurons, further purification of the crosslinked

proteins and mass spectrometric analysis of these purified protein complexes the  $\alpha 3$  subunit of the  $\text{Na}^+/\text{K}^+$  ATPase (NKA) was identified as a neuronal binding partner for agrin (Hilgenberg et al., 2006). Using  $\text{Na}^+$ -sensitive dyes it could be shown that agrin seemed to inhibit the function of  $\alpha 3\text{NKA}$  leading to an increase in intracellular  $\text{Na}^+$  and depolarization of the membrane potential (Hilgenberg et al., 2006).

Although agrin does not seem to be essential for synapse formation in the CNS it may have an effect on synaptogenesis or synapse maturation that is not easily resolved due to compensatory effects. The answer to the question what the agrin receptor in the CNS is, still remains highly debated and many different roles during synapse development have been assigned to agrin highlighting the importance to further study this protein at the central synapse (Daniels, 2012).

### **1.3 Aims of this study**

This study aims at unraveling agrin's specific role during synaptogenesis of cortical neurons in conventional monolayer and microisland culture systems. Questions this study wants to address are: Does the addition of soluble agrin induce changes in the synaptic properties of cultured neurons? Do these changes affect the pre- or postsynaptic site? Is there a change in the number of synapses? What is the mechanism behind agrin signaling in the CNS?

The physiological effects of agrin incubation are analyzed using whole-cell patch clamp recordings of untreated and agrin-treated neurons. Analysis of miniature postsynaptic currents revealed an effect on the frequency and amplitude of mEPSCs in microisland and the frequency of mIPSCs in monolayer cultures. Using immunocytochemistry (ICC) and paired-pulse stimulation experiments changes in presynaptic release of neurotransmitter in the number of inhibitory and excitatory synapses were examined. Also the passive and active membrane properties of the neurons either treated with agrin or left untreated were compared resulting in data that suggests that agrin incubation does not influence passive properties e.g. the cells capacitance or active voltage-gated  $\text{K}^+$  current amplitudes of neurons.

Since PI3K has been shown to be activated by agrin in myotubes (Schmidt et al., 2012) this kinase was also of interest as a possible effector of agrin signaling in neurons. Therefore

experiments focused on PI3K signaling. The obtained results suggest an interaction of PI3K in agrin-mediated signaling in neurons.

To unravel the agrin receptor complex in neurons a possible interaction of endogenous agrin with soluble agrin was investigated utilizing patch clamp recordings of agrin-deficient neurons cultured on agrin-deficient astrocytes and conventional monolayer cultures of agrin-deficient neurons. The collected data indicate a necessary function for endogenous agrin in agrin-mediated signaling in the CNS.

In addition LRP4's involvement in the induction of the agrin-mediated effect on mEPSC frequency was also analyzed by patch clamp recordings of LRP4-deficient neurons cultured on LRP4-deficient astrocytes to confirm a possible interaction between agrin and LRP4 at the central synapse. The evaluation of these experiments indicates that LRP4 is needed for the upregulation of the mEPSC frequency after incubation with neuronal agrin of single excitatory neurons.

## 2. Materials and methods

### 2.1 Materials

#### 2.1.1 Animals

Pregnant C57BL6/N mice used for the preparation of wild type cultures were delivered by Charles River GmbH (Germany). Embryos were prepared at embryonic day 15 (E15). Agrin knock out mice were generated by a targeted mutation which introduced a neomycin cassette into the mice genome replacing the exons 32 and 33, encoding the “z” alternative splice exons (B in chick) of the agrin gene (Gautam et al., 1996). Agrin knock out mice were a kind gift from Prof. Dr. Markus Ruegg and were maintained at the MDC animal facility. Embryos from agrin heterozygous mice were prepared at embryonic day E15 or E18. LRP4<sup>mitt</sup> mice carrying a chemically induced mutation leading to an early stop of translation and a splice site mutation also leading to an early stop of translation (Weatherbee et al., 2006) were a kind gift from Dr. Annette Hammes-Lewin. Embryos from LRP4<sup>mitt</sup> heterozygous mice were prepared at embryonic day E15 or E18.

#### 2.1.2 Antibodies

Antibodies used for immunocytochemistry and western blots are listed in table 1.

**Table 1: List of primary antibodies used in this study**

Name	Manufacturer/Order number	Concentration
Goat anti-agrin K17	Santa Cruz/sc-6166	WB: 1:1000
Guinea pig anti-Vglut2	Synaptic Systems/135404	ICC: 1:200
Guinea pig anti-Vglut1	Synaptic Systems/135304	ICC: 1:600
Mouse anti-GAPDH	Novus Biological/NB300-221	WB: 1:1000
Mouse anti-gephyrin	Synaptic Systems/147011	ICC: 1:500
Mouse anti-GluA	Synaptic Systems/182411	ICC: 1:500
Mouse anti-MAP2a/b	Dianova/DLN-08583	ICC: 1 µg/ml
Mouse anti-neurofilament M	Leinco Technologies/N103	ICC: 7.5 µg/ml
Mouse anti-PSD95	Thermo Scientific/MA1-046	ICC: 1:200
Rabbit anti-agrin Rb46	Kröger lab	WB: 1:1000
Rabbit anti-AKT	Cell Signaling Technology 9272	WB: 1:1000
Rabbit anti-GFAP	Dako/Z0334	ICC: 1:500
Rabbit anti-pAKT (S473)	Cell Signaling Technology/9271	WB: 1:1000
Rabbit anti-pGSK3 beta (S9)	Cell Signaling Technology/9323	ICC: 1:100; WB: 1:1000
Rabbit anti-LRP4 (H-98)	Santa Cruz/sc-98775	WB: 1:200
Rabbit anti-VGAT	Synaptic Systems/131002	ICC: 1:1000

### 2.1.3 Agrin proteins

Expression and purification of neuronal chicken agrin: Expression and purification of the recombinant agrin proteins was done by the technicians of the Rathjen lab. Full-length neuronal chicken agrin carrying a seven amino acid insert near the N-terminus, a four amino acid insert at the A/y and an eight amino acid insert at the B/z splice site (agrin 7-4-8) was harvested from the medium of stably transfected HEK293 cells (a kind gift from Markus Ruegg) and purified by ion exchange using Q-Sepharose columns. Cells were kept in DMEM supplemented with 10% FCS, P/S and G418 (1:500). The medium was then changed to DMEM (without phenol red) and the cells were kept for one week under these conditions. The supernatant was harvested and centrifuged for 10 min at 2000 rpm at 4°C using a Heraeus Megafuge 1.0 R. The supernatant was again centrifuged for 10 min at 10000 rpm at 4°C using a Sorvall RC 6+ centrifuge and the supernatant incubated with Q-Sepharose equilibrated with 0.5 M NaCl/20 mM Tris pH 7.4 on a shaker overnight. A column was built with the Q-Sepharose and washed with 40 ml 0.5 M NaCl/20 mM Tris pH 7.4. Elution was done by switching to an elution buffer consisting of 2 M NaCl/20 mM Tris pH 7.4. Agrin-containing fractions were tested by silver stained SDS-gels, pooled and dialysed against PBS. The protein concentration was quantified with a UV spectro photometer and samples were run on a 6 % SDS polyacrylamide gel to analyze their molecular mass and appearance again. Full-length neuronal chicken agrin 7-4-8 was strongly recognized by the polyclonal anti-agrin antibody Rb46 (a kind gift from Prof. Stefan Kröger) in western blots and ran as a smear of around 600 to 400 kDa.

C-terminal neuronal chicken agrin carrying a four amino acid insert at the A/y and a 19 amino acid insert at the B/z splice site (agrin 4-19) was purified by wheat germ agglutinin lectin affinity chromatography. Elution was done by using 0.2 M  $\alpha$ -methyl-pyranoside. Agrin-containing fractions were as well tested by silver stained SDS-gels, pooled and dialysed against PBS. The C-terminal fragment showed a band at 95 kDa in silver stained SDS polyacrylamide gels.

In experiments agrin was applied in concentrations of 100 ng/ml, 1  $\mu$ g/ml or as indicated.

## 2.2 Methods

### 2.2.1 Cell culture

Preparation of coverslips for monolayer culture: Coverslips of 12 mm diameter were treated in a solution consisting of 4 pellets of NaOH dissolved in 10 ml ddH<sub>2</sub>O and 35 ml 70 % ethanol for one day on a shaker. After extensive washing with ddH<sub>2</sub>O coverslips were put in a 1 M solution of HCl overnight on a shaker. On the next day they were once again washed extensively with ddH<sub>2</sub>O and stored in absolute ethanol at 4°C. One day before seeding the cells, coverslips were sterilized with fire and put into a 24-well cell culture plate. 400 µl of poly-D-lysine in borate buffer was used as a coating agent and left overnight on the coverslips.

Preparation of coverslips for microisland cultures: The coverslips for microisland cultures were obtained from the laboratory of Prof. Dr. Rosenmund and were processed as described in the following:

30 mm coverslips were shaken overnight in 1 N NaOH. Coverslips were extensively washed in water followed by sterilization in 70 % ethanol and stored in absolute ethanol. The coverslips were briefly sterilized by fire and placed in the wells of a 6-well culture plate. To coat the coverslips 0.15 % low-melting agarose was liquefied in a microwave. 700-1000 µl of this solution was used to cover the glass and was quickly sucked off so that only a very thin layer of agarose attached to the glass. Agarose-coated coverslips were dried at room temperature and stored for later usage. To coat the agarose-containing coverslips with a growth-submitting substrate a custom-made stamp with small dots, which will create adhesive “islands”, was used. Three to four tissue papers were cut to fit in a 35\*10 mm petri dish and 300 µl of coating solution containing 0.85 mg/ml collagen I from rat tail (Gibco) and 0.1 mg/ml poly-D-lysine were used to soak the paper. The stamp was pressed against the papers and the adhesive substrate printed on the agarose-coated coverslips. After this step the coverslips were dried and sterilized under a sterile hood by UV-irradiation for at least 30 min. Coverslips were stored at room temperature for up to three month.

Glia cells: Postnatal day 0 to 2 (P0, P2) C57BL6/N pups were sacrificed and their cortices were removed. Bulbi olfactorii and hippocampi as well as the meninges were also removed. Cortices were transferred into Eppendorf tubes filled with 800 µl sterile PBS + 0.05 % Trypsin-EDTA (Gibco) and incubated for 15 min at 37°C and 800 rpm on a thermo shaker.

Trypsin solution was removed and the digestion stopped by adding 800 µl DMEM containing 10 % FCS + P/S. Cortices were triturated with a 1000 µl pipette and 400 µl of this solution transferred into a T75 flask filled with pre-warmed DMEM +10 % FCS + P/S. Medium was changed after the first day *in vitro* and consecutively after seven days. Cells were maintained in an incubator at 37°C for at least 14 days prior to seeding. In experiments requiring agrin and LRP4 mutant glia cells, cortices of E18 embryos were used instead of P0-P2 pups.

Seeding of glia cells: After at least 14 days *in vitro*, T75 flasks were vortexed for 1 min, medium was aspirated and the T75 flasks washed with sterile, pre-warmed PBS. PBS was exchanged with 5 ml of 0.05 % Trypsin-EDTA solution and cells were incubated for 1 min. Trypsin-EDTA solution was sucked off and the cells placed in an incubator for 4 min at 37°C until the cells visibly rounded up and started to detach. Cells were completely detached by hitting the sides of the flask. 7 ml of DMEM + 10 % FCS + P/S were added to stop the digestion. The solution was triturated 10 times with a 10 ml pipette and the solution transferred in a 15 ml Falcon tube. After resuspension a 10 µl aliquot of the solution was mixed with 10 µl of Trypan Blue (BioRad) and 10 µl of this mix were pipetted on a slide for automated cell counting in a BioRad TC-10 Cell Counter. After the cells were counted, they were diluted with DMEM + 10 % FCS + P/S and seeded at a density of 7100 cells/cm<sup>2</sup>. Each well was filled with 3 ml of cell suspension and cells were allowed to grow for 4-7 days.

Cortical cell cultures: Pregnant mice were sacrificed by cervical dislocation at day 15 of gestation. Embryos were transferred into sterile PBS and their heads cut off and transferred into petri dishes filled with 10 ml HBSS. Tails were collected for genotyping. Cortices were removed from the skull with fine forceps using a Stemi DRC microscope with an 1.6x objective (Zeiss). Bulbi olfactorii and meninges were discarded as well as the mid- and hindbrain. Cortex halves were collected in tubes filled with 9 ml HBSS. HBSS was exchanged with S1 solution and the cortices were incubated for 15 min at 37°C in a water bath. In the next step S1 solution was removed and the trypsinisation stopped by adding 9 ml of NB + 10 % FCS + P/S. After a further washing step with NB + 10 % FCS + P/S, cells were resuspended with fire-polished glass pipettes in 2 ml of NB + 10 % FCS + P/S supplemented with 20 µl of DNase I solution. Tubes were filled to 9 ml with NB + 10 % FCS + P/S and centrifuged for 4 min with 1000 rpm in an Eppendorf Centrifuge 5804. Medium was aspirated and cells resuspended in 2 ml of NB + 10 % FCS + P/S. Tubes were again filled to 9 ml with medium

and again centrifuged for 4 min with 1000 rpm. At this point the preparation was modified for the different types of cultures used in this work.

- a) Monolayer culture: Medium was aspirated and exchanged with 1 ml NB<sup>+</sup> + 10 % FCS + P/S. After resuspension a 10 µl aliquot of the solution was mixed with 10 µl of Trypan Blue and 10 µl of this mix were pipetted on a slide for automated cell counting in a BioRad TC-10 Cell Counter. Cells were diluted with NB<sup>+</sup> + 10 % FCS + P/S and seeded at a density of  $2.65 \times 10^5$  cells/cm<sup>2</sup>. They were kept in an incubator at 37°C and 95% O<sub>2</sub> + 5% CO<sub>2</sub> for 5 up to 15 days. Half of the medium was exchanged with NB<sup>+</sup> without FCS + P/S every 3 days.
- b) Microisland culture: Medium was aspirated and exchanged with 1 ml NB<sup>+</sup> without FCS + P/S. After resuspension a 10 µl aliquot of the solution was mixed with 10 µl of Trypan Blue and 10 µl of this mix were pipetted on a slide for automated cell counting in a BioRad TC-10 Cell Counter. Cells were diluted with NB<sup>+</sup> without FCS + P/S and seeded at a density of 425 cells/cm<sup>2</sup>. They were kept in an incubator at 37°C and 95% O<sub>2</sub> + 5% CO<sub>2</sub> for 5 up to 15 days. Half of the medium was exchanged with NB<sup>+</sup> without FCS + P/S every 7 days.

Agrin incubation experiments: Cell cultures were treated with different concentrations of neuronal full-length chicken agrin or C-terminal agrin by adding agrin directly to the culture medium. Medium was gently mixed and the cells were incubated at 37°C for three to five hours prior to any measurements. In experiments where the PI3K blockers wortmannin or LY294002 were applied cells that were incubated for three to five hours in culture medium supplemented with 1 µM of wortmannin or 50 µM of LY294002 served as controls. Cells were also treated with 1 µM wortmannin or 50 µM LY294002 in combination with 1 µg/ml soluble neuronal agrin respectively. For blocking mTOR signaling cells were incubated as in the other experimental setups with together with 1 µM rapamycin.

In the results section of this study agrin refers to the full-length form of neuronal chicken agrin in the incubation experiments. C-terminal neuronal chicken agrin is indicated as such in the experiments it has been used in.

Solutions:

NB + 10 % FCS + P/S:	450 ml Neurobasal medium 50 ml fetal calf serum 5 ml penicillin/streptomycin 100x
NB <sup>+</sup> + 10 % FCS + P/S:	170 ml Neurobasal medium 20 ml fetal calf serum 4 ml BME amino acids 4 ml B27 supplement 50x 250 µl GlutaMax 100x 100 µl β-mercaptoethanol 50 mM 2 ml penicillin/streptomycin 100x
NB <sup>+</sup> without FCS + P/S:	190 ml Neurobasal medium 4 ml BME amino acids 4 ml B27 supplement 50x 250 µl GlutaMax 100x 100 µl β-mercaptoethanol 50 mM 2 ml penicillin/streptomycin 100x
DMEM + 10 % FCS +P/S:	500 ml Dulbecco's modified Eagle medium 50 ml fetal calf serum 5.5 ml penicillin/streptomycin
S1 Solution:	22 ml Hank's buffered salt solution 2.5 ml 10x Trypsin solution (125 mg in 5 ml HBSS) 0.25 ml penicillin/streptomycin 100x 0.25 ml DNase I solution
Borate buffer:	1.24 g boric acid 1.9 g sodium tetra borate ad 400 ml ddH <sub>2</sub> O pH: 8.4
Poly-D-lysine solution:	5 mg poly-D-lysine 50 ml sterile borate buffer
Trypsin-EDTA solution:	5 ml Trypsin-EDTA 10x 45 ml sterile PBS
DNase I solution:	1.5 ml HBSS 10 kU DNase I from bovine pancreas

## 2.2.2 Genotyping of mutant mice by PCR and DNA electrophoresis

### 2.2.2.1 Preparation of genomic DNA

Tail cuts of mice were digested in 200  $\mu$ l tail lysis buffer supplemented with 2  $\mu$ l of proteinase K (Roche) at 57°C on a shaker for 4-12 hours. After full digestion proteinase K was inactivated by heating the solution to 85°C for 45 min on a shaker. Lysate was used as template for PCR-based genotypings or stored at -20°C for later use.

### 2.2.2.2 Genotyping of agrin mutant mice

The mixture for a single PCR reaction (25  $\mu$ l) contained the following reagents:

ddH <sub>2</sub> O:	16.6 $\mu$ l
10X PCR reaction buffer:	2.5 $\mu$ l
50 mM MgCl <sub>2</sub> :	1.25 $\mu$ l
2.5 mM dNTPs:	1 $\mu$ l
5' primer 10 $\mu$ M (WT: Ex31, KO: 77730):	1.25 $\mu$ l
3' primer 10 $\mu$ M (WT: Ex32rev, KO: 30234):	1.25 $\mu$ l
Taq-polymerase (Invitrogen) 5U/ $\mu$ l:	0.15 $\mu$ l
tail lysate:	1 $\mu$ l

The PCR program was designed as follows:

94°C	4 min
30 cycles – 94°C	30 s
58°C	30 s
72°C	45 s
end of loop	
72°C	5 min
4°C	$\infty$

10  $\mu$ l of PCR product supplemented with loading buffer were loaded on a 2 % agarose gel supplemented with ethidium bromide, electrophoresed at 120 V for 45 min and imaged on a ChemiDoc station (BioRad). The wild type reaction (WT) yielded a 300 bp product, the knock out reaction (KO) a 250 bp product, respectively (Figure 5).

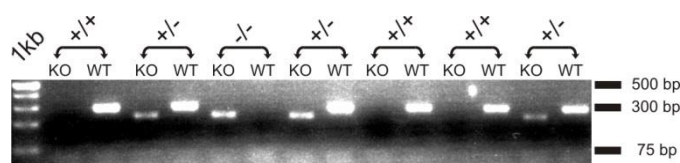


Figure 5: PCR products of an agrin genotyping showing WT-PCR products and KO-PCR products having a size of 300 bp and 250 bp, respectively.

### 2.2.2.3 Genotyping of LRP4 mutant mice

The mixture for a single PCR reaction (25  $\mu$ l) contained the following reagents:

ddH <sub>2</sub> O:	17.25 $\mu$ l
10X Thermopol buffer:	2.5 $\mu$ l
10 mM dNTPs:	0.5 $\mu$ l
5' primer 10 $\mu$ M (L4Hpfmf):	1.25 $\mu$ l
3' primer 10 $\mu$ M (43Br_FP):	1.25 $\mu$ l
Taq-polymerase (NEB) 5U/ $\mu$ l:	0.15 $\mu$ l
tail lysate:	2 $\mu$ l

The PCR program was designed as follows:

94°C		3 min
40 cycles –	94°C	15 s
	58°C	15 s
	72°C	20 s
end of loop		
	4°C	$\infty$

PCR products were digested with 0.5  $\mu$ l of HpyCH4V at 37°C overnight. 10  $\mu$ l of digested PCR product supplemented with loading buffer were loaded on a 2 % agarose gel supplemented with ethidium bromide, electrophoresed at 120 V for 45 min and imaged on a ChemiDoc station (BioRad).

The reaction yielded a 132 bp + 69 bp product for wild type animals (+/+), a 227 bp product for mutant animals (-/-) and 227 bp + 132 bp + 69 bp products for heterozygous animals (+/-) (Figure 6).

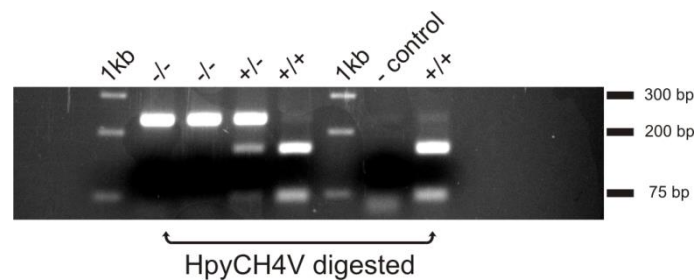


Figure 6: PCR products of a LRP4 genotyping. *Lrp4*<sup>mitt</sup> mutant PCR products (-/-) are not digested by HpyCH4V and have a size of 227 bp while digested products from wild type animals (+/+) show two bands of a size of 132 and 69 bp. PCR products from heterozygous animals yielded a combination of all three bands.

## Solutions and primers:

50x TAE buffer for agarose gels:	242 g Tris 57 ml glacial acetic acid 100 ml 0.5 M EDTA pH 8.0 ad 1 l ddH <sub>2</sub> O
1x TAE buffer:	100 ml 50x TAE buffer 900 ml ddH <sub>2</sub> O
2 % agarose gel:	100 ml 1x TAE buffer 2 g agarose 10 µl ethidium bromide
10x loading buffer:	25 % (v/v) Ficoll 100 mM Tris-HCl pH 7.4 100 mM EDTA 0.25% (w/v) xylene cyanol
Ex31:	CAGGGGATAGTTGAGAAG
Ex32rev:	GCTGGGATCTCATTGGTC
777302:	TCGCAAGTTCTAATTCCA
30234:	GGCAGGGCTAACACCAA
L4Hpmf:	GGTGAGGAGAACAGCAATGT
43Br_FP:	TCCCAGGGTCAGTGTAACGATG

All PCR primers being used in this thesis were synthesized by Eurofins MWG Operon.

### 2.2.3 SDS-PAGE and western blot

Sample preparation for membrane protein purification: Cortical tissue from mice of different ages was collected and the meninges, bulbi olfactorii and hippocampi were removed and the cortical tissue rapidly frozen on dry ice. Samples were stored at  $-80^{\circ}\text{C}$ . Tissues were homogenized in PBS supplemented with 0.34 M sucrose containing the proteinase blockers leupeptin (10  $\mu\text{M}$ ), aprotinin (0.1 mM), PMSF (0.1 mM), pepstatin A (10  $\mu\text{M}$ ). The homogenate was centrifuged at 800 g for 10 min at  $4^{\circ}\text{C}$  using an Eppendorf 5424-R bench centrifuge. The supernatant was collected and centrifuged at 100000 g for 15 min in a Sorvall RC M150 GX centrifuge. The supernatant contained the cytosolic fraction and was stored at  $-20^{\circ}\text{C}$ . The pellet containing the membrane fraction was stripped using 0.1 M DEA pH 11.5 and centrifugation at 100000 g for 15 min. The pH was neutralized by adding PBS after discarding the supernatant. The suspension was again centrifuged at 100000 g for 15

min and the pellet solubilized in 200  $\mu$ l TBS containing proteinase blockers and 1% CHAPS. In this solution the proteins were incubated for one hour on ice and again centrifuged at 100000 g for 15 min. The supernatant now contained the solubilized transmembrane proteins. Protein concentration was determined by measurement of UV absorbance at a wavelength of 280 nm with a Bio photometer (Eppendorf). Proteins were stored at -20°C until further use.

Sample preparation for PI3K experiments: Cortical neurons were incubated in medium containing 1  $\mu$ g/ml, 5  $\mu$ g/ml or 10  $\mu$ g/ml agrin for 10 or 30 min, washed with warm PBS and scraped from 24-well plate by adding 200  $\mu$ l ice-cold solubilization buffer containing the proteinase blockers leupeptin, aprotinin, PMSF, pepstatin A and 1 % CHAPS in Tris buffered saline solution. 0.1  $\mu$ M okadaic acid and 0.1  $\mu$ M calyculin A were added to block phosphatases. Wortmannin was added at 1  $\mu$ M to inhibit PI3K and untreated cells used as a negative control. The solution was centrifuged for 4 min at maximal speed on an Eppendorf 5424-R bench centrifuge. The supernatant was collected and again centrifuged for 15 min at 100000 g at 4 °C in a Sorvall RC M150 GX ultra centrifuge. The protein concentration of the supernatant was determined by measurement of UV absorbance at a wavelength of 280 nm with a Bio photometer (Eppendorf).

SDS-PAGE and western blot: Protein samples were diluted to the desired protein concentration by adding water and sample buffer and boiled for 3 min. 1-5  $\mu$ g of protein (depending on the experiment) was loaded per lane and analyzed by SDS-PAGE. 6 % SDS gels were used for agrin blots (7.5 % SDS gels for LRP4, 10 % SDS gels for PI3K) and samples were electrophoresed for one hour at 150 V. Separated proteins were blotted on nitrocellulose membranes in a transfer tank filled with cold blotting buffer and an ice block at 100 V for one hour. Membranes were stained with Ponceau S stain and washed with ddH<sub>2</sub>O. Blocking was done using PBS supplemented with 1% BSA for at least 30 min at room temperature. Primary antibodies were diluted in PBS/BSA and applied to the membranes overnight at 4°C on a shaker. Blots were washed three times for 5 min with PBS containing 0.5 % TWEEN 20 and incubated for one hour with secondary antibodies coupled to HRP diluted 1:20000 in PBS/BSA. After another step of washing in PBS/TWEEN blots were analyzed using the enhanced chemiluminescence kit (Thermo Scientific). The membranes were incubated with a solution comprised of one volume peroxide solution and one volume of luminol enhancer

and placed between plastic sheets without introducing bubbles. Images were acquired with a ChemiDoc station (BioRad) using different exposure times yielding optimal results.

Analysis of PI3K pathway blots: In experiments where the PI3K pathway was either stimulated with neuronal agrin or blocked by wortmannin blots were analyzed with ImageJ. The intensity of the bands was measured by placing a rectangular region of interest (ROI) around the bands and was normalized to the intensities of their respective GAPDH bands. Control values for pAKT and pGSK3 $\beta$  were compared with wortmannin- and agrin-treated levels of the proteins and statistically tested. Data showing strong increases in phosphorylation of AKT and GSK3 $\beta$  in cells treated with wortmannin were omitted. Data showing strong decreases in phosphorylation of AKT and GSK3 $\beta$  in cells treated with agrin compared to control cells were also omitted.

#### Solutions:

1 M Tris-HCl pH 8.8:	121.1 g Tris base fill to 800 ml with ddH <sub>2</sub> O adjust pH to 8.8 with HCl add ddH <sub>2</sub> O to 1 l
1 M Tris-HCl pH 6.8:	same as above but pH 6.8
10 % ammonium persulfate (APS):	0.1 g APS in 10 ml ddH <sub>2</sub> O
10x running buffer:	30.3 g Tris base 144 g glycine dilute in 1 l ddH <sub>2</sub> O
Blotting buffer:	100 ml 10x running buffer 200 ml methanol 690 ml ddH <sub>2</sub> O 10 ml 10% SDS solution
1x running buffer:	100 ml 10x running buffer 10 ml 10% SDS solution add ddH <sub>2</sub> O to 1 l

### 2.2.4 ELISA for agrin-agrin interaction

Biotinylation of agrin: To detect a possible agrin-agrin interaction agrin was covalently labeled with biotin. Agrin was incubated with Sulfo-NHS-LC-Biotin linker for one hour at room temperature in 20x molar excess. The reaction was quenched with ethanolamine (1 M stock, pH 8.0) using the same volume of ethanolamine as the biotin linker and the biotinylation confirmed by western blot analysis.

ELISA: 100 µl of agrin at a concentration range from 0.5 µg/ml to 0.125 µg/ml was immobilized in wells on a 96-well plate (Nunc). Adsorption was done at 4°C overnight. Empty wells and wells containing only PBS or PBS/BSA were used as negative controls; Rb46 was used as a positive control. The plate was washed three times with 200 µl washing puffer per well. Blocking was done with 200 µl of blocking buffer for 1 h at room temperature. The plate was washed again three times and the biotin-conjugated agrin was added in different dilutions. After two hours of incubation at room temperature the plate was again washed three times and 100 µl developing solution was applied to each well. The reaction was stopped with 100 µl of 6 N sulfuric acid. The plate was read on a Model 3550 microplate reader (BioRad) using a detection wavelength of 490 nm and a reference wavelength of 405 nm.

Solutions:

Block buffer:	1 g bovine serum albumin 500 µl TWEEN-20 ad 100 ml PBS
Washing buffer:	5 ml TWEEN-20 ad 1 l PBS
Detection solution:	15 ml citrate buffer 5 µl 30 % hydrogen peroxide solution 100 µl OPD

### 2.2.5 Immunocytochemistry

Staining of synapses: Immunocytochemistry was used to visualize synapses in microisland as well as in monolayer cultures of control and agrin-treated cells. Antibodies against the presynaptic markers VGlut1+2 (polyclonal GP, Synaptic Systems) for excitatory and VGAT (polyclonal Rb, Synaptic Systems) for inhibitory synapses as well as postsynaptic markers gephyrin (monoclonal mouse, Synaptic Systems) and PSD95 (monoclonal mouse, Thermo Scientific) were combined to show areas of co-localization, supposedly synapses. Cells were fixed in cold methanol fixation solution (for synapse staining) for 10 min at -20°C and washed with PBS for three times. After permeabilization with 0.1 % Triton X-100 in 0.1 % BSA containing PBS cells were again washed with PBS three times and incubated in blocking solution containing 1 % BSA in PBS. Antibodies were diluted in blocking solution (table 1). Cells were incubated for one hour in a chamber containing moist paper at room temperature with primary antibodies and washed three times with PBS. Secondary antibodies (raised in goat, Dianova) coupled to either Alexafluor-488, Alexafluor-594 or Cy3 were diluted 1:500 in 1 % BSA/PBS and when necessary DAPI was added 1:1000 to visualize nuclei. During 45 min of incubation the coverslips were kept in the dark in a moist atmosphere. Coverslips were washed three times with PBS and dipped into ddH<sub>2</sub>O and mounted on glass slides with mowiol. They were left to dry at room temperature in the dark overnight and kept at 4°C until further use.

Staining of AMPAR: AMPAR were visualized using anti-GluA antibodies (mouse monoclonal, Synaptic Systems) together with the presynaptic protein VGlut1+2 (polyclonal GP, Synaptic Systems). Cells were fixed in PBS containing 4 % formaldehyde for 10 min at room temperature. From this step on the same protocol was used as for the staining of synapses. This protocol was also used for the staining and detection of other proteins (e.g. GFAP, MAP2).

Solutions:

Methanol fixation solution:	90 ml methanol 10 ml glacial acetic acid
Formaldehyde fixation solution:	8 ml 37 % formaldehyde solution 66 ml PBS
PBS/BSA:	1 g bovine serum albumin ad 100 ml PBS

Permeabilization solution:            100 µl Triton X-100  
    0.1 g bovine serum albumin  
    ad 100 ml PBS

### **2.2.5.1 Confocal imaging of immuno-stained cultures**

Cells were imaged on a Carl Zeiss LSM700 confocal microscope using ZEN 2010 software and a PC for data acquisition. Images were taken using a 63x objective (Plan Apochrome 1.4 Oil DIC) and a zoom factor of 0.5. The soma of a neuron was placed in the center of the view field and Z-stack images were taken. Laser intensities and gain factors were adjusted for each channel to yield sufficiently illuminated pictures without oversaturating the image. For further analysis these stacks were transformed into 2D images and saved separately.

### **2.2.5.2 Analysis of confocal images**

Analysis of co-localization: Confocal images of control and agrin-treated cells were processed with ZEN2010 and co-localization assessed with the ImageJ (NIH) plug-in PunctaAnalyzer written by Barry Wark, which is available from the Eroglu Lab (c.eroglu@cellbio.duke.edu). The program was used according to the following instructions of the Eroglu group (Ippolito and Eroglu, 2010). A rectangular selection tool was selected in the ImageJ menu to determine the region of interest (ROI). The whole view field was selected as ROI (width = 203.23 µm, height = 203.23 µm). With this ROI selected the plug-ins menu "PunctaAnalyzer" was selected. In the "Analysis Options" window that appeared "Red Channel", "Green Channel", the first "Subtract Background" and "Set results file..." was selected. Next, a rolling ball radius of 50 was selected and the "White Background" option unchecked. A new window appeared alongside a mask corresponding to the red channel image. The threshold was adjusted until the red mask corresponded as well as possible to as many discrete individual puncta without introducing too much noise. This is the most subjective step of this protocol and it was taken care to develop a consistent approach. The minimum puncta size was set to 4 pixels and nothing else modified. The previous step was repeated for the green channel respectively. The plugin provided quantification corresponding to puncta in each channel separately and to co-localized puncta between the two channels. The co-localized puncta number was saved to an Excel sheet and subjected to statistical analysis using Mann-Whitney rank sum tests. Only cells with a clear and distinct staining for both channels were analyzed. Cells were blindly evaluated in respect to agrin treatment.

Analysis of pharmacological PI3K block: To test whether or not blocking of PI3K leads to a decrease of phosphorylated downstream targets we used immunocytochemistry employing antibodies raised against phosphorylated GSK3 $\beta$  (Cell Signaling Technology). Cultures were either untreated controls or treated with agrin (1  $\mu$ g/ml) or wortmannin (1  $\mu$ M). Cells were fixed as previously described. Images were acquired with the same microscope and objective as mentioned before. Special care was taken to always use the same laser intensities and gain settings for control and treated cells in the same experiment set. ImageJ was used for offline analysis to draw a ROI around the soma of a cell and to measure the mean intensity of the fluorescence signal. The data was then subjected to appropriate statistical tests (t-test if normally distributed or Mann-Whitney test if normal distribution was not given).

Analysis of AMPAR cluster area and density: Pictures were obtained as previously described using a 63x objective. Overview images were acquired employing a zoom factor of 0.5 or 1.5 for detailed images for offline analysis. Images were analyzed with ImageJ. AMPAR cluster area was determined after adjusting the threshold by zooming in on spots of co-localization with VGlut1+2 and drawing a ROI around it and measuring the area of the ROI. For the density of these spots the length of dendrites harboring these co-localizations was measured and the contained spots counted. The data was then subjected to appropriate statistical tests (t-test if normally distributed or Mann-Whitney test if normal distribution was not given).

### **2.2.6 Reverse transcription PCR & quantitative real-time PCR**

Preparation of total RNA: Pregnant mice were sacrificed and the cortices of E15 embryos were removed as described for the preparation of cell cultures. Cortical hemispheres were frozen at -80°C and stored at this temperature until further processing. Animals were genotyped and wild type as well as mutant littermates selected for each specific experiment. For the preparation of total RNA the Qiagen Rneasy Kit was used. Only DEPC-treated plastics were used in all the following steps to avoid degradation of RNA by RNases. Samples were always kept on ice. Homogenization buffer was freshly prepared by adding 12  $\mu$ l of  $\beta$ -mercaptoethanol to 1200  $\mu$ l of RLT buffer. This mix was shortly vortexed and 600  $\mu$ l of RLT-mix pipetted onto the tissue samples. Samples were triturated with a 1000  $\mu$ l pipette until the tissue was completely dissolved. Samples were centrifuged at maximal speed on an Eppendorf 5424-R bench centrifuge for 3 min at 4°C. The supernatant was transferred in a

fresh 1.5 ml Eppendorf tube, 350  $\mu$ l of 70 % ethanol was added and the solution vortexed. After this step 700  $\mu$ l of this solution were applied to one RNeasy spin column. After 60 s centrifugation at 8000 g the flow-through was discarded and the column tapped on a piece of paper to remove excess buffer. 700  $\mu$ l of RW1 were applied to the column followed by 60 s centrifugation at 8000 g. Flow-through was again discarded and the column tapped on a piece of paper. 500  $\mu$ l of RPE buffer were applied in the next step and the column centrifuged for 60 s at 8000 g. Flow-through was again discarded and 500  $\mu$ l RPE buffer were again applied to the column followed by 2 min of centrifugation at 8000 g. In the final step RNA was eluted in a fresh collection tube by adding 40  $\mu$ l of DEPC-treated ddH<sub>2</sub>O to the spin filter and centrifugation for 2 min at 8000 g. A 1  $\mu$ l aliquot of total RNA was diluted 1:20 in DEPC-treated ddH<sub>2</sub>O and the concentration quantified in a Bio photometer (Eppendorf). Reverse transcription: To transcribe the total RNA into cDNA SuperScript II reverse transcriptase was used. 5  $\mu$ g of RNA were chosen as a template for reverse transcription. For each reaction a PCR tube was prepared with the following reagents:

Oligo (dT) Mix:	1 $\mu$ l
dNTPs 2.5 mM:	1 $\mu$ l
5 $\mu$ g total RNA:	x $\mu$ l
ddH <sub>2</sub> O:	to 12 $\mu$ l

The mixture was heated to 65°C for 5 min in an Eppendorf Master Cycler Gradient PCR machine and quickly chilled on ice. After that the following reagents were added to the tubes:

5x first-strand buffer:	4 $\mu$ l
0.1 M DDT:	2 $\mu$ l

The contents were mixed with a 100  $\mu$ l pipette and incubated for 2 min at 25°C in the PCR machine. Afterwards 1  $\mu$ l (200 U) of SuperScript II RT was added and mixed by pipetting. After further incubation at 25°C for 10 min, the reaction was incubated at 45°C for 50 min and inactivated by heating to 70°C for 15 min. cDNA was diluted 1:100 and quantified an UV-photometer. For real-time quantitative PCR the SYBR Select Master Mix (Applied Biosystems) was used in these experiments according to the manual.

A single reaction consisted of the following components:

SYBR Green Master Mix:	10 $\mu$ l
Forward primer 10 pM:	0.5 $\mu$ l
Reverse primer 10 pM:	0.5 $\mu$ l
ddH <sub>2</sub> O:	8 $\mu$ l
cDNA template (40 ng):	1 $\mu$ l

Each gene was investigated at least in triplicate on 96-well plates suitable for real-time PCR. The standard cycling mode was selected on the 7500 Fast Real Time PCR cycler (life technologies) which comprised the following steps:

UDG Activation:	50°C	2 min	
AmpliTaQ polymerase activation:	95°C	2 min	
Denature:	95°C	15 s	40 cycles
Anneal/Extend:	60°C	1 min	40 cycles

Analysis of melting curves: The mean cycle threshold ( $C_T$ ) values for each gene were calculated and used to determine the  $\Delta C_T$  value to normalize the mRNA amount to the actin reference of the specific animal. Values that deviated strongly from the others of the same sample were excluded when calculating  $C_T$ .

$$\Delta C_T^{WT} = C_T^{WT} \text{ target} - C_T^{WT} \text{ actin} \quad \& \quad \Delta C_T^{KO} = C_T^{KO} \text{ target} - C_T^{KO} \text{ actin}$$

In the next step the normalization to the wild type sample was done which gives the  $\Delta\Delta C_T$  value

$$\Delta\Delta C_T = \Delta C_T^{WT} \text{ target} - \Delta C_T^{KO} \text{ target}$$

The last calculation is used to calculate the relative fold change (F) showing a higher transcription or lowered transcription of the target gene in the sample.

$$F = 2^{-\Delta\Delta C_T}$$

Fold changes from different preparations were used to determine statistically significant changes in mRNA levels of wild type and mutant mice by using the t-test.

List of primers for real-time quantitative PCR:

Agrin:	Agrin_F:	GCACACCTTCGAGAGAGACC	
	Agrin_R:	CTATGGGCTCTTTGCTCCTG	product size: 206 bp
CAR:	CxadrFor:	ACT CTC AGT CCC GAA GAC CA	
	CxadrRev:	TGCGTCGCCAGACTTGACAT	product size: 179 bp
Actin:	Aktin For:	CGTGGGCCGCCCTAGGCACCA	
	Aktin Rev:	CTTAGGGTTCAGGGGGGC	product size: 238 bp
$\alpha$ 3-Na <sup>+</sup> /K <sup>+</sup> ATPase:	A3_F:	CATTGTCACTGGTGTGGAGG	
	A3_R:	GAAGGGTGTGATCTCAGGGA	product size: 100 bp
LRP4:	LRP4_F:	GCAACTGCACCACCTCCATG	
	LRP4_R:	CACAGGAAGTGGTCAGAGGC	product size: 168 bp
$\alpha$ -dystroglycan:	aDys_F:	CACCACTCGAATCCGTACT	
	aDys_R:	AAAATAGGTTCCCACCCAGG	product size: 116 bp

Primers were specifically designed to include all possible isoforms of each gene investigated.

## 2.2.7 Electrophysiology

### 2.2.7.1 Components of the electrophysiology set-up

The patch clamp set-up comprised the following components: an upright microscope Axioscope 2 FS plus (Zeiss) set upon a vibration isolated table (Newport). Cells were visualized with phase contrast optics using a 40x Achromatic objective (0.8 w Ph 2; Zeiss) and a 16x Zeiss ocular. The holding chamber for tissue slices or coverslips was custom-made from acrylic glass and mounted on micromanipulators that were operated manually (Luigs & Neumann). The head stage of the EPC-10 patch clamp amplifier (HEKA Elektronik) and the electrode for extracellular stimulations were also mounted on micromanipulators powered by Mini 25 (Luigs & Neumann) motors being controlled by an external SM III-5 controller unit (Luigs & Neumann). A stimulus isolator model 2200 (A-M Systems) to transform the applied stimuli for extracellular stimulations, a gravity-fed perfusion system and peristaltic pump system were used when necessary. All components mentioned above were located in a Faraday's cage and centrally grounded. Electrophysiological recordings were acquired with a EPC-10 patch clamp amplifier (HEKA Elektronik), analog signals digitized and saved on a Windows XP personal computer. The amplifier was controlled, protocols edited and run with the Windows version of TIDA 5.24 (HEKA Elektronik).

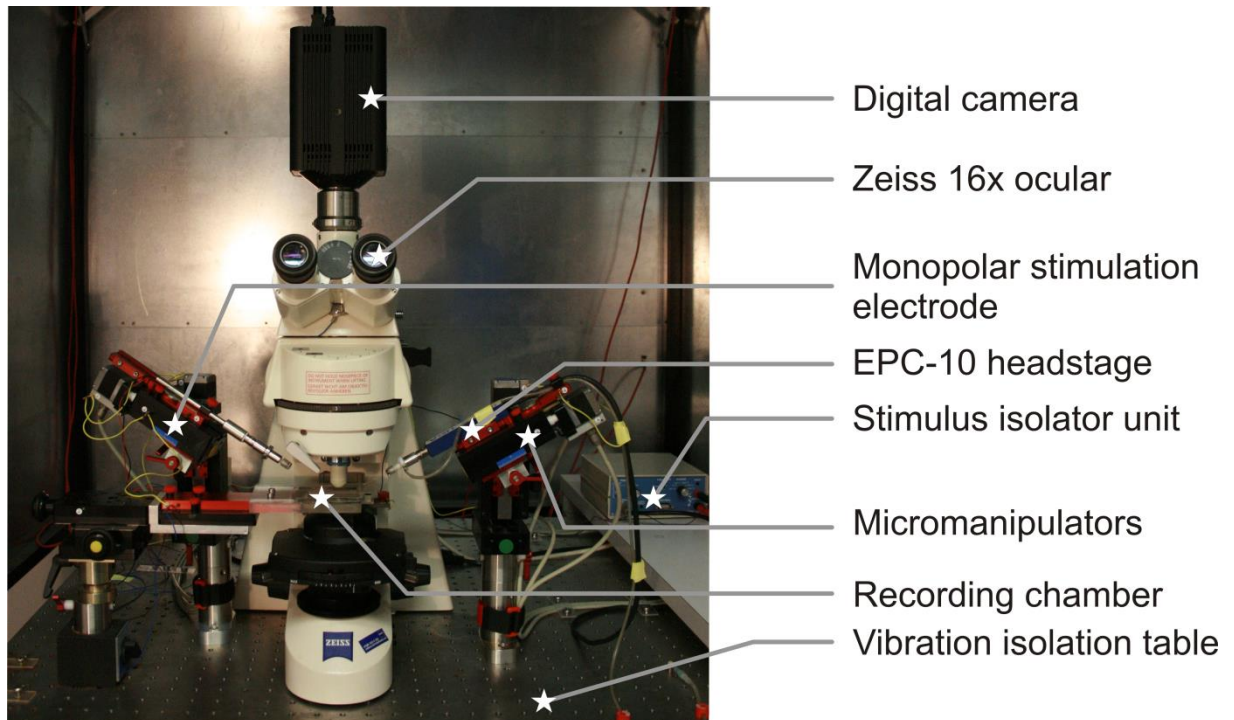


Figure 7: Patch clamp set-up comprised of an upright microscope, stimulation and recording electrodes mounted on micromanipulators, the recording chamber, a stimulus isolation unit, a vibration isolation table and a Faraday's cage.

#### 2.2.7.2 Patching a cell

Coverslips were removed from cell culture plates with fine forceps and attached to the recording chamber using a small drop of grease. They were submerged in pre-warmed extracellular solution containing the drugs needed for the experiment. The recording chamber was screwed to the micromanipulators and cells were visually inspected using a 40x water immersion objective. After a suitable cell was selected, meaning a healthy neuron with a phase bright soma, a pipette pulled from Kwik-Fil 1B150F-4 borosilicate glass (World Precision Instruments) using a model P-97 micropipette puller (Sutter Instruments Co.) was filled with intracellular solution and mounted on the head stage. Positive pressure was given using a 5 ml syringe to prevent clogging and the pipette was moved into the bath solution. The pipettes had resistances of around 2-5 M $\Omega$  when filled with intracellular solutions. The offset voltage ( $V_{\text{offset}}$ ) between pipette and bath solution was cancelled and the pipette advanced to the neuron until the current response of the 10 mV test pulse started to decrease, signaling the vicinity of the pipette tip to the cell's membrane. The positive pressure was removed and the membrane patch under the pipette sucked into its opening. Under normal conditions a giga seal, which is the increase of the resistance indicating a tight "seal" between pipette and membrane patch, formed within seconds. The holding potential was adjusted to - 70 mV and the fast capacitive transients were cancelled. The membrane

patch was then ruptured by gentle suction leading to an electrical connection between the cell and the pipette. The access resistance ( $R_a$ ) was compensated as much as possible (round 30-60 %) without inducing membrane potential oscillations. The whole cell patch clamp configuration was thus achieved (Figure 8) and the cell could now be investigated with different voltage and current clamp protocols.

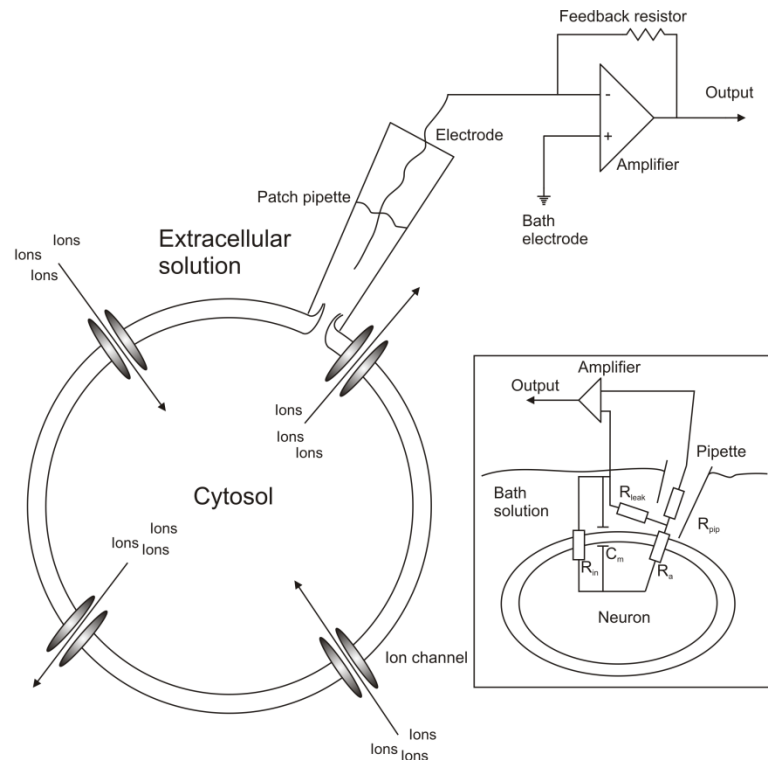


Figure 8: A scheme of a cell being patched in whole cell configuration. The currents measured by the Ag/AgCl electrode are due to ionic fluxes through different ion channels of the cell. The electrode is connected to an amplifier (the head stage) which is also connected to the bath solution for grounding and uses a feedback resistor to maintain the desired holding potential. Recorded currents are further processed and digitalized by the EPC-10 amplifier and stored on a personal computer. The inset shows an equivalent circuit for the whole cell patch clamp configuration with the different resistors that shape the electrical properties of a cell.

### 2.2.7.3 Determining the passive membrane properties of a cell

The passive membrane properties are comprised of the cell's capacitance ( $C_m$ ) and its input resistance ( $R_{in}$ ) (Figure 8). The access resistance ( $R_a$ ) is a good indicator for a sound recording. It can be easily determined by measuring the maximal transient current ( $I_{max}$ ) which is induced if a cell's membrane potential is depolarized by + 10 mV ( $\Delta U$ ) (Figure 9A, Figure 10A). The following formula is used to determine the access resistance:

$$R_a = \Delta U / I_{max}.$$

Cells exceeding an uncompensated access resistance of 30 MΩ were discarded and not included in the analysis. The input resistance of a cell could be computed by measuring the offset current ( $I_{\text{offset}}$ ) of the current response (Figure 9B) and dividing  $\Delta U$  by it.

$$R_{\text{in}} = \Delta U / I_{\text{offset}}$$

To determine the membrane capacitance of a cell a 200 ms voltage change was induced in its membrane potential by + 10 mV for 10 times. The acquired trace was averaged and the integral of the current response, the charge of the membrane, was determined, giving rise to the membrane capacitance (Figure 9A) as can be deduced by these formulae:

$$C_m = 1/\Delta U * \int I dt = \text{Charge}/\Delta U = \text{pF}; \text{Charge} = \text{pA} * \text{s} = \text{pC}.$$

The specific membrane resistance ( $R_{\text{spec}}$ ) was calculated by multiplying the input resistance ( $R_{\text{in}}$ ) with the specific membrane capacitance  $1\mu\text{F}/\text{cm}^2$ :

$$R_{\text{spec}} = R_{\text{in}} * 1\mu\text{F}/\text{cm}^2.$$

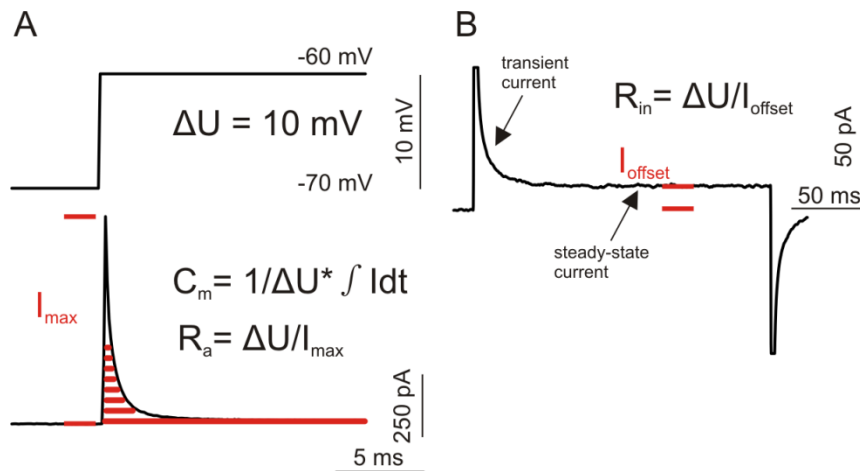


Figure 9: A + 10 mV voltage pulse was given to a neuron clamped at - 70 mV. The maximal current ( $I_{\text{max}}$ ) can be measured to calculate the access resistance ( $R_a$ ) of this cell. By integrating the current response of the cell to the applied pulse one can also determine the membrane capacitance ( $C_m$ ) (A). The offset current ( $I_{\text{offset}}$ ) can be calculated as the difference between the baseline of the pulse and the steady-state of the measured current response. This value is then used to calculate the input resistance ( $R_{\text{in}}$ ) of the cell (transient currents truncated) (B).

#### 2.2.7.4 Determining the active membrane properties (voltage-gated sodium & potassium currents)

To determine sodium ( $\text{Na}^+$ ) and potassium ( $\text{K}^+$ ) current amplitudes and current densities a voltage clamp protocol was used in which the membrane voltage was successively stepped up from - 70 mV to + 30 mV in 10 mV increments. After this protocol 10 hyperpolarizing pulses to - 90 mV were given and used as a correction of passive membrane changes induced

by the depolarizing voltage steps (Figure 10B). Voltage-gated Na<sup>+</sup> currents could not be investigated when miniature postsynaptic currents were recorded due to Na<sup>+</sup> channel blockade by tetrodotoxin (TTX) in the bath solution. Current-voltage relationships could be easily plotted as an IV curve, giving further insights in the properties of the investigated currents.

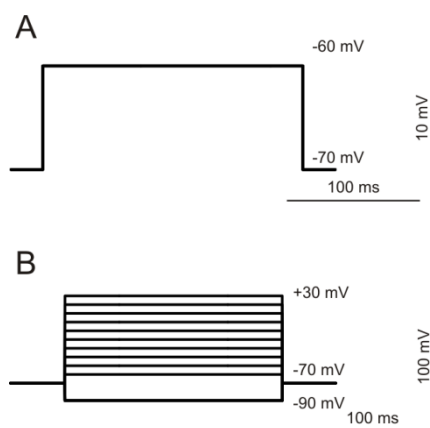


Figure 10: A 10 mV depolarizing voltage step is used to determine the passive membrane properties of a neuron (A). For the analysis of active membrane properties of a cell the membrane potential is successively stepped from -70 mV to +30 mV in 10 mV steps (B). This protocol is used to determine the amplitudes of sodium and potassium currents and generate current-voltage (IV) curves.

#### 2.2.7.5 Recordings of miniature postsynaptic currents (mPSCs)

Miniature postsynaptic currents were recorded in the presence of 1  $\mu$ M TTX to block Na<sup>+</sup> current derived (action potential-derived) events. For all experiments involving monolayer cultures 1  $\mu$ M TTX, 20  $\mu$ M DNQX and 100  $\mu$ M APV were added to the extracellular solution (EC) to block glutamate receptors (AMPA and NMDA receptors) or 20  $\mu$ M bicuculline to block GABA-A receptors. In microisland cultures no further drugs besides TTX were applied since inhibitory and excitatory postsynaptic currents of single neurons could be easily distinguished by their decay time kinetics because in this culture system only monoaxonal inputs are present (Figure 11A). Miniature postsynaptic currents were recorded at a holding potential ( $V_h$ ) of -70 mV in voltage clamp mode by using a 10\*10 s recording protocol. Offline analysis of the recorded events was done using PeakCount (programmed by Christian Henneberger). Amplitude, decay time constant, rise time and frequency were calculated by its algorithms and exported for further statistical analysis.

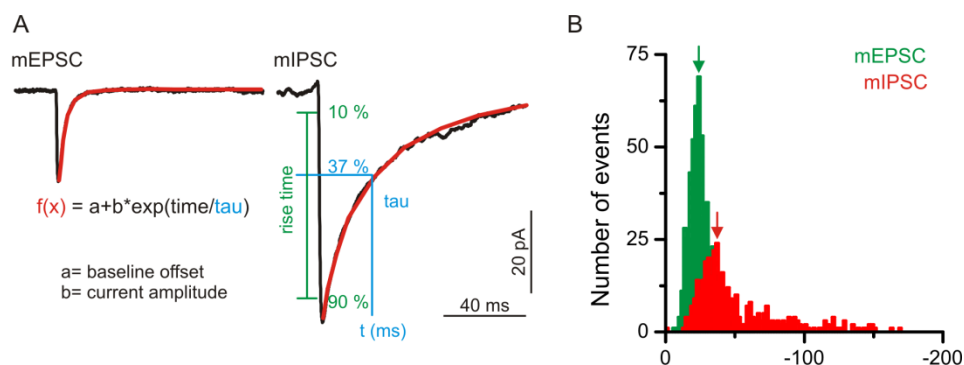


Figure 11: Miniature postsynaptic events from an excitatory (mEPSC) and inhibitory cell (mIPSC). Amplitudes as well as decay times ( $\tau$ ) of the events are shown. Single exponential fits (red) were used to determine  $\tau$  (blue). Also shown is the time interval which was used to measure the rise times (green) of events (A). Histogram showing the amplitude distribution of mEPSCs (green) and mIPSCs (red) (B). Arrows point at the peak of the histogram showing the point used to determine the quantal size of the mPSCs in these two cells. 518 mEPSCs were analyzed having a quantal size of 24.44 pA and 352 mIPSCs with a quantal size of 37.25 pA. The bin size was for the histogram in B was 2 pA.

### 2.2.7.6 Determining the quantal size of miniature postsynaptic events

The quantal size was determined by histograms of the mPSC amplitude distribution of a neuron using Origin7.0. The peak of the histogram was measured to give the value of the quantal size of the mPSCs in a given cell. The selected bin size was 2 pA and only cells with >100 events were analyzed (Figure 11B).

### 2.2.7.7 Analysis of voltage-gated calcium currents (VGCC)

To investigate the properties of voltage-gated  $\text{Ca}^{2+}$  channels normal extracellular solution was changed to EC solution containing 1  $\mu\text{M}$  tetrodotoxin, 10 mM barium chloride, 2 mM 4-amino pyridine and 20 mM tetraethyl ammonium chloride to block voltage-gated potassium channels. Sodium chloride was reduced to 70 mM and extracellular calcium was omitted. IC solution was changed to a cesium chloride-based solution (Table 2). In this way calcium currents could be recorded without activation of voltage-gated sodium and potassium currents. The normal voltage clamp protocol used for the analysis of  $\text{Na}^+$  and  $\text{K}^+$  currents was used in this set of experiments (Figure 10B).

### 2.2.7.8 Analysis of neurotransmitter release by extracellular stimulation with a monopolar electrode

In monolayer cultures where autapses were rarely encountered cells had to be extracellularly stimulated by a monopolar Ag/AgCl electrode to elicit inhibitory postsynaptic currents (eIPSCs). The stimulation pipette was filled with extracellular solution and advanced to a distance of 50-100  $\mu\text{m}$  from the neuron being recorded in whole cell mode. Trigger pulses of 1 V were given by the EPC-10 amplifier to the stimulus isolation unit at defined

interstimulus intervals either 100 ms for ten times with a wait between stimuli of 5 s (Figure 12D) or varying interstimulus intervals (Figure 12E). Stimuli had a current intensity between 10-100  $\mu$ A to elicit a synaptic response. If no response was seen during stimulation, the stimulation electrode was moved around until IPSCs were encountered. Paired-pulse recordings of evoked inhibitory postsynaptic currents (eIPSCs) were made in the presence of 20  $\mu$ M DNQX and 100  $\mu$ M APV in the bath solution to block glutamate receptor currents. The neurons were clamped at a holding potential of -70 mV. Neurotransmitter release in microisland cultures was studied in single neurons making autaptic connections without the need for extracellular stimulation (Figure 12A-C).

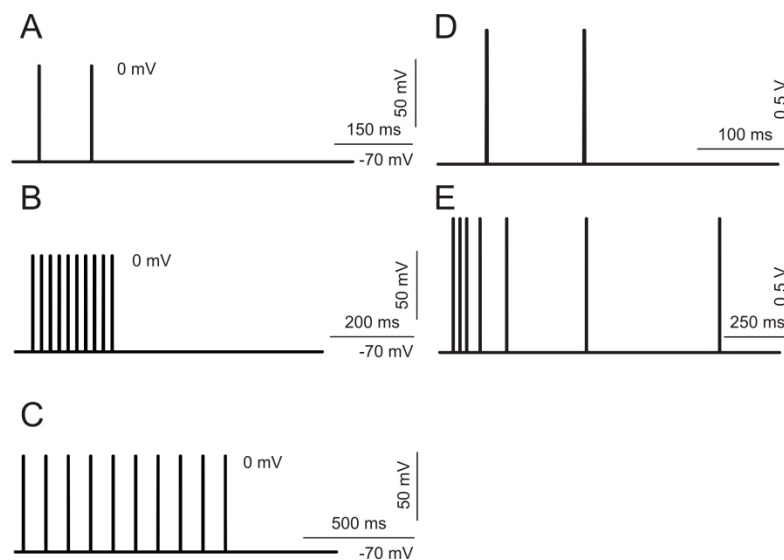


Figure 12: Different pulse protocols used in paired-pulse and high frequency stimulation experiments. To study autaptic connections two depolarizing pulses of 70 mV were given at an interstimulus interval of 100 ms and repeated 10 times (A). For high frequency stimulations excitatory cells were stimulated at 50 Hz (B) and inhibitory cells at 10 Hz (C) and repeated 10 times. For extracellular stimulations the amplifier gave two 1 V trigger pulses to the stimulus isolation unit at an interstimulus interval of 100 ms (D) or at varying interstimulus intervals (E). The stimulus intensity was of the pulses in D and E was 10-100  $\mu$ A.

### 2.2.7.9 Analysis of autaptic neurotransmitter release

Autaptic connections were revealed by a brief (1 ms) step of the membrane potential to 0 mV. EC solution in these experiments contained 20  $\mu$ M DNQX and 100  $\mu$ M APV for the investigation of inhibitory autaptic currents in monolayer cultures and no blockers of GABA or glutamate receptors in microisland cultures since postsynaptic currents of single neurons could be easily classified by their decay kinetics. The paired-pulse ratios were determined for interstimulus intervals (ISI) of 100 ms (Figure 12A). For high-frequency stimulation experiments the neurotransmitter release of single neurons was stimulated at 10 Hz (ISI = 100 ms; Figure 12C) for inhibitory cells or at 50 Hz (ISI = 20 ms; Figure 12B) for excitatory

cells, repeating the stimulus regime 10 times with a pause of 5 s between stimuli and averaging the responses.

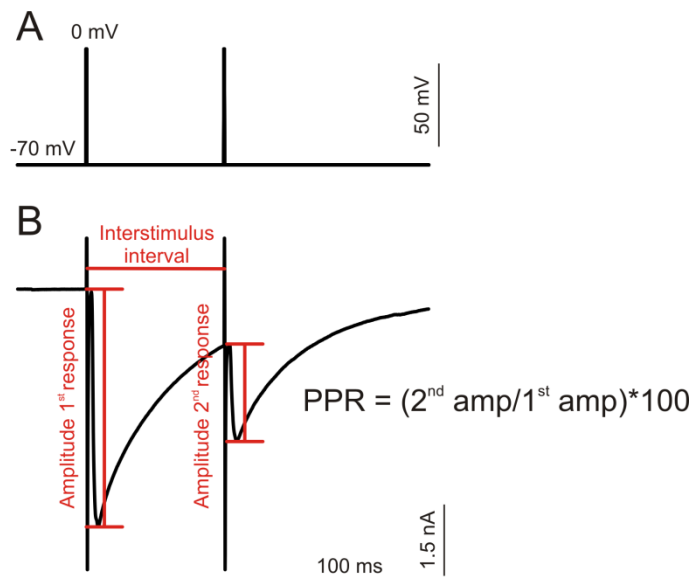


Figure 13: Stimulation of autapses was done using the recording pipette by briefly increasing the membrane potential of the patched cell to 0 mV for 1 ms (A). The time between the two pulses is the interstimulus interval (ISI). The amplitudes of the two current responses were used to determine the paired-pulse ratio (PPR) of the evoked IPSC of the investigated cell (B).

### 2.2.7.10 Determining the quantal content of evoked postsynaptic currents

The quantal content of evoked postsynaptic events was determined by dividing the values of the mean amplitudes of the first synaptic response with the mean values of the quantal size of either excitatory or inhibitory postsynaptic currents. The quantal content gives a rough estimate on how many vesicles are released during stimulation be it extracellularly or autaptically.

### 2.2.7.11 Analysis of the readily releasable pool by high osmolality sucrose stimulation

To stimulate the release of synaptic vesicles in monolayer cultures EC solution was supplemented with 500 mM sucrose. This solution (~ 20  $\mu$ l) was applied locally using a CellTram device (Eppendorf) during the recording of a 2x100 s long voltage clamp file in the presence of 1  $\mu$ M TTX, 20  $\mu$ M DNQX and 100  $\mu$ M APV in EC bath solution. The membrane potential was held at -70 mV and sucrose containing bath solution was washed away before further experiments were conducted. The current response to the sucrose stimulation was integrated using TIDA to determine the charge and the decay kinetics (Figure 14).

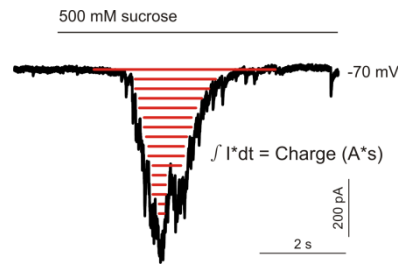


Figure 14: Voltage clamp recording of a cell whose vesicle release was stimulated by local application of a high osmolality sucrose solution. The current response of the cell was integrated to measure the charge of the response, which corresponds to the size of readily releasable vesicle pool.

### 2.2.7.12 Solutions for electrophysiological experiments

The following section contains the composition of all electrophysiological solutions that have been used in this study. Blockers listed in table 4 were added to the solutions in the indicated concentrations where applicable.

Table 2: Solutions for electrophysiological experiments

EC solution	NaCl-based	MW (g/mol)	Concentration (mM)	Weight for 1l (g)
NaCl		58.44	105	6.136
KCl		74.56	3	0.224
HEPES		238.3	10	2.383
Glucose H <sub>2</sub> O		198.1	5	0.991
CaCl <sub>2</sub> *2H <sub>2</sub> O		147.02	2	0.294
MgCl <sub>2</sub> *6H <sub>2</sub> O		203.3	1	0.203

Adjust to pH 7.3 with 1 M HCl  
Adjust osmolality to ~ 250 mOsm

IC solution	KCl-based	MW (g/mol)	Concentration (mM)	Weight for 100 ml (g)
KCl		74.56	90	0.6710
NaCl		58.44	3	0.0175
EGTA		380.35	5	0.1902
HEPES		238.3	5	0.1192
Glucose H <sub>2</sub> O		198.1	5	0.0991
CaCl <sub>2</sub> *2H <sub>2</sub> O		147.02	0.5	0.0074
MgCl <sub>2</sub> *6H <sub>2</sub> O		203.3	4	0.0813

Adjust pH to 7.3 with 1 M KOH  
Adjust osmolality to ~ 220 mOsm

For the analysis of voltage-gated calcium channels (VGCC) the ionic composition of the standard extracellular solution was modified. Sodium chloride was reduced and complemented with tetraethyl ammonium chloride. The intracellular solution was also changed to a cesium chloride-based solution resulting in a block of currents mediated by voltage-gated potassium receptors.

**Table 3: Solutions for VGCC experiments**

EC solution	VGCC	MW (g/mol)	Concentration (mM)	Weight for 1l (g)
NaCl		58.44	70	4.091
KCl		74.56	3	0.224
HEPES		238.3	10	2.383
Glucose H <sub>2</sub> O		198.1	10	1.981
TEA-Cl		165.7	20	3.314
MgCl <sub>2</sub> *6 H <sub>2</sub> O		203.3	2	0.407

Adjust to pH 7.3 with 1 M HCl  
Adjust osmolarity to ~ 250 mOsm/l

IC solution	VGCC	MW (g/mol)	Concentration (mM)	Weight for 100 ml (g)
CsCl		168.36	90	1.5152
EGTA		380.35	10	0.1902
HEPES		238.3	5	0.1192
Glucose H <sub>2</sub> O		198.1	5	0.0991
CaCl <sub>2</sub> *2 H <sub>2</sub> O		147.02	0.5	0.0074
MgCl <sub>2</sub> *6 H <sub>2</sub> O		203.3	4	0.0813

Adjust to pH 7.3 with 1 M CsOH  
Adjust osmolarity to ~ 220 mOsm/l

### 2.2.7.13 List of inhibitors used in electrophysiological experiments

This table contains a list of the used blockers and their concentration.

**Table 4: Blockers used in patch clamp experiments**

Inhibitor name	Target	Company	Concentration
4-AP (4-amino pyridine)	K <sup>+</sup> channels	Alexis	2 mM
Bicuculline	GABA <sub>A</sub> receptor	Alexis	20 μM
DL-APV	NMDA receptors	Tocris	100 μM
DNQX	AMPA/kainate receptors	Tocris	20 μM
LY294002	PI3K	Sigma Aldrich	50 μM
Rapamycin	mTOR	Cayman Chemical	1 μM
Tetraethylammonium chloride	K <sup>+</sup> channels	Sigma Aldrich	20 mM
Tetrodotoxin	Na <sup>+</sup> channels	Almone Labs	1 μM
Wortmannin	PI3K	Sigma Aldrich	1 μM

### 2.2.7.14 Offline analysis and statistics

All electrophysiological data was analyzed offline using TIDA 5.24. Voltage clamp traces of miniature postsynaptic currents were analyzed using PeakCount programmed by Christian Henneberger. Statistical analysis was done using Origin 7.0, SigmaStat5.0 and Microsoft Excel. Data was checked for normal distribution using the Kolmogorov-Smirnov test of SigmaStat3.5 and subjected to one way ANOVA or t-test. Data that failed the test was investigated using the Mann-Whitney rank sum test or ANOVA on ranks. All data in the text corresponds to mean values ± SEM.

## 2.2.8 List of chemicals and equipment

The following tables contain the chemicals and equipment that were used in this thesis.

**Table 5: List of chemicals used in this study**

Name	Manufacturer
2-mercaptoethanol	Sigma-Aldrich
37 % formaldehyde	Merck
Acetic acid	Merck
Acryl amide	Bio-Rad
Agarose NEEO Ultra-Qualität	Carl Roth
Ammonium persulfate	GE Healthcare
Aprotinin	Carl Roth
B27	Gibco
Barium chloride	Merck
BME amino acid solution	Sigma-Aldrich
Boric acid	Sigma-Aldrich
BSA fraction V	Biomol
Calcium chloride dihydrate	Merck
Calyculin A	New England Biolabs
Cesium chloride	Sigma-Aldrich
Cesium hydroxide	Sigma-Aldrich
CHAPS	Merck
DAPI	Dianova
Dihydrogen sodium phosphate	Merck
DMEM	Invitrogen
DMSO	Merck
DNase I type II from bovine pancreas	Sigma-Aldrich
dNTPs Mix (2.5mM each)	Invitrogen
EDTA	Merck
EGTA	Merck
Ethanol	Merck
Ethidium bromide	AppliChem
Fetal calf serum	Gibco
Fura-2 AM	Molecular Probes
G418 Geneticin	Life technologies
Glucose	Merck
GlutaMax I (100x)	Gibco
Glycine	Merck
HBSS	Gibco
HEPES	Sigma-Aldrich
Hydrochloric acid 32% solution	Merck
Isopropanol	Merck

Leupeptin hemisulfate salt	Sigma-Aldrich
Magnesium chloride hexahydrate	Merck
Methanol	Merck
Molecular mass standards for SDS-PAGE	BioRad
Mowiol	Calbiochem
Neurobasal medium	Gibco
Okadaic acid	Enzo Life Sciences
o-Phenylenediamine (OPD)	Sigma-Aldrich
PBS	Biochrom (L182-50)
Penicillin/streptomycin	Invitrogen
Pepstatin A	Sigma-Aldrich
PFA	Merck
PMSF	Enzo Life Sciences
Poly-D-lysine	Sigma-Aldrich
Potassium chloride	Merck
Proteinase K	Roche
Q-Sepharose High Pure	GE Healthcare
SDS solution 10%	Bio-Rad
Sodium chloride	Merck
Sodium hydroxide	Sigma-Aldrich
Sodium tetraborate	Sigma-Aldrich
Sucrose	Merck
Sulfo-NHS-LC-Biotin	Pierce
Sulphuric acid	Merck
SYBR Select Master Mix	Life technologies
TEMED	GE Healthcare
Tris	Merck
Triton X-100	Merck
Trypsin EDTA 10%	Gibco
Trypsin from bovine pancreas	Invitrogen
Tween-20	Sigma-Aldrich
Wheat germ agglutinin	Sigma-Aldrich

**Table 6: Equipment**

<b>Name</b>	<b>Manufacturer</b>
EPC-10 Patch Clamp Amplifier	HEKA Elektronik Dr. Schulze GmbH
Mini 25 micromanipulators	Luigs & Neumann
SM-5 III Controller	Luigs & Neumann
Analog Stimulus Isolator Model 2200	A-M Systems
Spot Insight 2 mega sample CCD camera	Visitron Systems GmbH

Axioskop 2 FS plus	Carl Zeiss
PI 16x ocular	Carl Zeiss
40x Achromplan 0.80 w Ph objective	Carl Zeiss
Vibration isolation table	Newport
Model P-97 Flaming Brown Micropipette Puller	Sutter Instruments
CellTram Air applicator	Eppendorf
Vapor Pressure Osmometer 5520	Vapro
ChemiDoc XRS	Bio Rad
GelDoc XR+ Imaging System	Bio Rad
Model 3550 Microplate Reader	Bio Rad
TC-10 automated cell counter	Bio Rad
Biophotometer	Eppendorf
UVvette	Eppendorf
Centrifuge 5424R	Eppendorf
Sorvall RC M150GX	Thermo Scientific
CB150 incubator	Binder
LSM 700 confocal microscope	Carl Zeiss
63x Plan-Apochrom 1.4 Oil DIC objective	Carl Zeiss
Stemi DRC stereomicroscope	Carl Zeiss
Megafuge 1.0 R	Heraeus
Sorvall RC 6+ (Rotor SS34)	Thermo Scientific

**Table 7: Kits**

<b>Name</b>	<b>Manufacturer</b>
SuperSignal West Dura Chemiluminescent Substrate	Thermo Scientific
RNeasy Mini Kit	Qiagen

**Table 8: DNA polymerases**

<b>Name</b>	<b>Manufacturer</b>
Taq DNA Polymerase recombinant	Invitrogen
Taq DNA Polymerase with Thermopol buffer	NEB
SuperScript II Reverse Transcriptase	Life Technologies

## 3. Results

### 3.1 Cortical microisland cultures

Agrin has been intensively studied at the NMJ for the last two decades where it is essential for its formation and maintenance. Although agrin is expressed in the developing brain its function is still not known and debated. By using a sophisticated microisland culturing system to cultivate single cortical neurons, prepared from E15 mouse embryos, on astrocyte islands and electrophysiology as a tool to measure synaptic function, agrin's effect on the synapse formation or stabilization was investigated by application of full-length neuronal chicken agrin containing an insert with four amino acids at the A site and eight amino acids at the B splice site onto the cultured single neurons.

#### 3.1.1 Characterization of single neurons in microisland cultures

Since the microislands should be composed of astrocytes growing on defined spots, cultures were first subjected to ICC to test this. Antibodies raised against the microtubule associated protein 2a/b (MAP2a/b) were used to label the dendrites of neurons growing on an astrocyte monolayer and antibodies against glial fibrillary acidic protein (GFAP) were chosen to stain these astrocytes. Nuclei were stained with DAPI. All microislands investigated at DIV12-15 harbored GFAP-positive cells, but not every cell was stained showing that there are other cell types present, most probably fibroblasts (Figure 15). Astrocytes were of varying shapes and sometimes very large and flat or displaying pronounced cytoplasmic protrusions. Next it was necessary to characterize the electrophysiological properties of single neurons in this culture system. Different DIV were studied to analyze the passive membrane properties of the cells. As expected the cell capacitance of the cultivated neurons increased with longer culturing periods (capacitance DIV5-6 =  $38.2 \pm 2.1$  pF; DIV10-11 =  $47.3 \pm 3.8$  pF; DIV12-15 =  $68.2 \pm 3.2$  pF; Figure 16) highlighting the growth of the cells. This increase in cell capacitance coincided with changes in input resistance. Young neurons displayed very high input resistances that reduced drastically with longer culturing periods ( $R_{in}$  DIV5-6 =  $1787.1 \pm 146.8$  M $\Omega$ ; DIV10-11 =  $963.0 \pm 105.3$  M $\Omega$ ; DIV12-15 =  $684.1 \pm 53.1$  M $\Omega$ ; Figure 16). Cells older than DIV15 were not analyzed because neurons should have ongoing maturational processes of their synaptic properties for the experiments conducted in this study. Maximal  $K^+$  current amplitudes in voltage clamp mode at DIV 5-6 were small (maximal current amplitude =  $1211 \pm 94$  pA) but still very prominent (Figure 17A). The maximal current

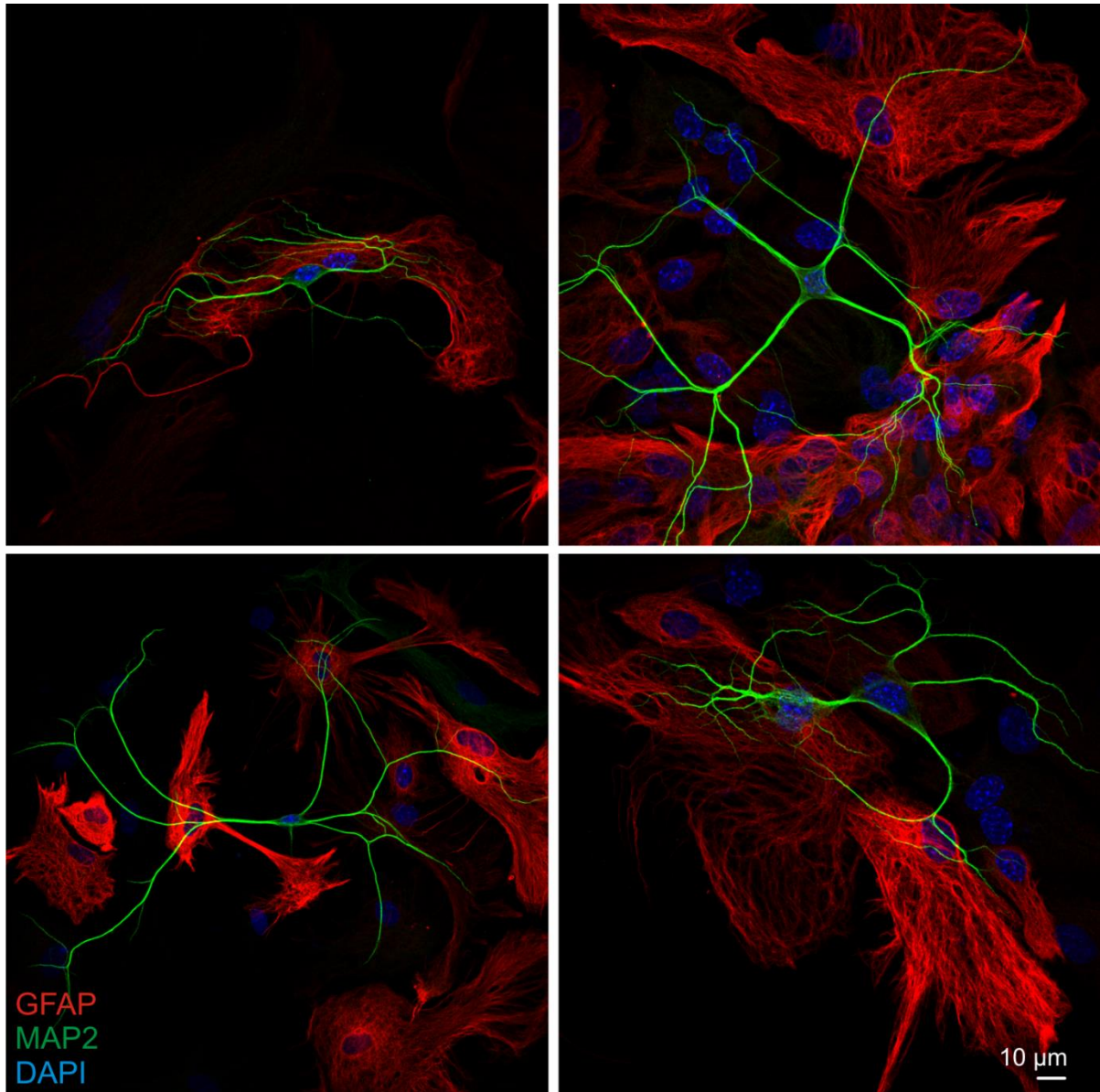


Figure 15: Single MAP2a/b-positive neurons growing on GFAP-positive astrocytes. Neurons at DIV14 were stained with anti-MAP2a/b antibodies and astrocytes with anti-GFAP antibodies. Microislands contained individual neurons with several processes that are branched. Some DAPI-stained nuclei are visible whose cell bodies are not GFAP-positive suggesting that these cells might be fibroblasts.

amplitude was double the size in cells that were cultured for 10-11 days ( $2510 \pm 229$  pA; Figure 17C) and was further increased at 12-15 days in culture ( $3772 \pm 156$  pA; Figure 17C). To further characterize  $K^+$  currents their current-voltage relationship was visualized in an IV-plot (Figure 17B). An increase in conductance with age is apparent from the slope of the respective IV curves. Not only the maximal amplitude of the  $K^+$  currents increased with prolonged culturing periods but also the respective current densities (DIV5-6:  $34.8 \pm 3.2$  pA/pF; DIV10-11:  $56.3 \pm 4.3$  pA/pF; DIV12-15:  $61.4 \pm 3.3$  pA/pF; Figure 17C). These results reflect a normal development of voltage-gated  $K^+$  currents in these neurons and they are in accordance with the results obtained from monolayer cultures (see chapter 3.2.1).

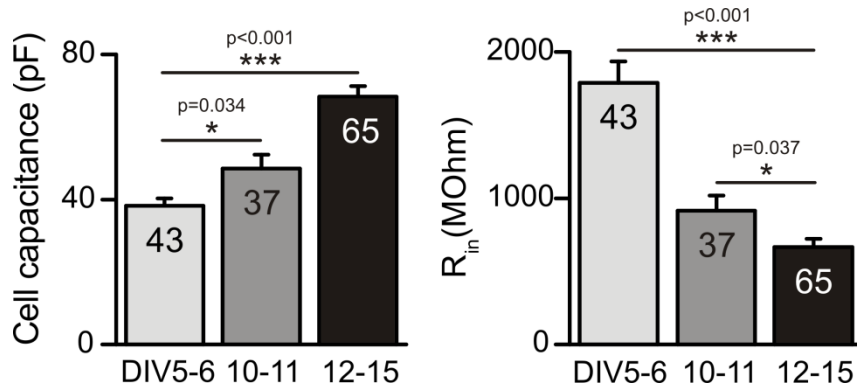


Figure 16: Characterization of the passive membrane properties of single neurons grown on astrocyte microislands. Cell capacitance increases with age, whereas the input resistance decreases, respectively. Statistical analysis was done using Mann-Whitney rank sum tests or t-test. Numbers in columns represent individual cells measured. Bar plots represent mean values + SEM.

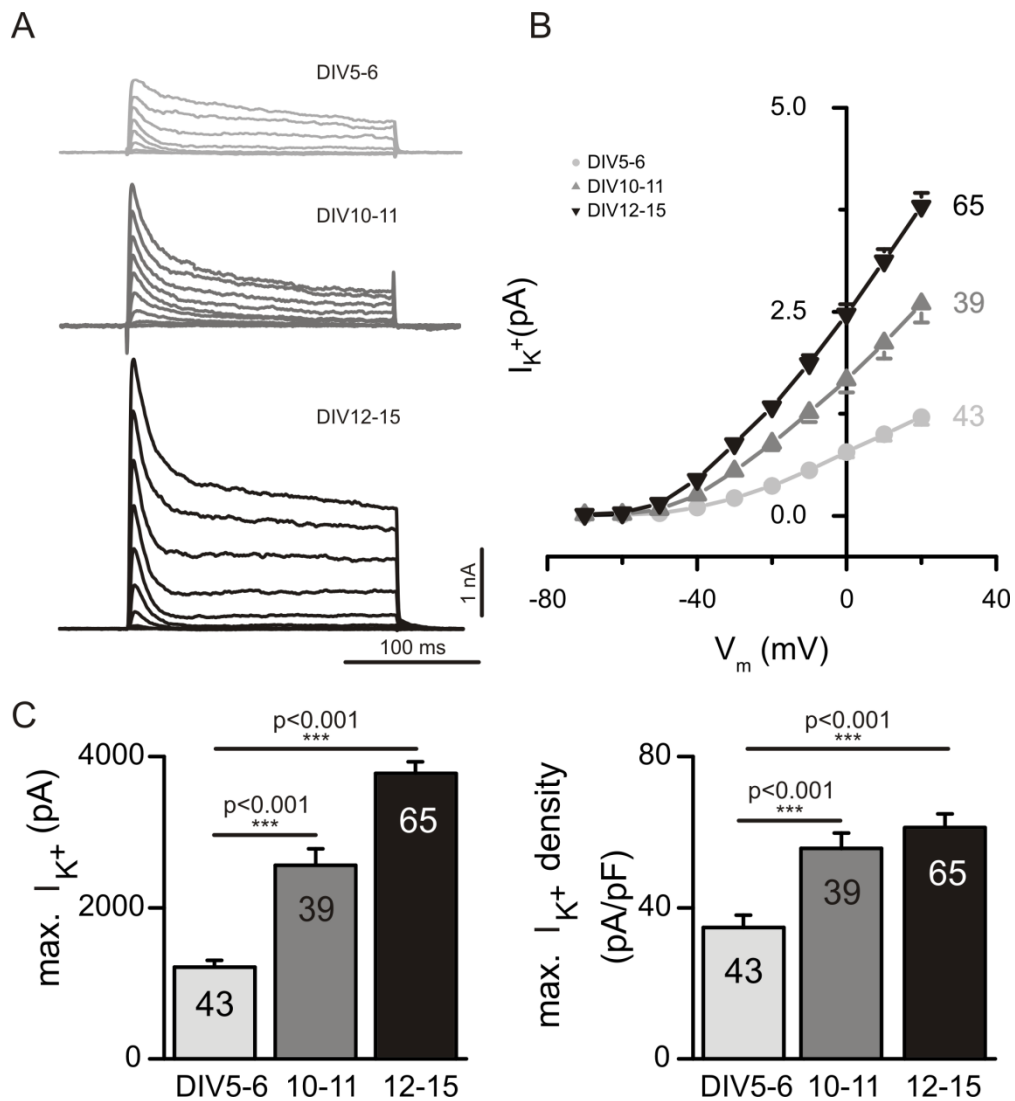


Figure 17: Active membrane properties of single neurons grown on astrocyte microislands. Potassium current traces recorded in voltage clamp mode at different DIV (A) and their respective current/voltage relationship graph (IV-plot) (B). Maximal potassium currents as well as potassium current density were increasing with increased culturing periods (C). The increase in maximal current amplitude was highly significant in “older” neurons compared to “younger” cells. All statistical tests were done using Mann-Whitney rank sum test. Numbers in columns in C represent individual cells measured. Bar plots represent mean values + SEM.  $K^+$  currents were recorded in the presence of TTX.

Since in this set of experiments also miniature postsynaptic currents were analyzed, TTX was present in the bath solution which meant that voltage-gated Na<sup>+</sup> currents were blocked in the recordings of the active membrane properties.

Miniature postsynaptic currents of excitatory and inhibitory neurons were also investigated. The frequency of these currents increased with prolonged culturing from  $0.176 \pm 0.146$  Hz (DIV5-6) to  $1.207 \pm 0.221$  Hz (DIV12-15) for mEPSCs and from  $1.488 \pm 0.993$  Hz (DIV5-6) to  $2.050 \pm 0.391$  Hz (DIV12-15) for mIPSCs. mIPSC frequency was the highest at DIV10-11 ( $4.225 \pm 0.968$  Hz). The amplitudes of the mPSCs were not significantly changed during the culture periods, whereas decay and rise time kinetics did not change during maturation in culture. Note that only 34.9 % of the recorded neurons at DIV5-6 were synaptically active whereas from 98.4 % of the cells at DIV12-15 mPSCs could be recorded (Figure 18). This shows that neurons undergo changes during *in vitro* cultivation.

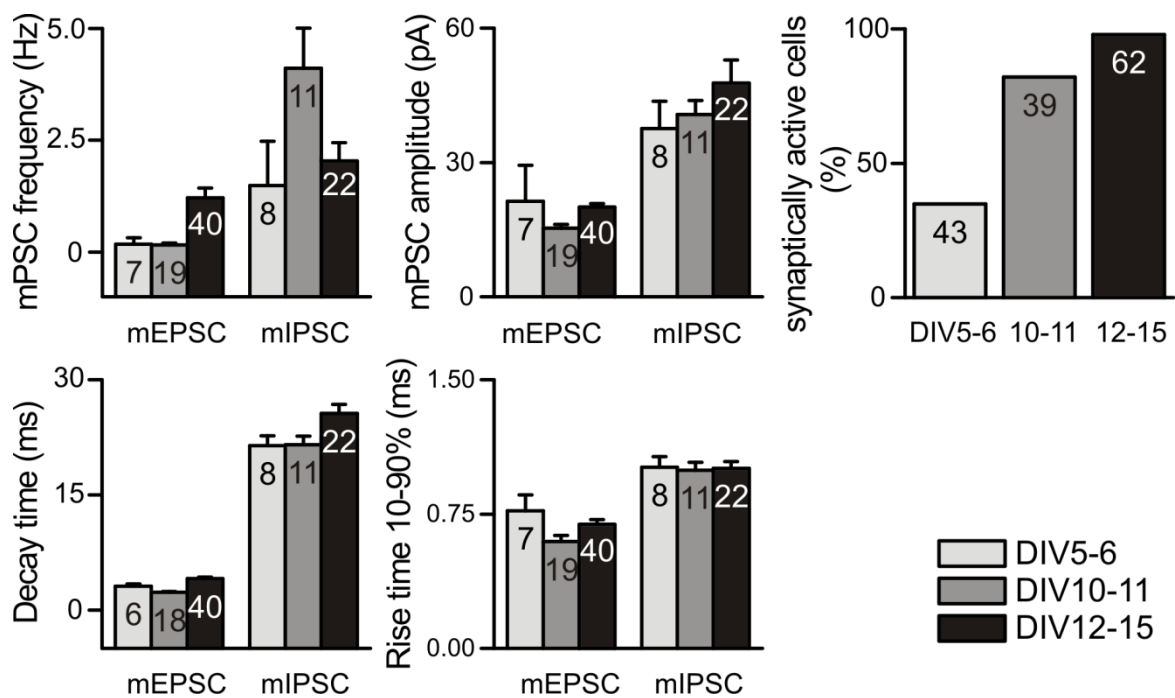


Figure 18: Synaptic properties of single neurons grown on astrocyte microislands. mEPSC and mIPSC frequency, amplitude and decay times increased with prolonged culturing, while rise times remained stable. Note that only around 1/3 of all investigated neurons at DIV5-6 were synaptically active. Numbers in columns represent individual cells measured. Bar plots represent mean values + SEM.

### 3.1.2 Comparison of inhibitory and excitatory neurons shows distinct differences in their electrophysiological properties

Since microisland cultures allow the analysis of single excitatory or inhibitory neurons the electrophysiological properties of these cells were compared. Figure 19A shows two phase contrast images of typical excitatory and inhibitory cells serving as examples. Excitatory cells

most of the time had a round soma with somatic diameters ranging from 13-24  $\mu\text{m}$  whereas inhibitory cells were more elliptic in shape with somatic diameters of 8-17  $\mu\text{m}$ . The cell types could be electrophysiologically distinguished by the decay kinetics of their respective mPSCs (compare voltage clamp traces recorded at  $V_h = -70$  mV in presence of TTX in Figure 19A and Figure 21C) and by pharmacological block of the mPSCs (Figure 21B). mIPSCs were characterized by long decay kinetics and larger amplitudes (Figure 19B and Figure 21C) whereas mEPSCs showed short decay kinetics and small amplitudes as can be seen in the averaged traces of the mPSCs of the two recorded cells (Figure 19B). Histograms of 2 pA bin size revealed that mEPSC amplitudes cluster around a narrow band of around 20 pA whereas mIPSCs have a wider range of amplitudes (Figure 19B).

Excitatory and inhibitory cells not only showed differences in their postsynaptic currents but also in their passive and active membrane properties. Inhibitory neurons were characterized by a significantly smaller somatic diameter ( $11.9 \pm 0.4$  vs.  $14.9 \pm 0.4$   $\mu\text{m}$ ;  $p < 0.001$ ), smaller cell capacitance ( $58.3 \pm 2.9$  vs.  $77.2 \pm 2.1$  pF;  $p < 0.001$ ) and higher  $R_{in}$  ( $761.6 \pm 49.8$  vs.  $623.7 \pm 24.5$  M $\Omega$ ;  $p = 0.012$ ) compared to excitatory neurons (Figure 20A). Of all cells patched 66.5 % were excitatory and 33.5 % inhibitory (Figure 20A, right). Differences in the active membrane properties were also very prominent. Figure 20B shows typical voltage clamp traces displaying  $\text{Na}^+$  and  $\text{K}^+$  currents evoked by a voltage clamp protocol (Figure 10B). The IV-plot revealed equal current-voltage relationships for  $\text{K}^+$  currents but significant differences in  $\text{Na}^+$  currents between excitatory and inhibitory cells (Figure 20C).  $\text{Na}^+$  current amplitudes induced by voltage steps ranging from -50 to +20 mV were significantly smaller in inhibitory cells compared to excitatory cells (Figure 20C) as can be seen in their respective IV-curves. Maximal  $\text{Na}^+$  currents were far greater in amplitude in excitatory cells compared to inhibitory cells ( $5.5 \pm 0.2$  vs  $3.9 \pm 0.3$  nA;  $p < 0.001$ ) but their current densities were similar ( $74.1 \pm 4.7$  vs  $67.96 \pm 4.8$  pA/pF;  $p = 0.06$ ). For  $\text{K}^+$  currents the cells exhibit exactly opposite characteristics. Here the maximal currents were of equal amplitudes ( $3.6 \pm 0.1$  vs  $3.9 \pm 0.2$  nA;  $p = 0.197$ ) but the current densities were significantly higher in inhibitory cells ( $75.6 \pm 4.2$  vs.  $50.8 \pm 2.1$  pA/pF;  $p < 0.001$ ; Figure 20D). These results may be caused by the changes found in the cell capacitance highlighting the difference in the size of these types of neurons.

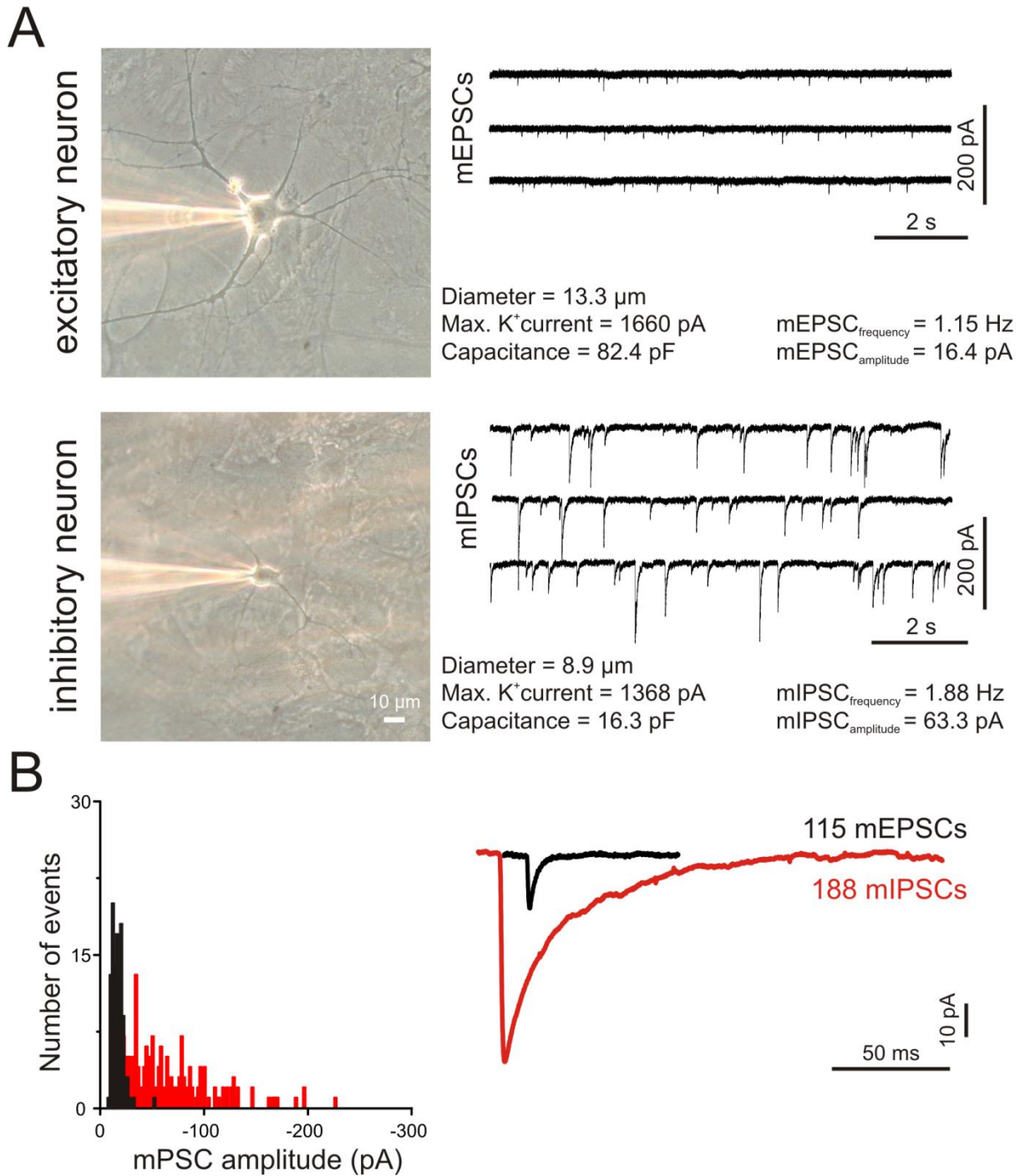
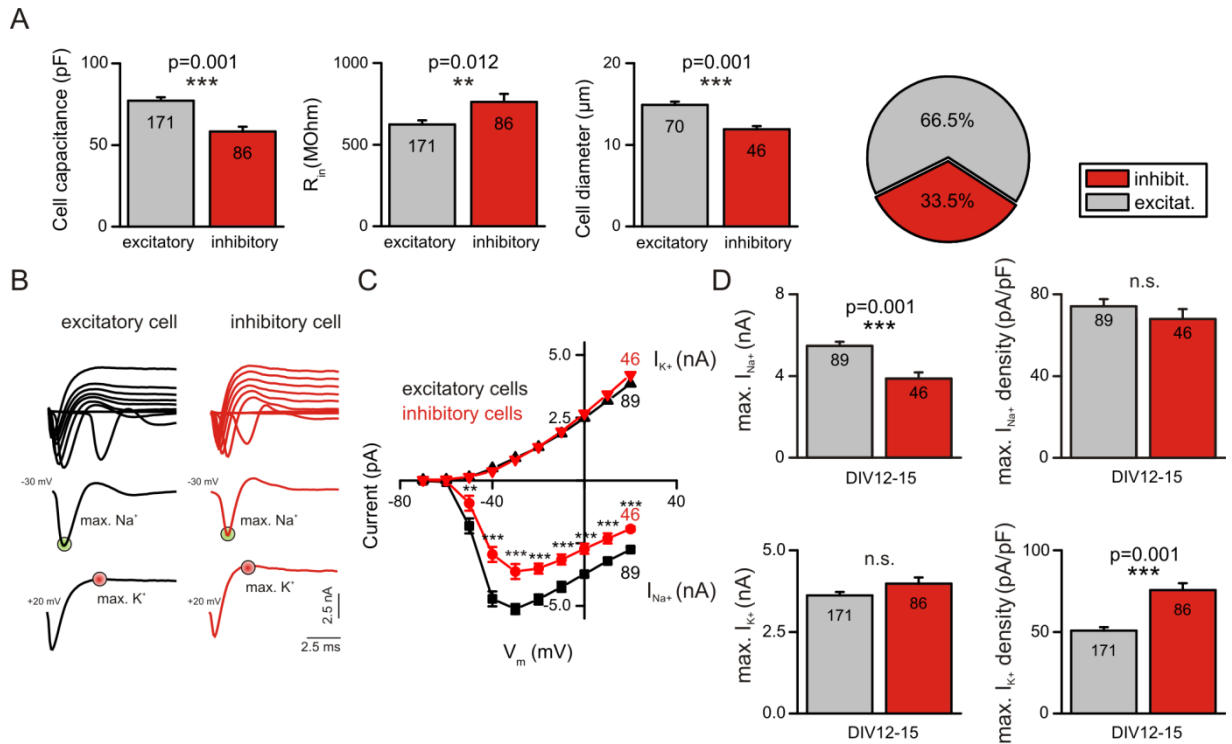


Figure 19: Comparison of excitatory and inhibitory neurons at DIV12-15. Excitatory neurons showed many differences compared to inhibitory cells. Note that excitatory neurons are larger than inhibitory neurons as seen in the phase contrast images (A, left) and seen by their respective cell capacitance. Synaptic events of excitatory cells were smaller in amplitude and decay time as can be seen in respective voltage clamp traces of the two neurons (A, right) and their averaged mEPSCs and mIPSCs traces (B, right). Histograms show that mEPSCs have a narrow amplitude maximum whereas mIPSCs are more variable in their amplitudes (B, left). mEPSCs and mIPSCs were recorded at a holding potential of -70 mV in the presence of TTX. Note the patch pipette visible in (A) coming from the left side.

A different distribution of  $\text{K}^+$  channels in inhibitory compared to excitatory cells may also be a valid explanation. It seemed as if more  $\text{K}^+$  channels/membrane area were present in the membrane of these neurons. In conclusion it is evident that inhibitory neurons differ greatly from excitatory cells in their passive and active membrane properties.



**Figure 20: Differences in passive and active membrane properties of single excitatory and inhibitory neurons at DIV12-15.** Excitatory cells exhibited a larger cell capacitance, smaller input resistance ( $R_{in}$ ) and cell diameter compared to inhibitory cells. Only 33.5% of the recorded cells were inhibitory neurons (A). Example traces of currents induced by a voltage clamp protocol to investigate Na<sup>+</sup> and K<sup>+</sup> currents showed smaller Na<sup>+</sup> current amplitudes in inhibitory cells (B). A corresponding IV-plot for the recorded Na<sup>+</sup> and K<sup>+</sup> currents showed the current-voltage relationship of the respective ionic currents. Notice the smaller Na<sup>+</sup> current in inhibitory neurons (C). The maximal Na<sup>+</sup> current amplitude in inhibitory cells was significantly smaller in comparison to excitatory cells whereas the K<sup>+</sup> current density was significantly higher in inhibitory neurons (D). p-values determined by Mann-Whitney rank sum test. Numbers in columns in A and D represent individual cells analyzed. Bar plots represent mean values + SEM.

### 3.1.3 Agrin increases the frequency of excitatory miniature postsynaptic currents in single cortical neurons.

As a first step agrin's effect on synaptic transmission in wild type cortical microisland cultures at DIV12-15 was investigated. Voltage clamp recordings were done three to five hours after incubation with 1  $\mu$ g/ml full-length neuronal chicken agrin with splice inserts containing 4 amino acids at the A/ $\gamma$  and eight amino acid inserts at the B/z site which led to a strong increase in the frequency of mEPSCs but not of mIPSCs (mEPSCs frequency  $1.21 \pm 0.22$  for control cells vs.  $2.70 \pm 0.40$  Hz for agrin-treated cells; Figure 21A). By using specific blockers against AMPA/ kainate (DNQX) and NMDA (APV) receptors combined with TTX to block action potential-induced postsynaptic events, glutamatergic mEPSCs could be abolished (Figure 21B, left) showing that events with short decay kinetics were really mediated by excitatory neurotransmitter release. The same was done for mPSCs with long decay kinetics using the GABA<sub>A</sub> receptor blocker bicuculline indicating that these events were indeed mIPSCs (Figure 21B, right). Agrin incubation not only affected the mEPSC

frequency but also their amplitude which increased from  $19.93 \text{ pA} \pm 1.0$  to  $23.95 \pm 1.2 \text{ pA}$  in agrin-treated neurons ( $p=0.011$ ; Figure 21C). Decay time constants of mEPSCs and mIPSCs were not influenced by agrin (mEPSCs:  $4.38 \pm 0.1$  vs.  $4.22 \pm 0.2 \text{ ms}$ ,  $p=0.389$ ; mIPSCs:  $25.53 \pm 1.1$  vs.  $23.35 \pm 1.3 \text{ ms}$ ;  $p=0.206$ ) as were their rise times (mEPSCs:  $0.695 \pm 0.027$  vs.  $0.689 \pm 0.018 \text{ ms}$ ,  $p=0.908$ ; mIPSCs:  $0.997 \pm 0.057$  vs.  $1.013 \pm 0.066 \text{ ms}$ ,  $p=0.852$ ). The quantal size of the mEPSCs and mIPSCs was also not changed by agrin-treatment (mEPSCs:  $18.25 \pm 1.10$  vs.  $19.83 \pm 0.91 \text{ pA}$ ,  $p=0.273$ ; mIPSCs:  $31.23 \pm 1.77$  vs.  $32.63 \pm 2.13 \text{ pA}$ ,  $p=0.616$ ; Figure 21C). Two most likely causes could attribute for the change in mEPSC frequency: a) changes of the presynaptic release machinery leading to more frequent spontaneous vesicle fusions or b) an increase in the number of excitatory synapses.

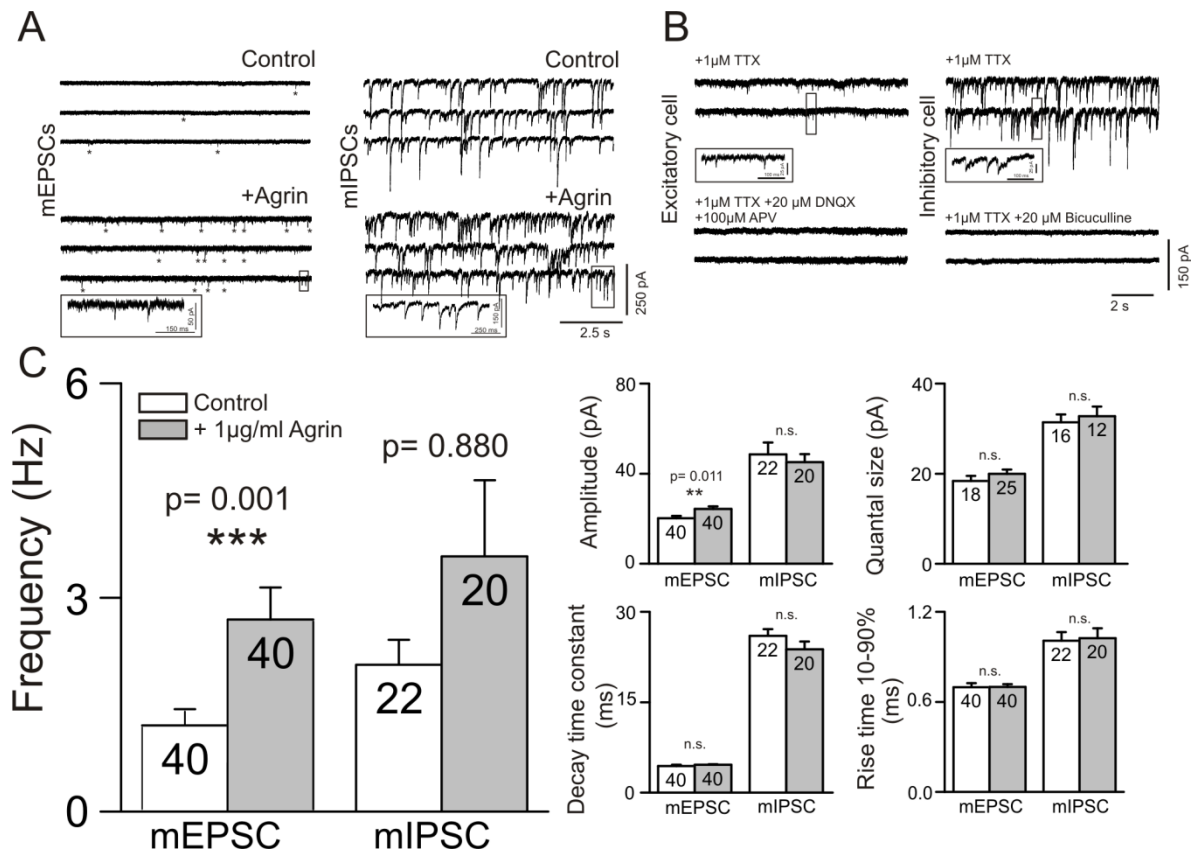


Figure 21: Agrin induces an increase in the frequency of mEPSCs. After agrin treatment excitatory neurons showed a strong increase in mEPSC frequency (A and C). Validation of excitatory and inhibitory postsynaptic currents was done by application of blockers. DNQX and APV blocked AMPA/kainate and NMDAR-mediated events with short decay times, bicuculline blocked GABA<sub>A</sub>R-mediated events with slow decay kinetics (B). mEPSC frequency as well as their amplitude was significantly altered by agrin treatment. Decay time constant, quantal size and rise time were not affected (C). p-values determined by Mann-Whitney rank sum test or t-test (for the rise time). Numbers in columns in C correspond to the number of analyzed cells. Bar plots represent mean values + SEM. mEPSCs and mIPSCs were recorded at a holding potential of  $-70 \text{ mV}$  in the presence of TTX.

### 3.1.4 Agrin induces excitatory synapses in microisland cultures

To test the possibility that agrin causes the effect on the frequency of mEPSC by the induction of new excitatory synapses immunocytochemistry was used. Antibodies against

the presynaptic proteins VGlut1+2 and antibodies against the postsynaptic scaffolding protein PSD95 were chosen to do co-localization studies in single neurons. After three to five hours of incubation with 1  $\mu\text{g}/\text{ml}$  neuronal agrin neurons were fixated and subjected to immunocytochemistry. The co-localized puncta were counted and a strong difference in the number of spots between control and agrin-treated cells was encountered (Figure 22A and B). Co-localized spots were more frequent in agrin-treated cells compared to control neurons ( $66.72 \pm 8.43$  spots for control neurons vs  $98.65 \pm 7.34$  spots for agrin-treated neurons). This effect was highly significant ( $p=0.001$ ; Figure 22C).

These findings are a strong evidence for the hypothesis that agrin induces the increase in mEPSC frequency by increasing the number of excitatory synapses.

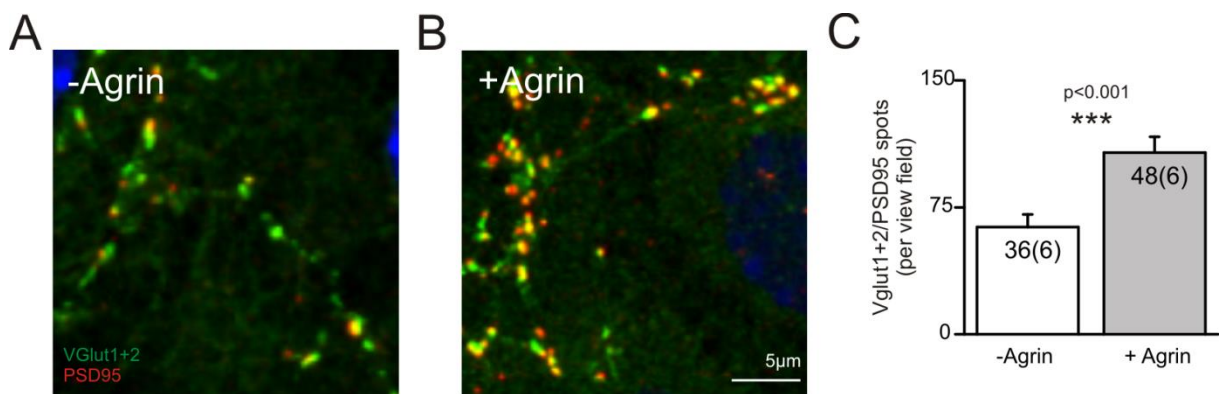


Figure 22: Excitatory synapses are induced by agrin stimulation. Excitatory synapses in single neurons at DIV12-15 were stained with antibodies against VGlut1+2 as a presynaptic marker and PSD95 as a postsynaptic marker. Agrin treated cells showed more co-localized spots of VGlut1+2 and PSD95 per view field than untreated control neurons appearing as yellow dots (A and B). 36 and 48 cells were analyzed in six independent experiments yielding a significant difference in the abundance of putative excitatory synapses in agrin-treated neurons compared to untreated cells (C). The p-value was determined by using a Mann-Whitney rank sum test. Numbers in columns in C represent investigated individual images (36 and 48) and how many different preparations were analyzed (6 and 6). Bar plots represent mean values + SEM.

### 3.1.5 Agrin treatment induces an increase in the number and size of synaptic AMPAR spots

Since AMPAR are highly mobile glutamate receptors it was important to test if the increase in mEPSC frequency and amplitude might be caused by recruitment of AMPARs to the synapse. Antibodies that recognize all postsynaptic AMPAR-specific GluR subunits (GluR1-4) and antibodies against VGlut1+2 as a presynaptic marker were applied. Control cells showed less co-localized AMPAR clusters on their dendrites than agrin-treated cells ( $0.054 \pm 0.006$  vs.  $0.109 \pm 0.007$  cluster/ $\mu\text{m}$ ;  $p<0.001$ ; Figure 23A, B and C). The area occupied by these AMPAR clusters was also increased in agrin-treated cells compared to untreated controls ( $0.372 \pm$

0.046 vs.  $0.598 \pm 0.031 \mu\text{m}^2$ ;  $p < 0.001$ ; Figure 23D, E and F) while the density of AMPAR on extrasynaptic parts of dendrites was not influenced (data not shown).

These data show that the mEPSCs frequency increase (Figure 21C) is caused by an increased number of excitatory synapses and the recruitment of AMPARs to these synapses. The increased area of AMPAR clusters could also be the cause for the increase in mEPSC amplitude seen in agrin-treated neurons (Figure 21C).

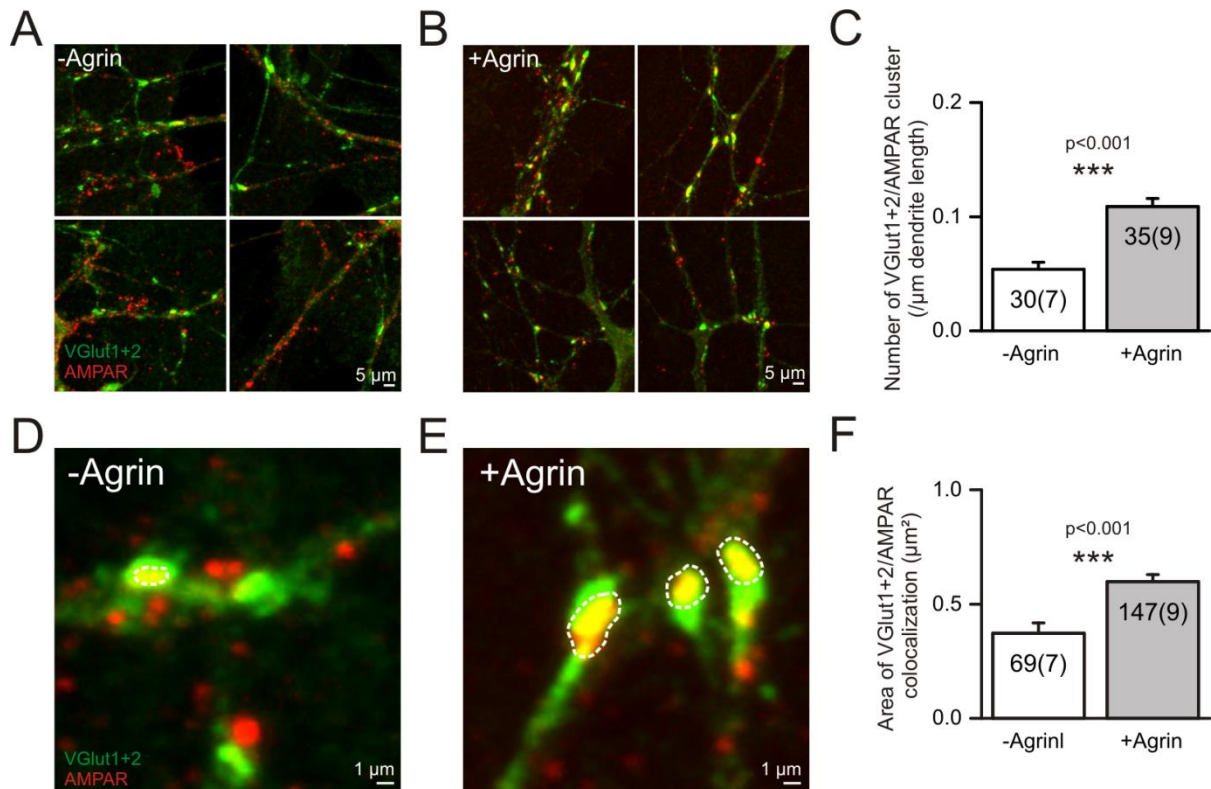


**Figure 23:** AMPAR are recruited to synapses after agrin treatment. Control neurons showed less co-localized AMPAR/VGlut1+2 spots than agrin-treated neurons (A, B and C). The area of co-localized AMPAR and VGlut1+2 immunofluorescence was significantly enlarged in agrin-treated neurons compared to controls (D, E and F). Data were collected from 7 to 9 different cells and 30-35 dendrites were measured as well as 69-147 AMPAR cluster were analyzed. Statistical analysis was done using a Mann-Whitney rank sum test. Numbers in C and F represent investigated individual images and how many different preparations were analyzed (number in parentheses). Bar plots represent mean values + SEM.

### 3.1.6 Autaptic neurotransmitter release in single neurons seems unaffected by agrin application

Autapses were only rarely seen in monolayer cultures (see chapter 3.2.5) but were always present in single neurons grown on microislands at 12-15 DIV. Autapses are a reliable tool to investigate presynaptic release of neurotransmitter because neurons in this case only receive single axonic inputs. After incubation with 1 μg/ml neuronal agrin for three to five hours the cells were subjected to different stimulus protocols (see Figure 12A-C). By giving two pulses at an interstimulus interval of 100 ms and comparing the amplitudes of the

current responses the paired-pulse ratio (PPR) could be determined. Is the first amplitude larger than the second the release probability is high and the PPR small, leading to a paired-pulse depression. All investigated excitatory cells showed paired-pulse depression but no changes in their paired-pulse ratio after agrin incubation ( $68.8 \pm 3.6\%$  for control vs.  $67.8 \pm 2.0\%$  for agrin-treated cells,  $p=0.625$ ). The amplitudes of the first evoked current response were significantly increased in agrin-treated neurons compared to untreated cells ( $833.8 \pm 75.0$  vs.  $636.79 \pm 104.8$  pA;  $p=0.009$ ; Figure 24C). Additionally the quantal content was also larger in agrin-incubated neurons ( $42 \pm 4$  vs.  $35 \pm 6$  vesicles;  $p=0.029$ ) compared to untreated controls (Figure 24F). The decay kinetics ( $4.82 \pm 0.2$  vs.  $5.00 \pm 0.2$  ms;  $p=0.651$ ) of the first current response were also not affected by agrin incubation (data not shown).

When the cells were stimulated at high frequency the release of neurotransmitter did not show any kind of difference between the agrin-incubated cells or the untreated control cells (Figure 24D and E). The normalized amplitudes of the EPSCs were the same in both conditions (Figure 24E). In a final conclusion it seems as if agrin treatment had no effect on the presynaptic release properties, namely the paired-pulse ratio, of excitatory neurotransmitters.

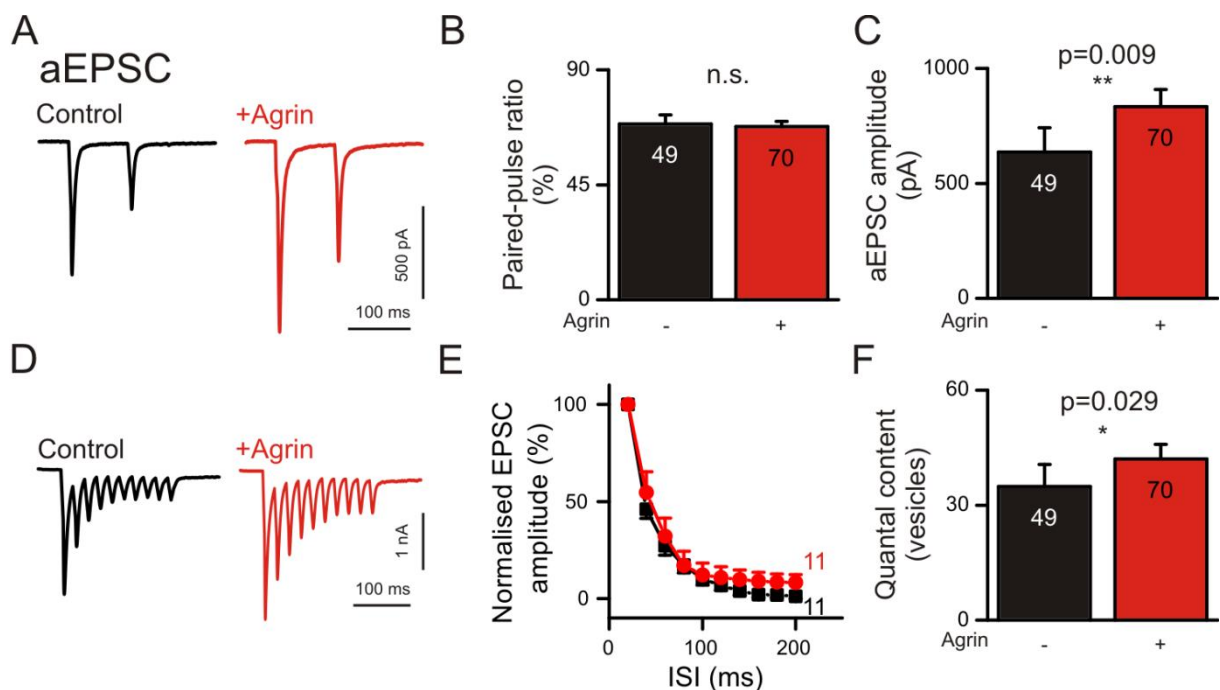
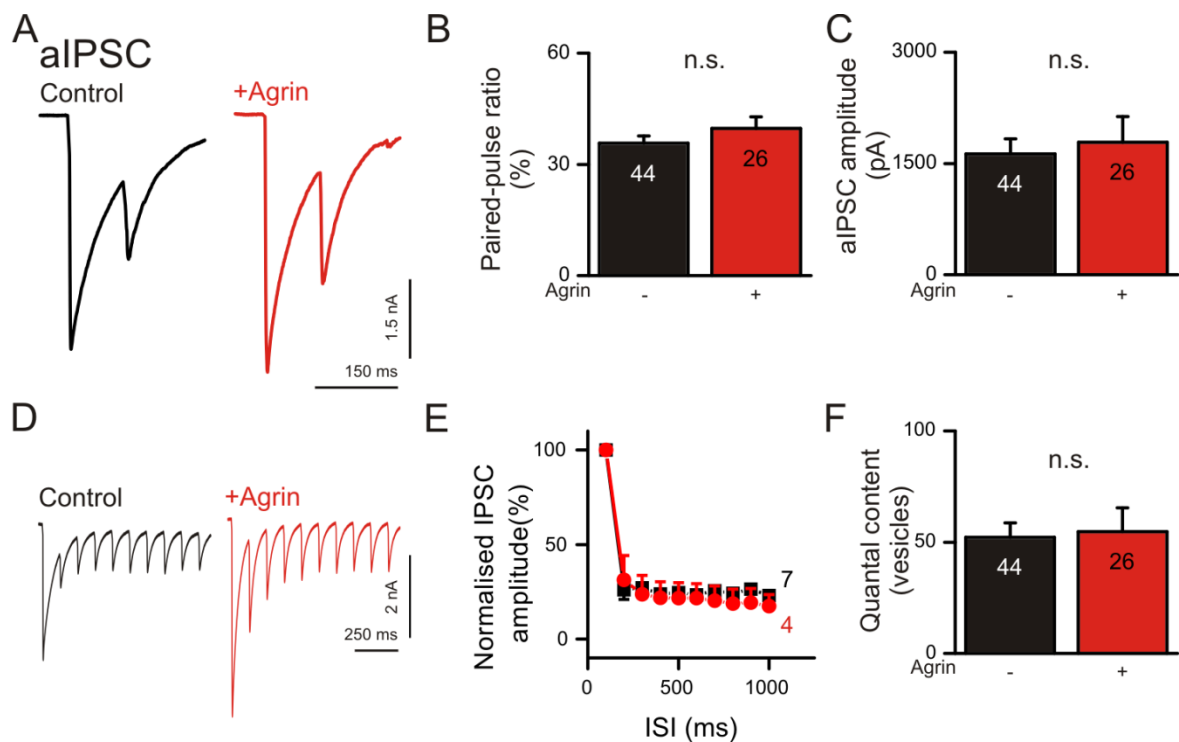


Figure 24: The paired-pulse ratio of autaptic EPSCs of single excitatory neurons at DIV12-15 is not influenced by agrin incubation. Evoked EPSCs of control and agrin-treated cells showed paired-pulse depression (A) but were not different from each other in regards to paired-pulse ratio (B) even though the amplitudes (C) and quantal content (F) were significantly changed by agrin incubation ( $1 \mu\text{g/ml}$ ) for three to five hours. High frequency stimulation also did not show differences in neurotransmitter release in treated and untreated cells (D and E). Statistical analysis was done using a Mann-Whitney rank sum tests. Numbers in columns in B, C and F represent individual cells measured. Bar plots represent mean values + SEM. aEPSCs were recorded at a holding potential of  $-70$  mV. Stimulation artifacts have been removed.

The same stimulus regime was used to investigate autaptic IPSCs. Paired-pulse recordings at an interstimulus-interval of 100 ms revealed no difference between IPSCs of agrin-treated cells and control cells (Figure 25A-F). In contrast to aEPSCs, aIPSCs showed no change in amplitude ( $1630.0 \pm 204.0$  vs.  $1785.0 \pm 349.3$  pA;  $p=0.329$ ), decay time kinetics ( $52.4 \pm 3.5$  vs.  $44.8 \pm 5.5$  ms;  $p=0.228$ ) and quantal content ( $36 \pm 2$  vs.  $40 \pm 3$  vesicles;  $p=0.813$ ; Figure 25B, C and F). The same holds true for high frequency stimulations. Normalized IPSC amplitudes of control and agrin-treated cells were almost identical (Figure 25E). These results suggest that agrin does not have an effect on the release of inhibitory neurotransmitter.



**Figure 25: Autaptic IPSCs of inhibitory neurons at DIV12-15 are not affected by agrin incubation.** Agrin treated cells showed no difference in paired-pulse ratio (A and B) compared with untreated control cells. All cells showed a prominent paired-pulse depression (A) but no changes in the amplitude (C) of the first current response or the quantal content (F). High frequency stimulation did not reveal differences in neurotransmitter release between treated and untreated cells (D and E). Numbers in columns in B, C and F represent individual cells measured. Statistical analysis was done using a Mann-Whitney rank sum tests. Bar plots represent mean values + SEM. aIPSCs were recorded at a holding potential of -70 mV. Stimulation artifacts have been removed.

### 3.1.7 Passive and active cell properties of single neurons are not affected by agrin incubation

When cells were treated with 1  $\mu\text{g/ml}$  of neuronal chick agrin for three hours it was crucial to determine whether agrin incubation had any effect on the passive and active membrane properties of the investigated single neurons or not. Investigating the input resistance as a means to determine changes in the membrane's conductance and measuring the cell's capacitance was performed in voltage clamp mode. The input resistance was not

significantly changed ( $718.2 \pm 40.1$  vs.  $614.0 \pm 23.1$  M $\Omega$ ;  $p=0.164$ ) but the cell capacitance seemed to be mildly affected by the incubation with neuronal agrin being increased ( $67.5 \pm 2.5$  vs.  $74.0 \pm 2.4$  pF;  $p=0.042$ ) in treated cells (Figure 26A). Therefore the specific membrane resistance was also analyzed, giving a more robust insight into apparent changes of the passive membrane properties. No significant change could be detected for agrin-treated and untreated control cells ( $45.89 \pm 2.8$  vs.  $42.9 \pm 1.7$  k $\Omega$ \*cm $^2$ ;  $p=0.932$ ). The active membrane properties were also investigated to test if agrin treatment could affect voltage-gated sodium and potassium currents. No difference in the current responses could be seen in their respective voltage clamp traces and IV-plot (Figure 26B and C). The maximal current amplitudes (Na $^+$  current:  $4.4 \pm 0.2$  vs.  $4.8 \pm 0.3$  nA;  $p=0.189$ ; K $^+$  current:  $3.8 \pm 0.1$  vs.  $4.1 \pm 0.2$  nA;  $p=0.353$ ) and the current densities (Na $^+$  current dens.:  $68.2 \pm 3.8$  vs.  $67.4 \pm 3.9$  pA/pF;  $p=0.708$ ; K $^+$  current dens.:  $61.4 \pm 3.3$  vs.  $61.4 \pm 5.4$  pA/pF;  $p=0.312$ ) for both Na $^+$  and K $^+$  currents were not affected by agrin treatment (Figure 26D).

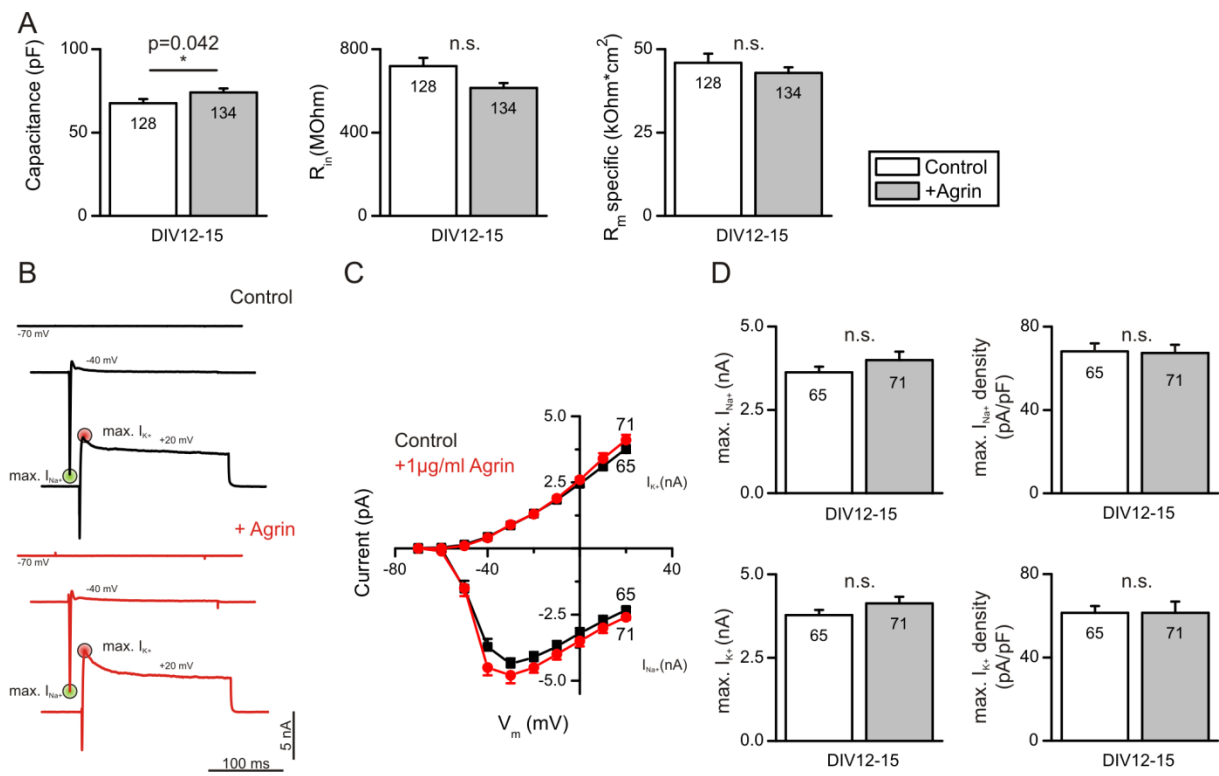


**Figure 26: Passive and active membrane properties of single neurons either untreated or incubated with neuronal agrin.** Cell capacitance was slightly increased after incubation with neuronal agrin but the input resistance as well as the specific input resistance were not affected (A). Sodium and potassium currents were also not affected by agrin treatment (B, C and D). No differences in the respective IV curves for both currents as well as in their maximal current amplitudes and current densities could be seen after agrin treatment (B-D). p-values determined by Mann-Whitney rank sum test. A test was used to test the maximal Na $^+$  current amplitudes. Numbers in columns in A, C and D represent individual cells measured. Bar plots represent mean values + SEM.

### 3.1.8 The agrin receptor LRP4 is expressed in cortical tissues and its expression is developmentally regulated

LRP4 has been recently discovered as the agrin receptor and plays crucial part in the formation of AChR clusters at the NMJ (Kim et al., 2008; Weatherbee et al., 2006; Zhang et al., 2008). First the expression of LRP4 in cortical tissues was assessed. To test a possible interaction with agrin in the central nervous system single LRP4-deficient neurons either untreated or treated with 1  $\mu\text{g}/\text{ml}$  agrin for three to five hours were subjected to electrophysiological analysis (see the following chapter 3.1.9).

LRP4 mutant mice showed some similarities to agrin and MuSK mutant mice. New born mice were cyanotic, did not move or breathe (Figure 27A) whereas their heterozygous and wild type littermates were normal in skin color and highly mobile (Figure 27B). Mutant mice also show disturbances in the morphology of their fore and hind limbs displaying a severe syndactyly compared to their wild type littermates which is specific for LRP4 mutants (Figure 27C and D).

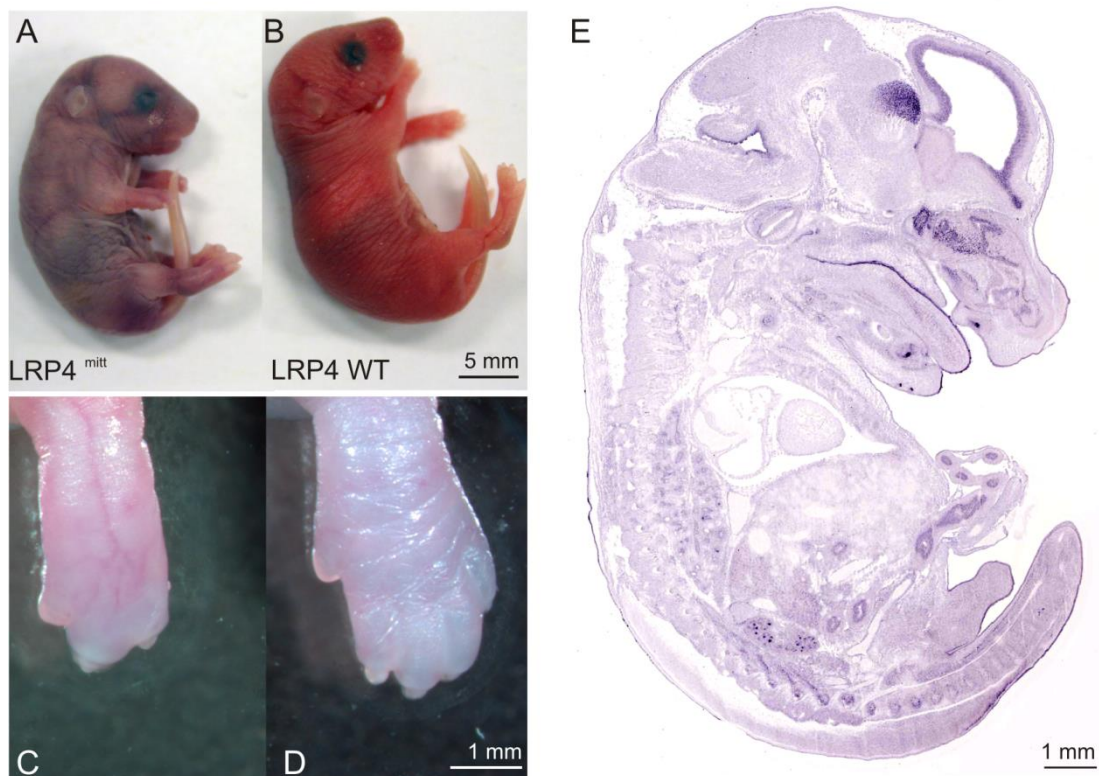
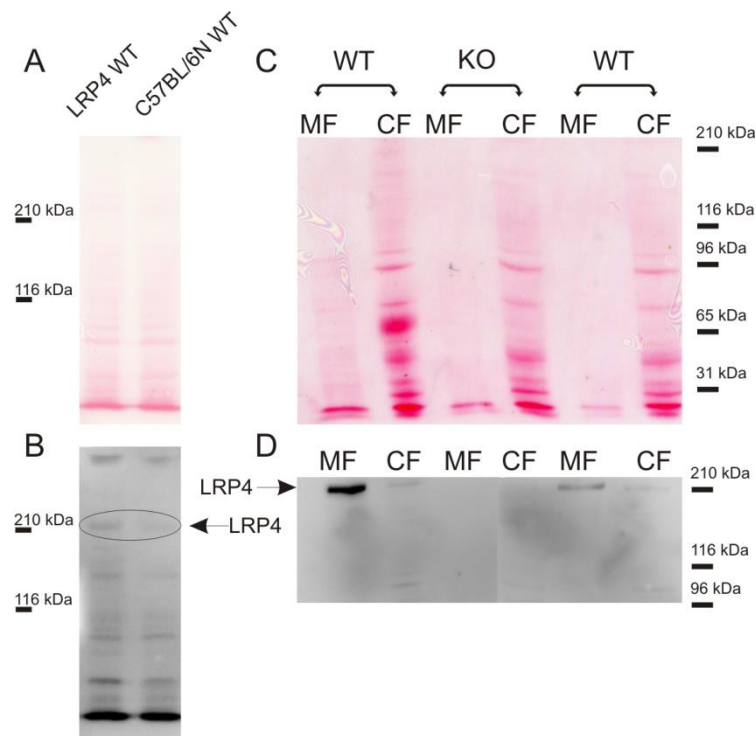


Figure 27: Comparison of LRP4 mutant and WT P0 mice. After birth the LRP4 mutants were cyanotic, not moving and breathing (A), whereas their WT littermates were highly mobile and healthy (B). An enlarged picture of the forelimbs shows the distinct bone phenotype of LRP4 mutant mice (C) in comparison to WT littermates (D). Mice suffer from syndactyly of the hind- and forelimbs whereas WT littermates show a normal development of the fore- and hind limbs. An E14.5 embryo *in situ* hybridization done with probes to detect mRNA of LRP4 highlights its expression in the cortex, the epithelium of the nasal cavity and the thalamus (E). Image in E taken from [www.genepaint.org](http://www.genepaint.org)

Although it had been previously shown that LRP4 is indeed expressed in the central nervous system e.g. by *in situ* hybridization (Figure 27E), western blot analysis of E15 C57BL/6N and LRP4 WT cortices was performed using a commercial antibody by Santa Cruz biotechnologies (sc-98775). LRP4 was detected as a single band at around 210 kDa in molecular weight (Figure 28B). Since crude extracts of cortices yielded a weak band a membrane fractionation was performed. LRP4 was now strongly enriched in the membrane fraction and almost completely absent in the cytosolic fraction (Figure 28D).

These data show that LRP4 is expressed not only at the neuromuscular junction but also at E15 in cortical tissues and is enriched in membrane fractions.



**Figure 28:** Western blot of LRP4 from E15 mouse cortices. LRP4 was expressed in E15 cortices of LRP4 WT embryos and C57BL/6N embryos of the same developmental stage. 5 µg of crude protein extracts for E15 cortices were loaded on a 6% SDS gel. Ponceau staining showed very weak bands above 116 kDa after blotting in the crude extracts (A). LRP4 appears as a weak band at just above 210 kDa after ECL development (B). Ponceau staining of WT and KO LRP4 E15 cortices after purification of the cytosolic (CF) and membrane fraction (MF). 2.5 µg MF proteins and 10 µg CF proteins were loaded on a 7% gel and the western blot membrane stained with ponceau (C). LRP4 was strongly enriched in the membrane fraction of WT but not KO tissue and absent from the cytosolic fraction as can be seen in the ECL-developed blot (D).

As a consequence of this experiment it was of importance to test whether LRP4 expression was developmentally regulated or not. Therefore cortices from animals of different ages were harvested and their membrane proteins fractionated. Western blotting and detection with the LRP4 antibody showed that LRP4 was indeed differentially expressed during development. High expression of LRP4 was seen at E20 to P10 decreasing again at P20 and being the lowest in adult cortices (Figure 29A and B).

These results corroborate the hypothesis that LRP4 is indeed differentially regulated during phases of cortical development.

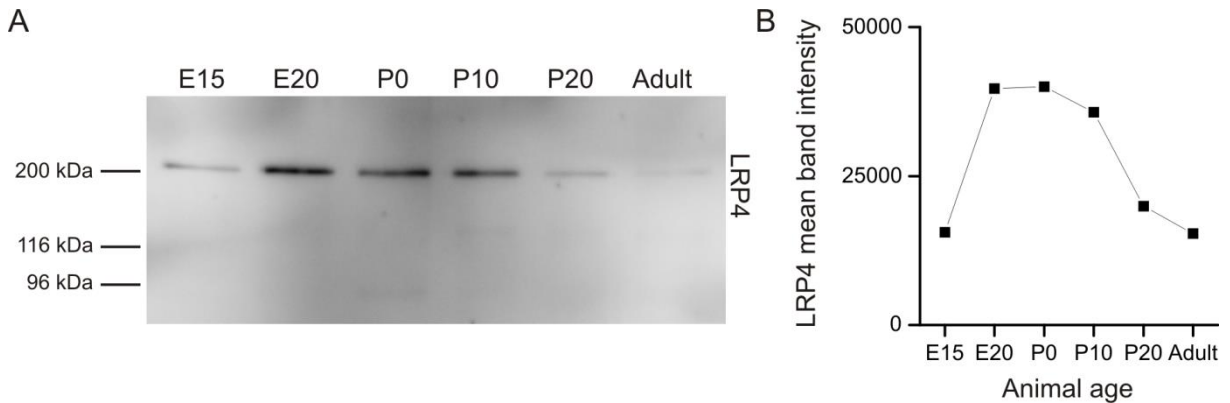


**Figure 29: Developmental regulation of LRP4 expression.** Cortical tissues from animals of different ages were harvested and their cytosolic and membrane proteins purified. Since LRP4 was only found in membrane fractions 1 µg/lane membrane protein was loaded on a 7.5 % SDS-gel and a western blot with LRP4 antibodies was done. LRP4 was strongly expressed in cortical tissues expression being the highest between E20 and P10 and only weak in adult tissue hinting to a possible function during phases of synapse development (A and B).

### 3.1.9 Agrin does not influence the mEPSC frequency of single excitatory neurons of LRP4 mutant cultures

Agrin and LRP4 are key players of synaptic organization at the NMJ and also expressed in the cortex of E15 embryos. So it was tempting to see whether the agrin-induced effect on mEPSCs was reproducible in LRP4 mutant neuron cultures. Therefore cortical neurons from LRP4-deficient embryos were cultured on LRP4-deficient astrocytes for 12-15 days *in vitro*. LRP4 mutant neurons exhibited differences in their passive and active membrane properties compared to wild type neurons. The input resistance in these neurons was significantly smaller compared to wild type cells ( $712.6 \pm 35.2$  vs.  $558.7 \pm 60.8$  MΩ;  $p < 0.001$ ; Figure 30A), the cell capacitance was significantly increased ( $69.3 \pm 2.7$  vs.  $80.1 \pm 4.7$  pF;  $p = 0.005$ ; Figure 30B) as was the soma diameter ( $13.4 \pm 0.4$  vs.  $15.3 \pm 0.5$  µm;  $p < 0.001$ ; Figure 30C).

Analysis of the maximal voltage-gated potassium currents showed that LRP4-deficient neurons exhibited higher current amplitudes compared to wild type cells ( $3559.8 \pm 141.8$  vs.  $4024.9 \pm 243.9$  pA;  $p = 0.009$ ; Figure 30D). The respective current density was comparable to the current density of wild type cells ( $57.8 \pm 2.8$  vs.  $54.9 \pm 3.9$  pA/pF;  $p = 0.983$ ; Figure 30E).

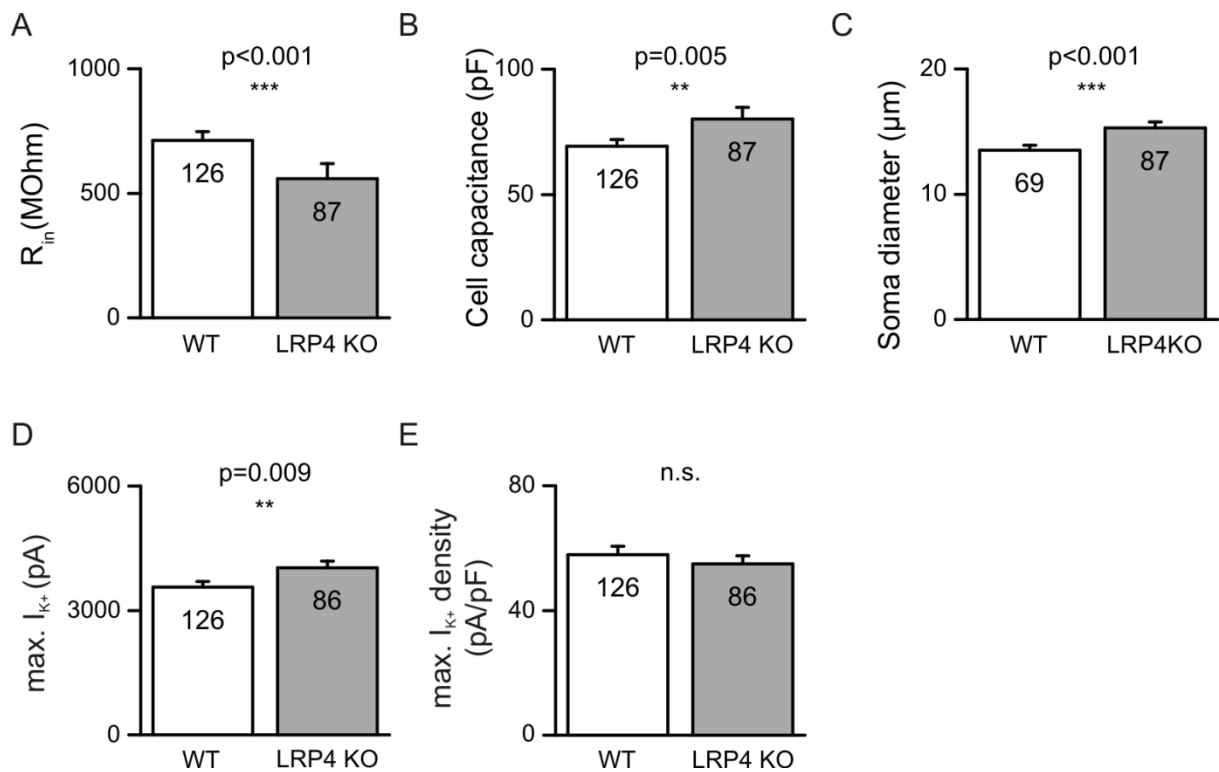


**Figure 30: Passive and active membrane properties of LRP mutant neurons.** LRP4 mutant neurons displayed a reduced input resistance compared to wild type C57BL/6N neurons (A). The cell capacitance in these neurons was significantly increased (B) as was their soma diameter (C). The maximal  $K^+$  current amplitude in LRP4 neurons was also significantly higher as in wild type neurons (D). This increase was not seen for the density of the  $K^+$  currents (E). Statistical analysis was done using Mann-Whitney rank sum tests. Numbers in columns in A to E represent individual cells investigated. Bar plots represent mean values + SEM. Note that WT refers to data collected from experiments with C57BL/6N wild type animals.

LRP4 mutant neurons were then analyzed for their synaptic transmission. In general LRP4 mutant cells were capable of forming functional excitatory (Figure 31A) and inhibitory synapses (data not shown). Since the agrin-induced effect was only seen in excitatory neurons those cells were the focus of the investigation. Comparison to untreated wild type neurons revealed that the frequency of mEPSCs was increased in untreated LRP4 mutant neurons ( $1.207 \pm 0.221$  vs.  $1.771 \pm 0.282$  Hz;  $p=0.047$ ; Figure 31B). Together with the differences in their passive and active properties these results are indicative of characteristics attributable to more “mature” neurons. After incubation with neuronal agrin LRP4-deficient neurons did not display a change in the frequency of mEPSCs ( $1.771 \pm 0.289$  vs.  $1.594 \pm 0.282$  Hz;  $p=0.356$ ; Figure 31C). The amplitude of these events did also not change due to agrin treatment ( $24.9 \pm 1.9$  vs  $21.8 \pm 1.0$  pA;  $p=0.109$ ; Figure 31D).

The absence of an agrin-mediated increase in the frequency and amplitude of mEPSCs from LRP4 mutant neurons indicates that LRP4 is important for the agrin-mediated effect seen in wild type neurons.

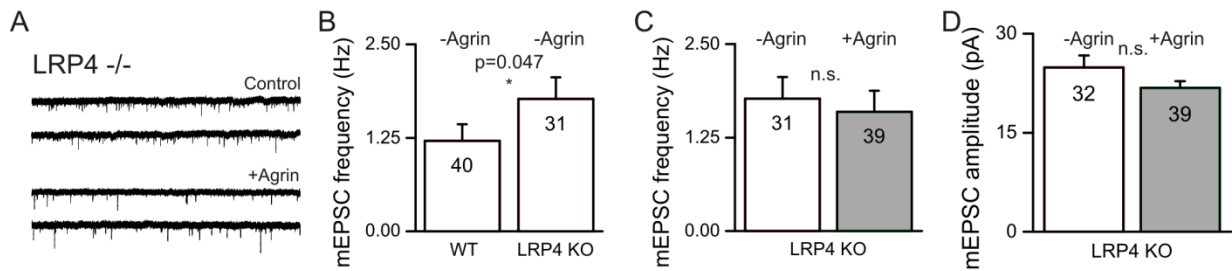


**Figure 31: Analysis of the synaptic properties of LRP4-deficient neurons.** Voltage clamp traces at  $-70$  mV holding potential show that LRP4-deficient neurons form functional synapses as can be seen by the recorded mEPSCs (A). The overall frequency of mEPSCs was higher compared to wild type neurons (B). Incubation with neuronal agrin did not increase the frequency of these events (C). The amplitudes of these events stayed on a similar niveau after adding agrin (D). Statistical significance was tested using Mann-Whitney rank sum tests. Numbers in columns in B to D represent individual cells investigated. Bar plots represent mean values + SEM. mEPSCs were recorded in presence of TTX. Note that WT refers to data collected from experiments with C57BL/6N wild type animals.

### 3.1.10 Agrin does not influence mEPSC frequency of single agrin-deficient excitatory neurons

Agrin's role on the synapse formation or maintenance was also investigated by analyzing agrin-deficient neurons grown on microislands of agrin-deficient astrocytes with electrophysiological means. Neurons cultured for a period of 12-15 days were recorded in whole cell patch clamp configuration and their passive as well as active membrane properties compared to the ones of wild type cells.

The agrin-deficient neurons showed no altered passive membrane properties compared to wild type cells. The input resistance was slightly higher as in the wild type ( $712.6 \pm 35.2$  vs.  $766.2 \pm 107.6$  M $\Omega$ ;  $p=0.690$ ; Figure 32A) but cell capacitance ( $69.3 \pm 2.7$  vs.  $71.7 \pm 5.2$  pF;  $p=0.596$ ; Figure 32B) and soma diameter ( $13.5 \pm 0.4$  vs.  $14.1 \pm 0.6$   $\mu$ m;  $p=0.261$ ; Figure 32C) were similar. Voltage-gated  $K^+$  currents ( $3559.9 \pm 141.8$  vs.  $2842.0 \pm 194.8$  pA;  $p=0.013$ ; Figure 32D) and their respective densities ( $43.8 \pm 3.4$  vs.  $57.8 \pm 2.8$  pA/pF;  $p=0.013$ ; Figure 32E) were significantly different between the two populations.

In conclusion agrin-deficient neurons are indistinguishable from their wild type counterparts in regards to their passive membrane properties but show significant differences in their  $K^+$  current properties compared to wild type neurons of the same developmental stage.

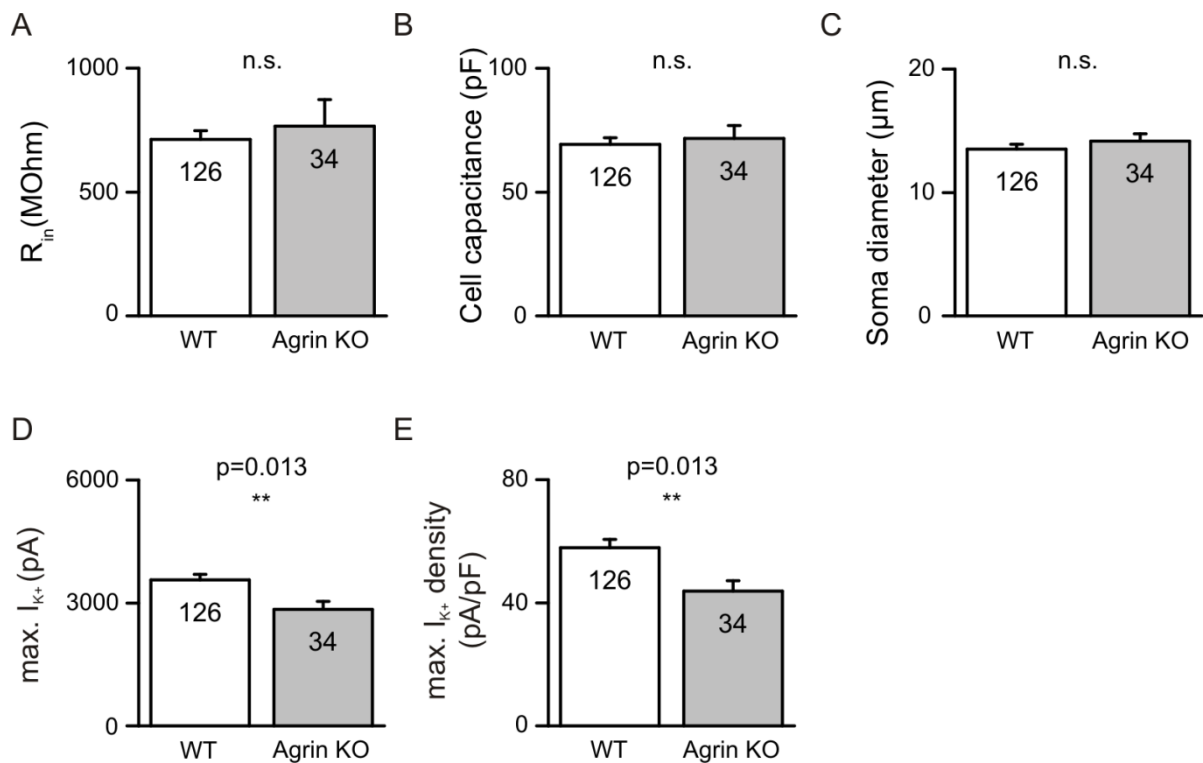


**Figure 32: Comparison of the passive and active membrane properties of C57BL/6N wild type and agrin-deficient neurons.** Input resistance (A), cell capacitance (B) and soma diameter (C) did not differ from their wild type counterparts in agrin-deficient cells. The maximal potassium current amplitude (D) and the respective current density (E) was significantly decreased in agrin-deficient neurons compared to wild type cells. Statistical significance was tested using Mann-Whitney rank sum tests. Numbers in columns in A to E represent individual cells investigated. Bar plots represent mean values + SEM. Note that WT refers to data collected from experiments with C57BL/6N wild type animals.

As has been shown in previous experiments (Li et al., 1999; Serpinskaya et al., 1999), agrin-deficient neurons were able to form functional synapses. Single neurons displayed mEPSCs (Figure 33A) or mIPSCs (data not shown) in the presence of TTX when recorded in whole cell patch clamp configuration. Only data for excitatory cells is discussed here because too few of the recorded cells were showing mIPSCs and the agrin-mediated effect was only seen for excitatory cells.

The mEPSC frequency of agrin-deficient neurons was slightly lower as in wild type cells ( $1.207 \pm 0.221$  vs.  $0.715 \pm 0.164$  Hz;  $p=0.648$ ) but not significantly changed (Figure 33B). After incubation with 1  $\mu$ g/ml neuronal agrin for three to five hours the frequency ( $0.715 \pm 0.164$  vs.  $1.085 \pm 0.401$  Hz;  $p=0.765$ ) of mEPSCs and their amplitude ( $22.6 \pm 1.6$  vs.  $22.4 \pm 1.6$  pA;  $p=0.932$ ) was not altered in agrin-deficient neurons (Figure 33A, C and D). Since agrin-deficient neurons did not show an increase in their mEPSC frequency or amplitude these data indicate that endogenous agrin is essential for the agrin-mediated effect on the excitatory synapses measured in wild type cultures.

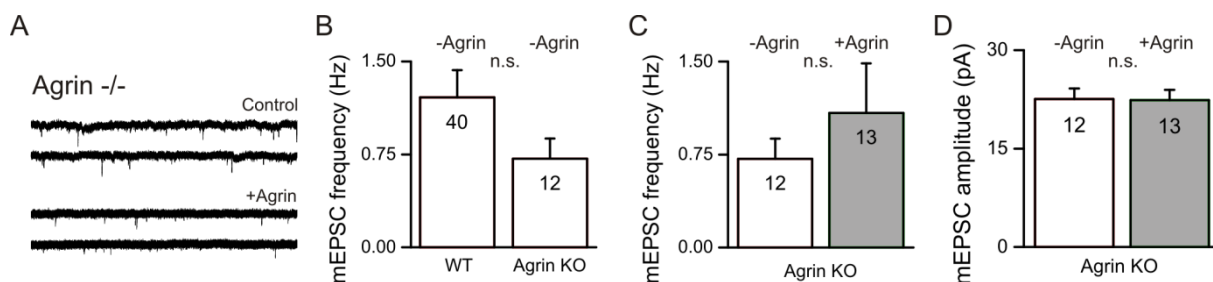


Figure 33: Analysis of the synaptic properties of agrin-deficient neurons. Voltage clamp traces at  $-70$  mV holding potential show that agrin-deficient neurons form functional synapses (A). The overall frequency of mEPSCs was lower compared to wild type neurons (B). Incubation with neuronal agrin did increase the frequency of these events but not to a significant level (C). The amplitudes of these events stayed on the same niveau after adding agrin (D). Significance tested by Mann-Whitney rank sum test and t-test (for D). Numbers in columns in B-D represent individual cells investigated. Bar plots represent mean values + SEM. mEPSCs were recorded at a holding potential of  $-70$  mV in the presence of TTX . Note that WT refers to data collected from experiments with C57BL/6N wild type animals.

### 3.1.11 Recombinant agrin does not interact with recombinant agrin in an ELISA-based binding assay.

As agrin-deficient neurons did not respond to extracellular application of neuronal agrin it was tempting to speculate that the agrin-mediated effect depended on the binding of soluble agrin to endogenously present agrin. To test this, an ELISA was used to detect a possible agrin-agrin interaction. One batch of agrin was therefore biotinylated with a sulfo-NHS-LC-biotin crosslinker and a different batch left unbiotinylated. Biotinylation was validated by western blot analysis using streptavidin coupled to horseradish peroxidase. Agrin-biotin conjugates were easily detected with streptavidin-HRP but not unconjugated agrin (Figure 34A). In a second western blot experiment Rb46, an antibody raised against agrin, was used which recognized biotinylated and unbiotinylated agrin (Figure 34B). To test the ELISA agrin-biotin was adsorbed to wells of ELISA-plates and incubated with streptavidin-HRP. Different dilutions of agrin-biotin and streptavidin-HRP were used to determine an effective range of concentrations. After measuring the absorbance of the ELISA reaction a high intensity at  $0.25$  and  $0.5$   $\mu\text{g/ml}$  streptavidin-HRP was detected (Figure 34C). A similar experiment was performed with unconjugated agrin and Rb46 recognizing the C-terminal part of chick agrin. In this experimental set up bound Rb46 antibodies were detected by goat-anti-rabbit HRP-coupled antibodies. At a dilution of  $1:4000$  to  $1:500$  of Rb46 the absorbance was very high with agrin concentrations ranging from  $0.125$  to  $0.5$   $\mu\text{g/ml}$  (Figure 34D). When unconjugated agrin was immobilized on the ELISA plates and incubated with agrin-biotin no binding between agrin and agrin was detected (Figure 34E). Wells coated with  $1\%$  BSA had a higher absorbance than agrin-coated ones indicating that agrin does not bind to agrin in this ELISA.

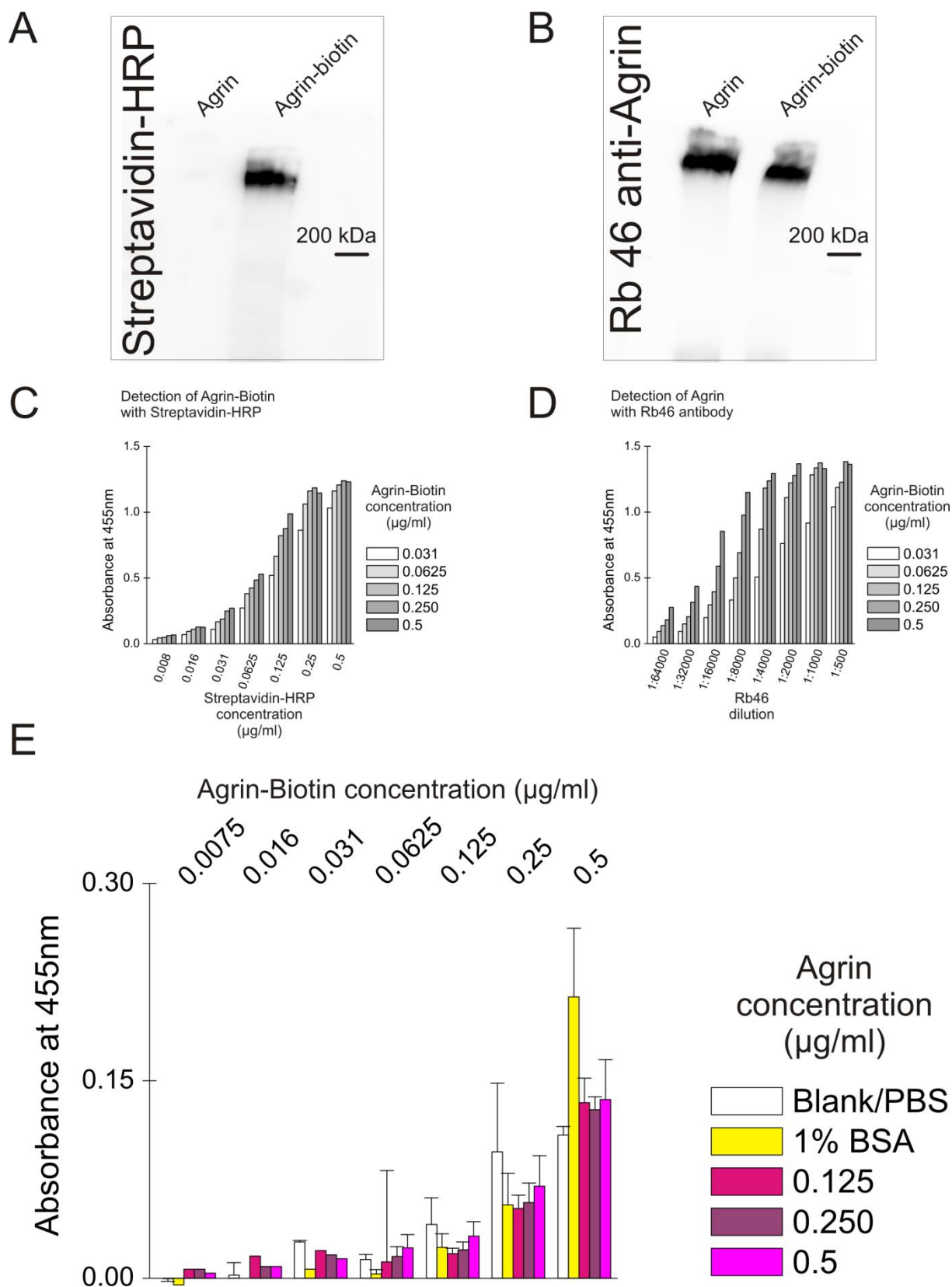


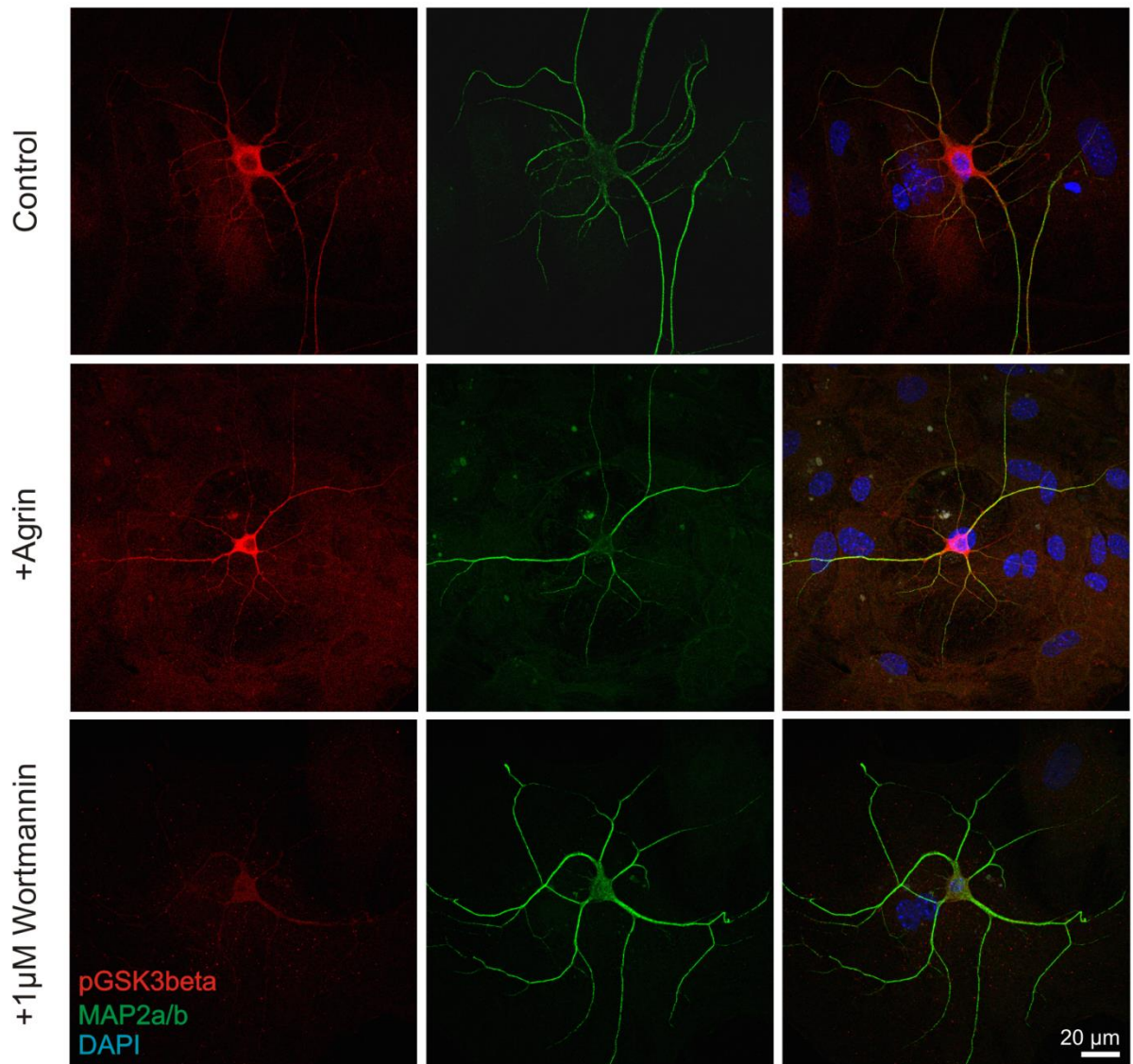
Figure 34: Agrin does not bind to agrin in ELISA tests. Agrin was biotinylated by chemical crosslinking and validity of the reaction tested with western blots. Only biotinylated agrin was detected by HRP-coupled streptavidin but both agrin or agrin-biotin conjugate was detected by Rb46 anti-agrin antibodies (A and B). Detection of agrin-biotin with streptavidin-HRP was tested with ELISA (C) as well as agrin detection with Rb46 antibodies, respectively (D). Different concentrations were tested but no strong agrin-agrin interaction could be shown in ELISA agrin-agrin binding studies; n=1 to 4 (E). Bar plots represent mean values + SEM.

### 3.1.12 PI3K activation is involved in agrin-mediated signaling

Since agrin induced a robust increase in PI3K downstream target phosphorylation in cultured myotubes (Schmidt et al., 2012) this was also tested in microisland cultures of cortical neurons to find a possible agrin-induced pathway that could account for the changes seen in excitatory cells after stimulation with neuronal agrin. Western blots are not sensitive enough to study individual neurons so immunocytochemistry was chosen as a tool to monitor changes in PI3K downstream target phosphorylation. Antibodies against pGSK3 $\beta$  were applied to cells that had been incubated with neuronal agrin three to five hours prior fixation to read out PI3K activity as well as antibodies against MAP2a/b to mark neuronal dendrites. The fluorescence of the soma was measured and set to 100% for untreated control neurons. These cells showed a basal amount of pGSK3 $\beta$ . In neurons incubated with agrin the fluorescence of pGSK3 $\beta$  increased significantly ( $64.3 \pm 4.8$  vs.  $86.1 \pm 5.5$  MFI;  $p=0.015$ ; Figure 35A and B). By incubating cells with the PI3K blocker wortmannin the mean fluorescence intensity (MFI) of pGSK3 $\beta$  could be significantly lowered below the level of control neurons ( $64.3 \pm 4.8$  vs.  $45.5 \pm 3.9$  MFI;  $p=0.005$ ; Figure 35A and B). Three different preparations were analyzed and a total of 37-64 cells were evaluated. This shows that agrin indeed activated PI3K in neurons.

As a next step towards analyzing agrin-mediated PI3K activation electrophysiological experiments on single neurons incubated with PI3K blockers together with neuronal agrin were conducted (Figure 36). Cells were treated with PI3K blockers wortmannin and LY294002 alone as controls and together with neuronal agrin for three to five hours. 1  $\mu$ M wortmannin as well as 50  $\mu$ M LY294002 did not abolish mEPSCs under control conditions, but the agrin-specific effect on the mEPSC frequency was completely blocked ( $1.391 \pm 0.377$  vs.  $1.402 \pm 0.325$  Hz;  $p=0.893$ ; Figure 36C). Wortmannin-treated cells showed a similar frequency of mEPSCs as untreated control cells ( $1.391 \pm 0.377$  vs.  $1.21 \pm 0.221$  Hz;  $p=0.803$ ). Treatment with LY294002 lowered the mEPSC frequency and also prevented the agrin effect (frequency of LY294002-treated cells  $0.801 \pm 0.356$  vs.  $0.865 \pm 0.321$  Hz in agrin/LY294002-treated cells;  $p=0.574$ ; Figure 36C).

A



B

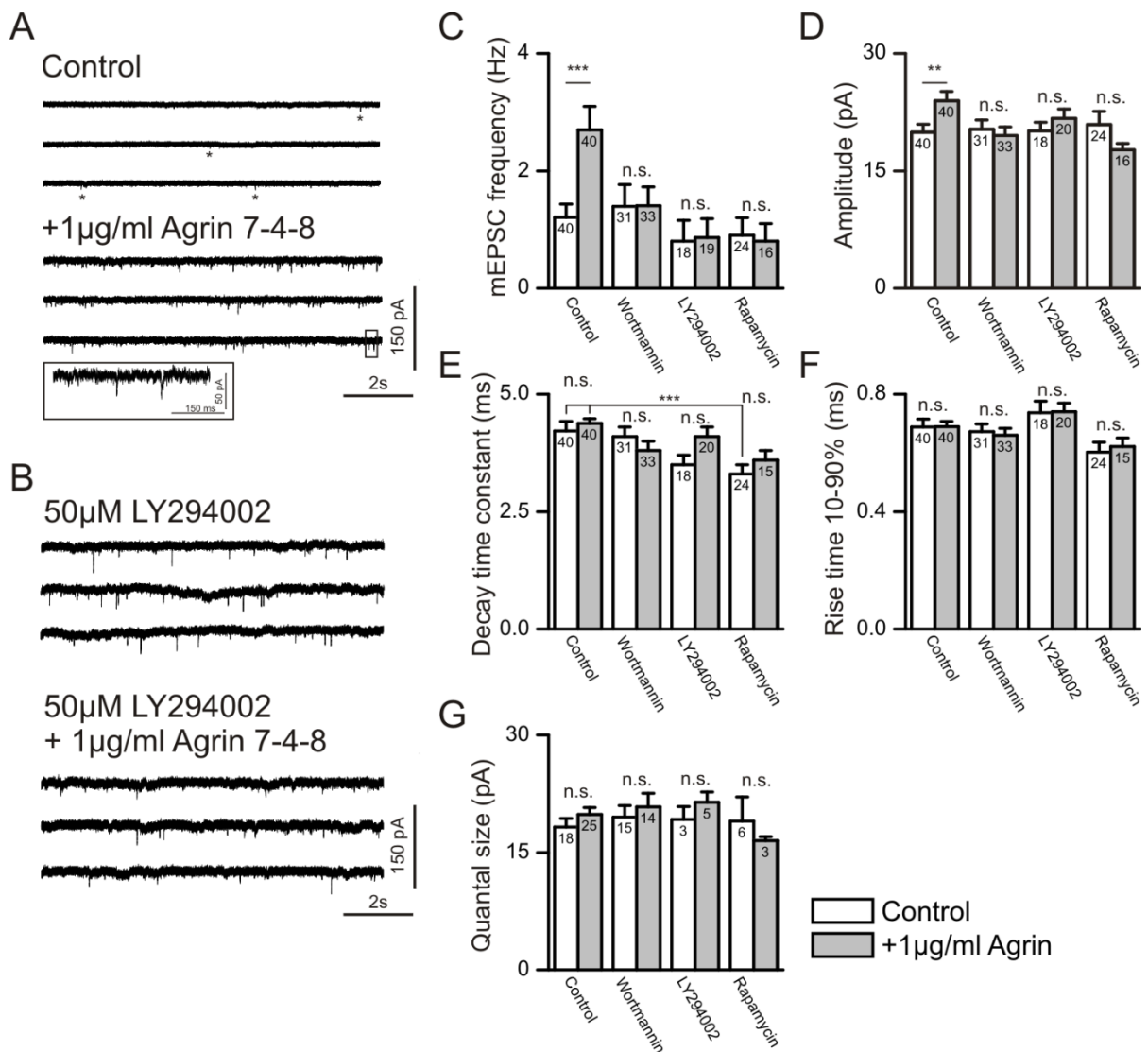


Figure 35: Agrin activates PI3K in single neurons and increases pGSK3β fluorescence. Antibodies against MAP2a/b as a marker for neurons and pGSK3β were used to study PI3K activity in neurons at DIV12-15. Stimulation with agrin led to an increase in pGSK3β fluorescence indicating an activation of PI3K (A and B). Wortmannin treatment reduced fluorescence of pGSK3β significantly below the control levels (A and B). p-Values were determined using Mann-Whitney rank sum test. Numbers in columns in B represent the number of analyzed cells. Bar plots represent mean values + SEM.

Since mammalian target of rapamycin (mTOR) is also implicated to play a role in synapse function and in dendrite outgrowth together with PI3K (Kumar et al., 2005; Urbanska et al., 2012), cells were also treated with the specific mTOR blocker rapamycin. Like LY294002 and wortmannin 1  $\mu$ M of this substance also abolished the agrin-mediated increase of the mEPSC frequency ( $0.947 \pm 0.288$  vs.  $0.832 \pm 0.275$  Hz;  $p=0.912$ ; Figure 36C).

Other properties of the miniature postsynaptic currents were not affected by agrin treatment in the presence of these blockers. The increase in the mEPSC amplitude after agrin incubation as could be observed in wild type control cells, was not seen in any of the drug-treated groups of neurons (Figure 36D). Decay and rise times in the respective groups were also not changed by agrin (tested with One-way ANOVA,  $p>0.05$ ) and stayed at values that were comparable to wild type cells (Figure 36E and F). Only rapamycin has an influence on the decay kinetics leading to a decrease that was statistically significant when control cells (only treated with rapamycin) were compared to wild type control cells ( $3.3 \pm 0.2$  vs  $4.2 \pm 0.2$  ms; tested with One-way ANOVA). Quantal size of the mEPSCs was also not changed in any of the treatment groups (Figure 36G).

These findings highlight a possible mechanism of agrin-mediated signal transduction via PI3K and mTOR leading eventually to the increase in mEPSC frequency and amplitude of agrin-treated neurons.



**Figure 36: Involvement of PI3K and mTOR in agrin-mediated signaling.** Voltage clamp analysis of cells treated with agrin and agrin together with PI3K blockers wortmannin (1 µM) or LY294002 (50 µM) or mTOR blocker rapamycin (1 µM) prevented the agrin-mediated increase in mEPSC frequency. For examples see A and B. Asterisks in A mark mEPSCs. Agrin incubation did not change other properties of mEPSCs e.g. amplitude (D), decay time (E), rise time (F) or quantal size in the treatment groups (tested with One-way ANOVA). mEPSCs frequencies after agrin incubation in WT control neurons were significantly increased (Mann-Whitney rank sum test,  $p=0.001$ ; C). The amplitude in WT control cells was also altered after agrin incubation (Mann-Whitney rank sum test,  $p=0.011$ ; D). The decay time constants of mEPSCs are also not affected by agrin (E). Only rapamycin-treated cells show differences in their control values compared to WT control decay times and agrin- treated cells (One-way ANOVA,  $p<0.001$ ; E). Rise times were similar between all treatment groups (F) as well as quantal sizes (G) (tested with One-way ANOVA). Numbers in columns in C, D, E, F and G represent investigated individual cells. Bar plots represent mean values + SEM. mEPSCs were recorded at a holding potential of -70 mV in the presence of TTX.

### 3.1.13 Voltage-gated $Ca^{2+}$ currents of single neurons are not affected by agrin application

Since it had been shown that agrin induced changes in voltage-gated calcium channels (VGCC) (Bandi et al., 2008) it was of interest to test this also in microisland cultures of cortical neurons. After three to five hours of incubation with neuronal agrin neurons were subjected to a voltage clamp protocol similar to the one used to determine the IV curves in other experiments (Figure 10B) in a bath solution blocking  $K^+$  and  $Na^+$  currents and with a

CsCl-based intracellular solution to isolate  $\text{Ca}^{2+}$  currents (chapter 2.2.7.12; Table 3). Maximal VGCC current amplitudes did not differ in untreated controls and agrin-treated neurons (Figure 37A) so current density in relation to the applied membrane potential was investigated (Figure 37B). The current densities at different membrane potentials were used to plot a graph. This graph illustrated that the current densities of treated and untreated cells did not differ at different holding potentials (Figure 37B) with maximal current densities at a holding potential of -10 mV. The maximal calcium current density was also not affected by incubation with agrin ( $5.64 \pm 0.46$  vs.  $5.85 \pm 0.61$  pA/pF;  $p=0.742$ ; Figure 37C). The cell capacitance was slightly increased in agrin-treated cells ( $61.5 \pm 3.4$  pF vs.  $70.65 \pm 3.7$  pF;  $p=0.07$ ; Figure 37C) but not to a significant level.

The data suggests that agrin is unable to induce changes in the VGCC currents in single cultured neurons.

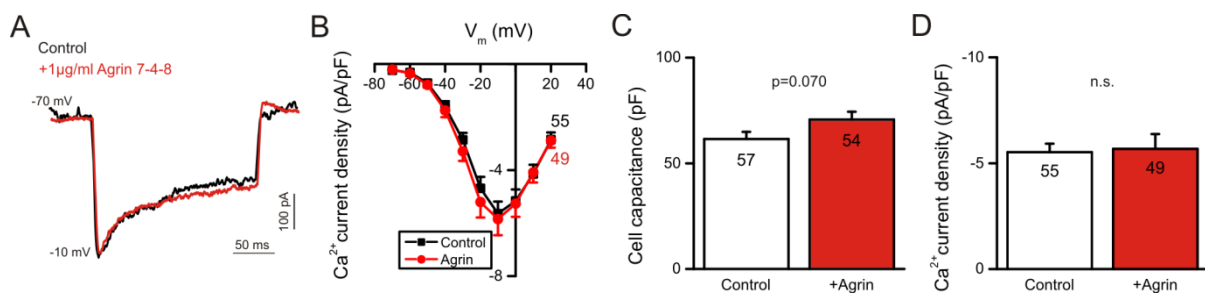


**Figure 37: Agrin is not able to influence voltage-gated  $\text{Ca}^{2+}$  currents in single neurons. Voltage-gated calcium currents induced at a membrane potential of -10mV seem to have similar amplitudes in control cells when compared to agrin treated cells (A). Current densities do not vary between control and treated cells (B and D). The cell capacitance in agrin-treated cells is slightly increased but not to a significant level (C). The p-value in C was determined using a t-test, the one in D using a Mann-Whitney rank sum test. Numbers in columns in C and D represent investigated individual cells. Bar plots represent mean values + SEM.**

## 3.2 Monolayer cortical cultures

A second culture system besides the microisland system was also used to investigate agrin's role in synapse formation. By using a conventional monolayer culture system to cultivate embryonic cortical neurons and electrophysiology as a tool to measure synaptic function, agrin's effect on the synapse development or maturation was investigated by incubating the cells with neuronal chicken agrin in these monolayer cultures.

### 3.2.1 Characterization of conventional monolayer cultures of cortical neurons

In a first step the culture system was characterized by using electrophysiological approaches to analyze the cultivated cortical neurons prepared from wild type embryos at E15. Cultures at DIV6-8 were already forming extensive neurite arborizations (data not shown). After 14 days *in vitro* a complex network of neuronal cells had formed as shown in a phase contrast image of a coverslip containing  $2.65 \cdot 10^5$  cells/cm<sup>2</sup> (Figure 38A). During prolonged cultivation the neurons underwent changes in their respective passive and active membrane properties. "Young" neurons at DIV6-8 were characterized by a high input resistance ( $R_{in}$ ) compared to "older" cells at DIV13-15 ( $1019.2 \pm 75.6$  M $\Omega$  vs.  $311.9 \pm 42.7$  M $\Omega$ ;  $p < 0.001$ ; Figure 38B). Respectively, the cell capacitance of DIV6-8 neurons was lower compared to DIV13-15 neurons ( $49.2 \pm 1.6$  vs.  $77.3 \pm 4.5$  pF;  $p < 0.001$ ; Figure 38C). The specific membrane resistance was also analyzed and significantly decreased in neurons cultured for 13-15 days *in vitro* compared to neurons at DIV6-8 ( $49.1 \pm 3.7$  vs.  $20.8 \pm 2.1$  k $\Omega$ \*cm<sup>2</sup>;  $p < 0.001$ ; Figure 38F). The active membrane properties were only investigated for voltage-gated K<sup>+</sup> currents since TTX was present in the bath solution in this set of experiments thus blocking voltage-gated Na<sup>+</sup> currents. Neurons at DIV6-8 had smaller maximal K<sup>+</sup> current amplitude compared to the neurons that were cultivated for 13-15 days ( $2079.2 \pm 104.3$  vs.  $3895.4 \pm 345.3$  pA;  $p < 0.001$ ) but the respective current densities were not significantly changed ( $49.8 \pm 3.4$  vs.  $54.1 \pm 5.9$  pA/pF;  $p = 0.721$ ; Figure 38D and E). The data show clearly that neurons in culture undergo developmental changes reflected in a decrease in their input resistance and increases in membrane capacitance and K<sup>+</sup> current amplitudes.

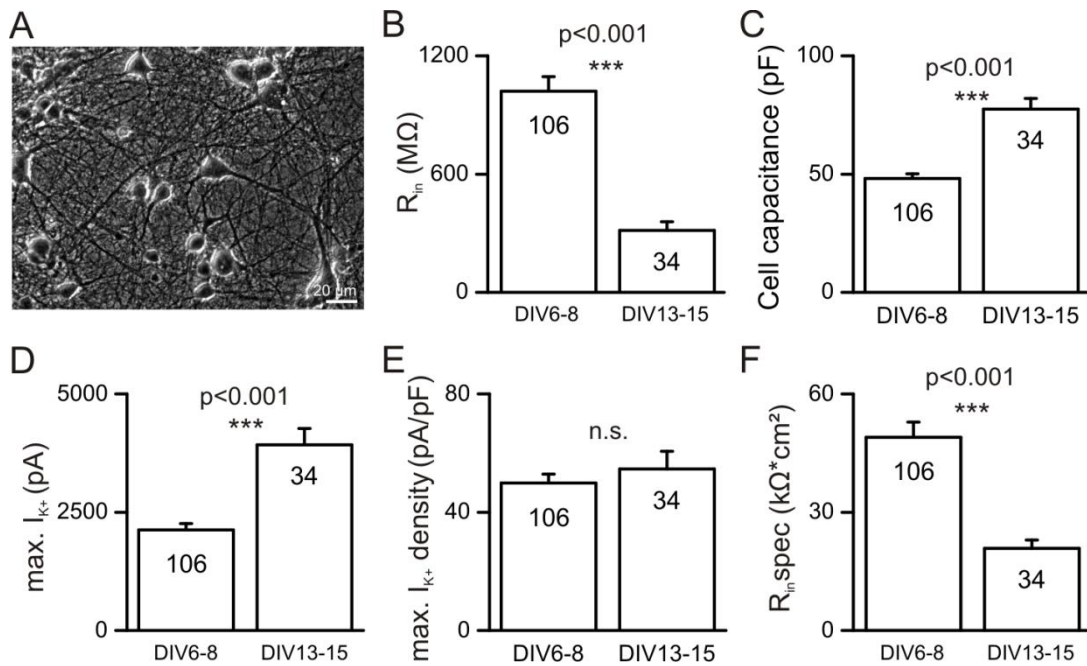


**Figure 38:** Analysis of developmental changes in the passive and active membrane properties of monolayer cell cultures of cortical neurons. Cortical cells in culture formed extensive neurite networks at DIV14 as seen in phase contrast optics (A). Cells underwent a strong reduction in their input resistance (B) and a strong increase in cell capacitance (C) with prolonged culture periods. The voltage-gated  $K^+$  current properties also showed a strong increase in the amplitude of the maximal currents (D) induced at a holding potential of +30 mV but no increase in the respective current densities (E). The specific input resistance was also strongly reduced in “older” neurons compared to “young” ones (F). All statistical analysis was done using Mann-Whitney rank sum tests. Numbers in columns in B to F represent the number of recorded neurons. Bar plots represent mean values + SEM.

### 3.2.2 Agrin increases inhibitory miniature postsynaptic currents of cortical neurons in monolayer cultures

In previous experiments in our lab (unpublished data by Jadwiga Schreiber; data not shown) cultured neurons were incubated with neuronal chicken agrin which resulted in an increase of their mIPSC frequency. This effect was thoroughly investigated in the scope of this study. To record these events 20  $\mu$ M DNQX, 100  $\mu$ M APV and 1  $\mu$ M TTX was added to the extracellular solution to block AMPAR/kainate, NMDAR and voltage-gated  $Na^+$  currents. Voltage clamp recordings at -70 mV holding potential revealed that incubation with 100 ng/ml full-length neuronal chicken agrin with splice inserts containing 4 amino acids at the A/y and eight amino acid inserts at the B/z site for three to five hours led to a significant increase in the frequency of mIPSCs ( $0.207 \pm 0.027$  vs.  $0.428 \pm 0.063$  Hz;  $p=0.008$ ; Figure 39A and C) in cultured neurons at DIV6-8. This increase was not observed in more “mature” cultures ( $0.438 \pm 0.102$  vs.  $0.575 \pm 0.154$  Hz;  $p=0.47$ ; Figure 39B and C) at DIV13-15. No other properties (amplitude, rise and decay times) of the mIPSCs were changed besides the frequency signifying an effect not generated by modulating receptor composition and density (Figure 39D).

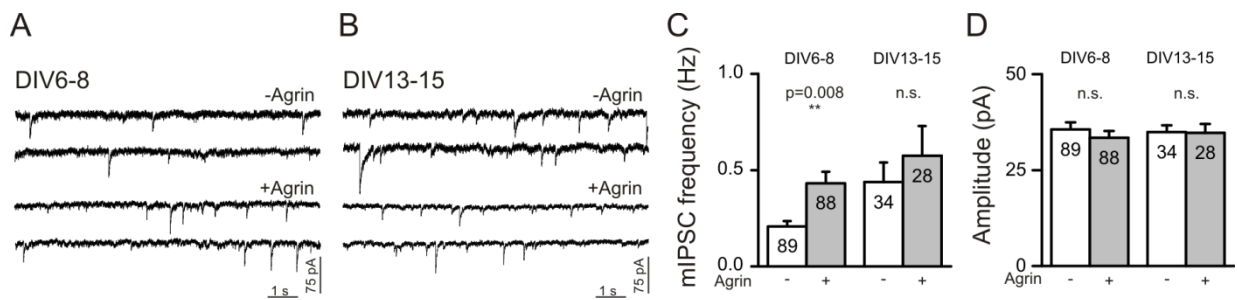


**Figure 39: Agrin influences the frequency of mIPSCs in monolayer cultures.** Treatment with 100 ng/ml neuronal agrin for three to five hours resulted in an increase in mIPSC frequency in neurons at DIV6-8 as can be seen in the voltage clamp traces recorded in presence of APV, DNQX and TTX at a holding potential of -70mV (A and C). No such increase was seen in neurons at DIV13-15 (B and C). The amplitudes of mIPSCs were also not influenced by agrin application (D). Statistical analysis was done using a Mann-Whitney rank sum test. Numbers in columns in C and D represent investigated cells. Bar plots represent mean values + SEM.

Not only agrin's effect on mIPSCs was investigated but also on mEPSCs. The recorded neurons were cultured for 13-15 days since glutamatergic synapses were encountered only at later stages. To record mEPSCs 20  $\mu$ M bicuculline and 1  $\mu$ M TTX was added to the extracellular solution to block GABA<sub>A</sub>R and voltage-gated Na<sup>+</sup> currents. Voltage clamp recordings at -70 mV showed that treatment with neuronal agrin yielded no significant changes in mEPSC frequency ( $1.029 \pm 0.339$  vs.  $0.712 \pm 0.243$  Hz;  $p=0.965$ ; Figure 40A and B) and amplitude ( $22.9 \pm 1.3$  vs.  $20.2 \pm 1.4$  pA;  $p=0.249$ ; Figure 40C) in the investigated neurons.

Since the effect measured is specific for GABAergic synapses additional experiments were primarily done in monolayer cultures focussing on this type of synapse.

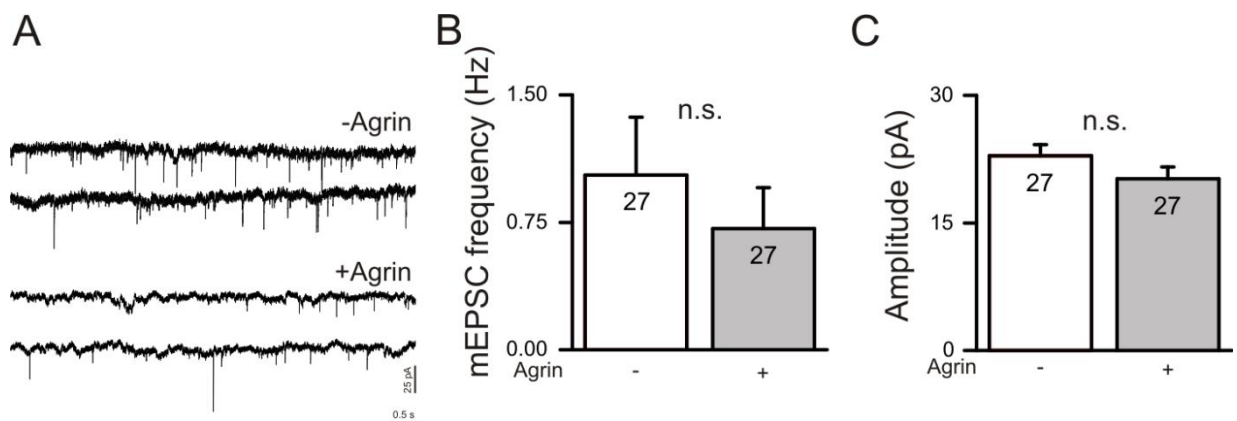


**Figure 40: Agrin does not influence the frequency of mEPSCs.** Voltage clamp traces recorded in the presence of 20  $\mu$ M bicuculline and 1  $\mu$ M TTX from neurons cultured for 13 to 15 days *in vitro* show that there is no increase in mEPSC frequency after treatment with 100 ng/ml agrin (A and B). The amplitudes of these events are not influenced by agrin, too (C). Statistical analysis was done using a Mann-Whitney rank sum test in B and was done using a t-test in C. Numbers in columns in B and C represent the number of investigated cells. Bar plots represent mean values + SEM.

As no effect of neuronal agrin could be seen at excitatory synapses at DIV 13-15 cells at earlier developmental stages were also subjected to agrin treatment to detect a critical time

point when agrin might be of importance. mEPSCs were recorded from cells as young as DIV10 up to DIV15. Incubation with 1 $\mu$ g/ml neuronal agrin for 3-5 h only caused a significant increase in mEPSC frequency in cells at DIV11 but not at any earlier or later stage (Figure 41). mEPSC frequency in DIV10 cells was identical in untreated and agrin treated cells ( $0.811 \pm 0.211$  vs.  $0.831 \pm 0.259$  Hz,  $p=0.903$ ) as was the respective amplitudes of these events ( $23.9$  vs.  $22.2 \pm 2.0$  pA,  $p=0.601$ ). At DIV11 agrin incubation led to an increase in the mEPSC frequency compared to untreated control cells ( $0.377 \pm 0.094$  vs.  $0.710 \pm 0.158$  Hz;  $p=0.033$ ) but did not influence the amplitude ( $17.7 \pm 1.5$  vs.  $19.7 \pm 1.4$  pA;  $p=0.134$ ) of these events (Figure 41B, D and E). If cells were cultured for a few more days (DIV13-15) they again became unresponsive to agrin and no increase in mEPSC frequency was apparent ( $1.125 \pm 0.331$  vs.  $1.418 \pm 0.393$  Hz;  $p=0.965$  Figure 41C, D and E). It seems that agrin-dependent effects on mEPSCs are either very time specific or somehow overshadowed in these kind of culture.

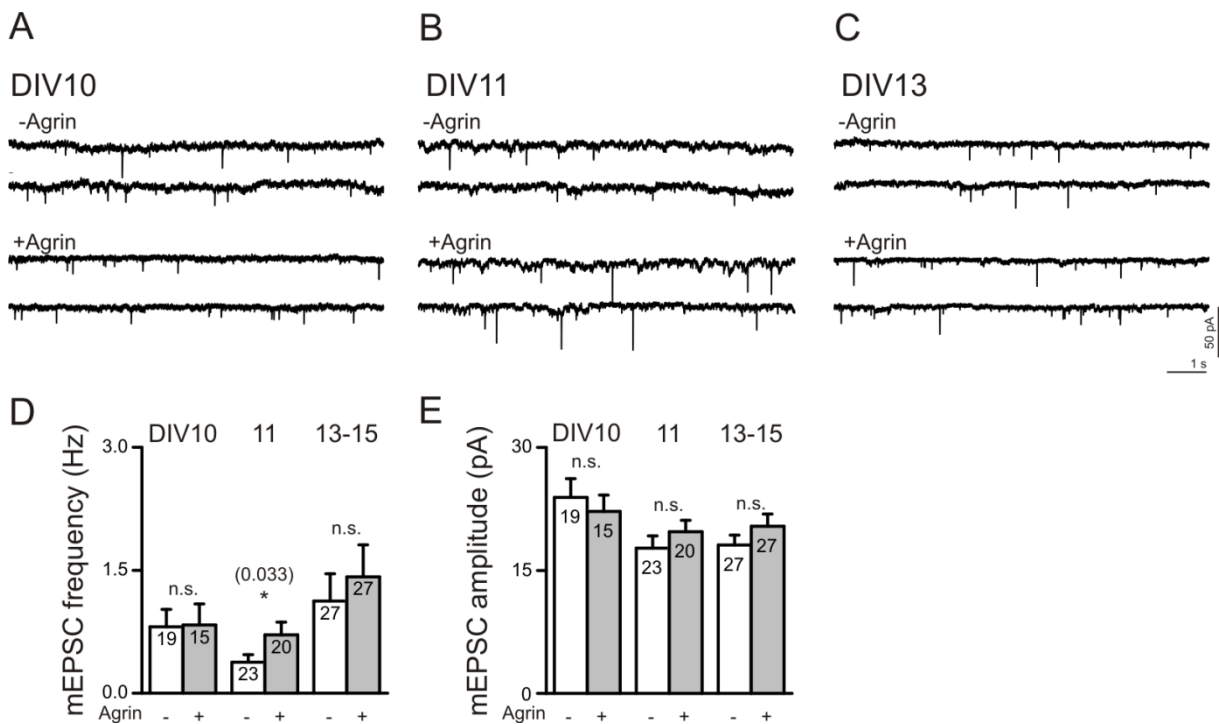


**Figure 41: Agrin only influences mEPSCs at a certain stage of maturation.** Voltage clamp traces show mEPSCs at different stages in neuronal development untreated and treated with 1  $\mu$ g/ml agrin for 3-5h (A-C). Analysis of the frequency of these events showed only at stage DIV11 a significant increase (Mann-Whitney rank sum test) (D). Amplitudes of the events were not affected by agrin treatment (E). Numbers in columns in D and E represent investigated cells. Bar plots represent mean values + SEM. mEPSCs were recorded in presence of 20  $\mu$ M bicuculline and 1 $\mu$ M TTX at a holding potential of -70 mV.

### 3.2.3 The agrin-mediated effect on mIPSCs of cortical neurons is time and concentration dependent

After establishing that agrin affected the mIPSC frequency after incubation for three to five hours it was of interest to find out if this effect was immediate or needed even more time to become stronger. Therefore incubation with 100 ng/ml agrin was done using varying time intervals (one, three and seven hours) and neurons at DIV6-8. Untreated cells served as controls. The mIPSC frequency was not influenced after one hour of incubation since agrin-treated neurons showed a similar mIPSC frequency as untreated cells ( $0.227 \pm 0.064$  vs.  $0.207 \pm 0.027$  Hz;  $p=0.829$ ; Figure 42A and B). After three hours a robust increase in mIPSC frequency was seen in the agrin-treated cells ( $0.428 \pm 0.63$  vs.  $0.207 \pm 0.027$  Hz;  $p=0.008$ ; Figure 42A and B). This increase was also seen in cells that were incubated for seven hours with neuronal agrin ( $0.587 \pm 0.130$  vs.  $0.207 \pm 0.027$  Hz;  $p<0.001$ ; Figure 42A and B).

These results implicate that the effect on the mIPSC frequency may be due to remodeling processes including protein synthesis that take a few hours' time.

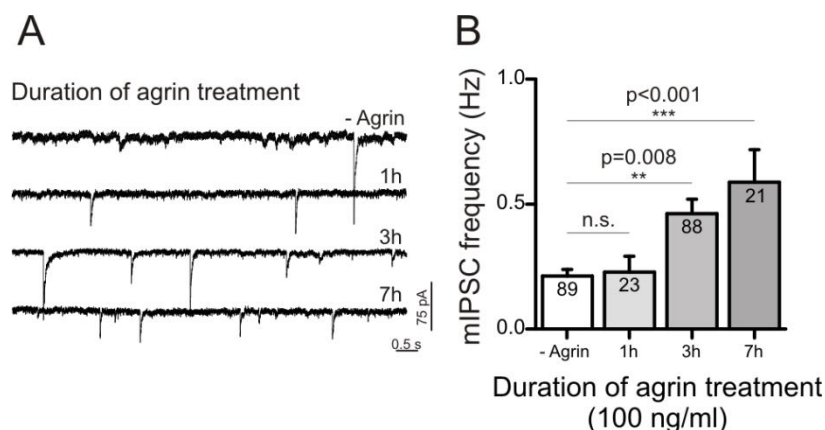


**Figure 42: Incubation time dependence of the agrin-mediated effect on mIPSCs.** Voltage clamp traces recorded at  $V_h = -70$  mV in the presence of TTX, DNQX and APV show that mIPSC frequencies were significantly increased after 3h incubation with 100 ng/ml neuronal agrin and stayed elevated after 7h of incubation (A and B). Significance level was tested using Mann-Whitney rank sum tests. Cells were subjected to Grubb's outlier test and one outlier was removed from each condition. Numbers in columns in B represent investigated cells. Bar plots represent mean values + SEM.

To study if the effect on mIPSC frequency was dependent on the concentration of agrin and maybe could be increased with higher amounts of protein, cells at DIV6-8 were incubated for three to five hours in culture medium supplemented with 100, 500 or 1000 ng/ml neuronal agrin. The mIPSC frequency was significantly increased at all concentrations tested. Concentrations of 100 ng/ml ( $0.428 \pm 0.063$  vs.  $0.207 \pm 0.027$  Hz;  $p=0.008$ ), 500 ng/ml ( $0.508 \pm 0.121$  vs.  $0.207 \pm 0.027$  Hz; p-value =0.003) or higher ( $0.476 \pm 0.128$  vs.  $0.207 \pm 0.027$  Hz;  $p=0.002$ ; Figure 43A and B) induced a significant increase in the frequency of the mIPSCs.

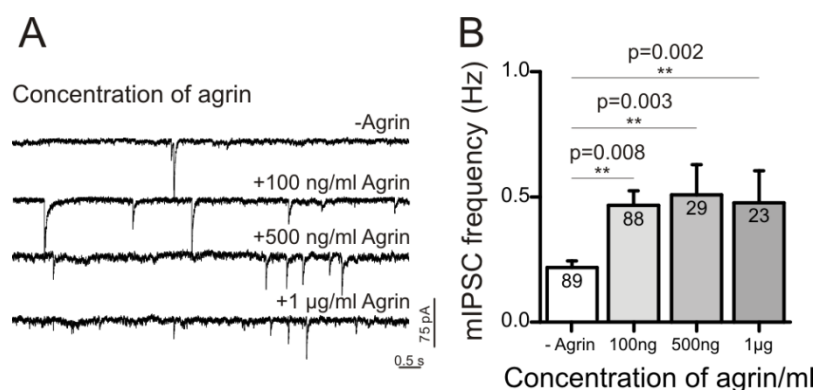


Figure 43: Dose dependence of the agrin-mediated effect on mIPSCs. Voltage clamp traces recorded at  $V_h = -70$  mV in the presence of TTX, DNQX and APV show that mIPSC frequencies were significantly increased after 3-5h incubation with 100 ng/ml, 500 ng/ml and 1  $\mu$ g/ml neuronal agrin (A and B). Significance level was tested using Mann-Whitney rank sum tests and a Kolmogorov-Smirnov test (1 $\mu$ g). Cells were subjected to Grubb's outlier test and one outlier was removed from each condition. Numbers in columns in B represent investigated cells. Bar plots represent mean values + SEM.

### 3.2.4 The induction of inhibitory synapses in monolayer cultures is not affected by agrin incubation.

The increase in mIPSC frequency measured after treatment with neuronal agrin may have been caused by an increase in the number of inhibitory synapses. Thus immunocytochemistry was used on DIV6-8 old cultures of neurons and the presynaptically localized vesicular GABA transporter (VGAT) together with the postsynaptic scaffolding protein gephyrin chosen as markers for these synapses. The analysis of co-localized spots in untreated control and agrin-treated cells revealed no visible change in inhibitory synapse number. Figure 44A shows example cells for both groups. In the images one can clearly see yellow spots that represent co-localization and thus inhibitory synapses. In both conditions an equal number of stained synapses was counted (Figure 44A and B). The mean number of spots ( $22.89 \pm 3.64$  vs.  $21.78 \pm 3.08$ ;  $p=0.843$ ; Figure 44C) clearly showed that there is no change in inhibitory synapse number caused by the addition of neuronal agrin. Daily mean values from individual experiments showed equal numbers of synapses (data not shown) further stressing the fact that agrin treatment does not influence inhibitory synapse number in this culture system.

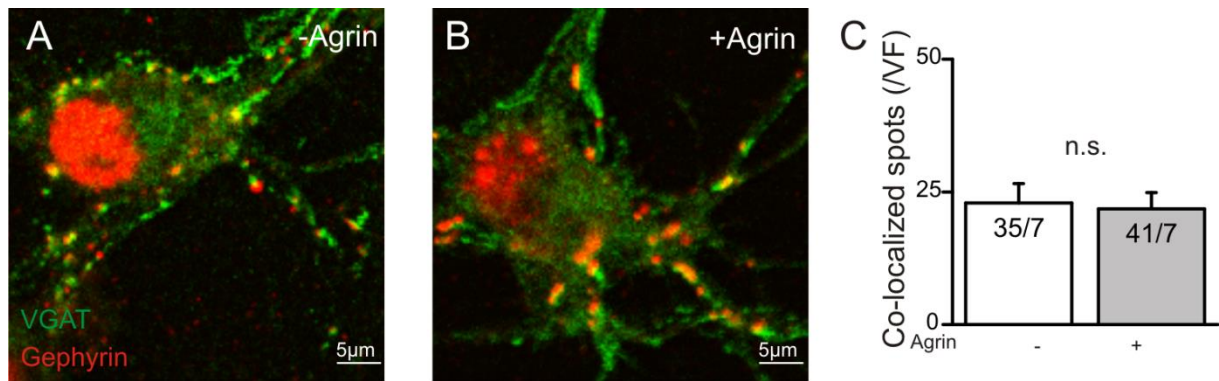


Figure 44: Inhibitory synapse number of cortical neurons is unchanged after agrin incubation. Inhibitory synapses were stained using antibodies against presynaptic VGAT and postsynaptic gephyrin after treatment with 100 ng/ml neuronal agrin for three to five hours. Agrin-treated cells and control cells exhibited equal numbers of inhibitory synapses seen as yellow dots in A and B. Mean values of the co-localized spots per view field show no change after incubation with agrin (C). Data was subjected to a Mann-Whitney rank sum test resulting in p-values >0.05. Numbers in columns in C represent individual images (35 and 41) and preparations that were analyzed (7 and 7). Bar plots represent mean values + SEM.

### 3.2.5 Presynaptic release of neurotransmitter of cortical neurons is not affected by agrin incubation

As the results of the co-localization experiments indicated no changes in inhibitory synapse number presynaptic neurotransmitter release was analyzed as a possible explanation for increased mIPSC frequency after agrin treatment. Extracellular stimulation with a monopolar electrode was used as a means to investigate the paired-pulse ratio (PPR) of agrin-treated cells (Figure 45A). When successfully stimulated, presynaptic axon terminals released neurotransmitter leading to a current response in the postsynaptic neuron that was recorded from in whole cell patch clamp configuration. By giving two pulses at an interstimulus interval of 100 ms and comparing the amplitudes of the current responses the PPR could be determined. Is the first amplitude larger than the second the release probability is high and the resulting PPR small, leading to a paired-pulse depression. The opposite is true for paired-pulse facilitation. Typical recordings in the presence of 20  $\mu$ M DNQX and 100  $\mu$ M APV can be seen in Figure 45B. Changes in the amplitude of the first current response were not recorded after three to five hours of agrin incubation (100 ng/ml) for the evoked IPSCs ( $758.3 \pm 94.5$  vs.  $772.9 \pm 104.2$  pA;  $p=0.603$ ; Figure 45C). The decay kinetics of the first current response of the IPSCs also did not exhibit changes due to agrin treatment ( $51.57 \pm 4.9$  vs.  $47.29 \pm 6.2$  ms;  $p=0.379$ ; Figure 45D). All investigated neurons showed a prominent paired-pulse depression indicating a high release probability of neurotransmitter (Figure 45B) but were not affected by agrin treatment ( $34.5 \pm 5.4$  vs.  $36.1 \pm 5.9$  %;  $p=0.767$ ; Figure 45E).

Sometimes autaptic connections were encountered in this monolayer culture system. In this special case of synapse a neuron forms synaptic connections with itself (Figure 45F). If autapses are present the neuron can be stimulated by using the patch pipette. Autaptic responses did not differ significantly from extracellularly stimulated responses in their amplitudes ( $753.9 \pm 172.1$  vs.  $758.3 \pm 94.5$  pA;  $p=0.928$ , Figure 45C and H). After agrin treatment the amplitude of the first response increased slightly ( $748.9 \pm 172.1$  vs.  $994.3 \pm 302.0$  pA;  $p=0.379$ ; Figure 45G and H). The decay kinetics of the first current response of the IPSC also did not exhibit changes due to agrin treatment ( $35.1 \pm 5.4$  vs.  $52.9 \pm 7.5$  ms;  $p=0.054$ ; Figure 45I). Agrin-treated cells appeared to have larger amplitudes of their synaptic current responses compared to untreated control cells thus leading to a smaller PPR ( $15.1 \pm 4.4$  vs.  $36.6 \pm 11.0$  %;  $p=0.369$ ; Figure 45J) but without statistical significance due to high variability.

The data suggest that also the presynaptic release of GABA neurotransmitter is most likely not influenced by the incubation with neuronal agrin.

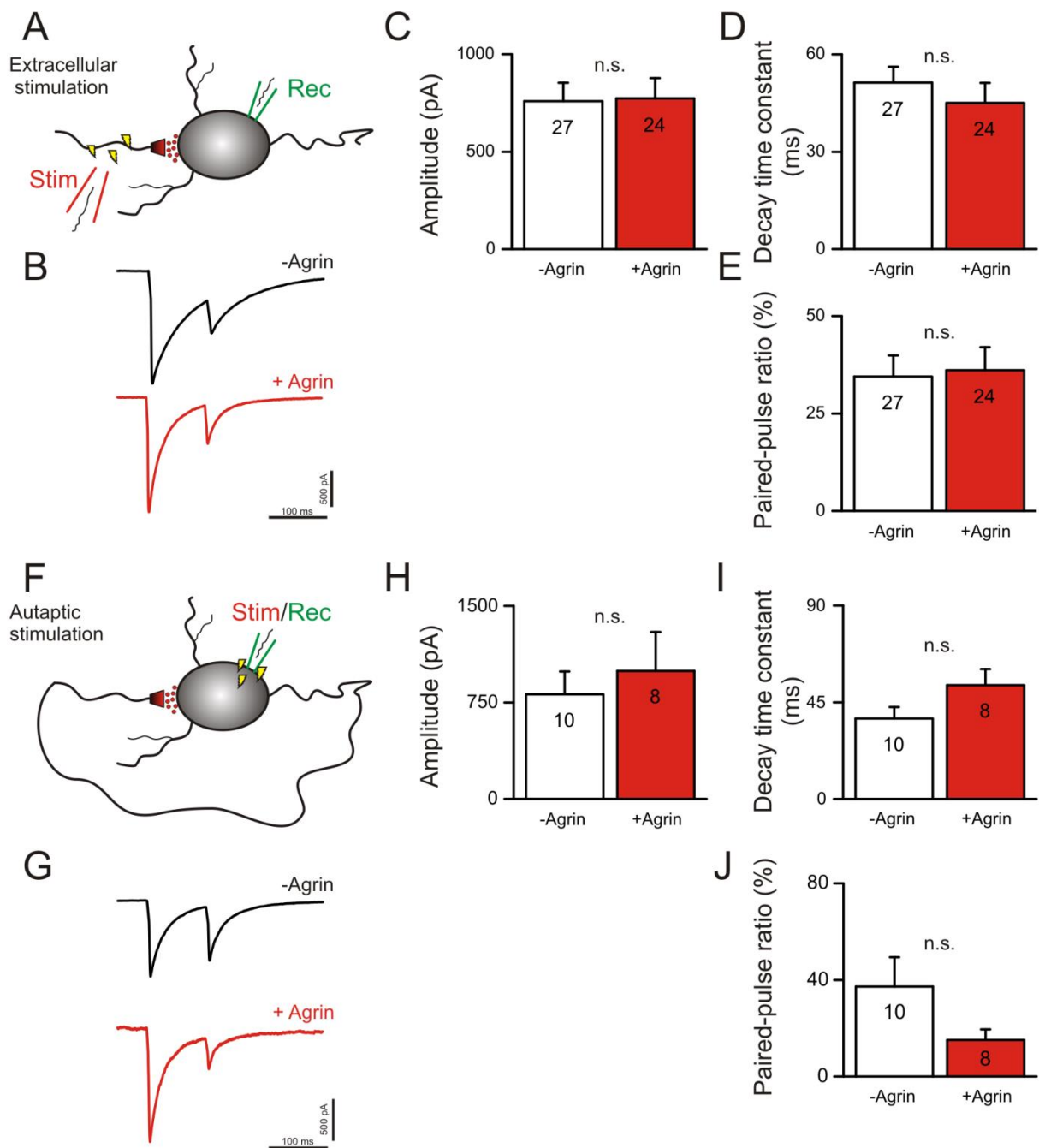
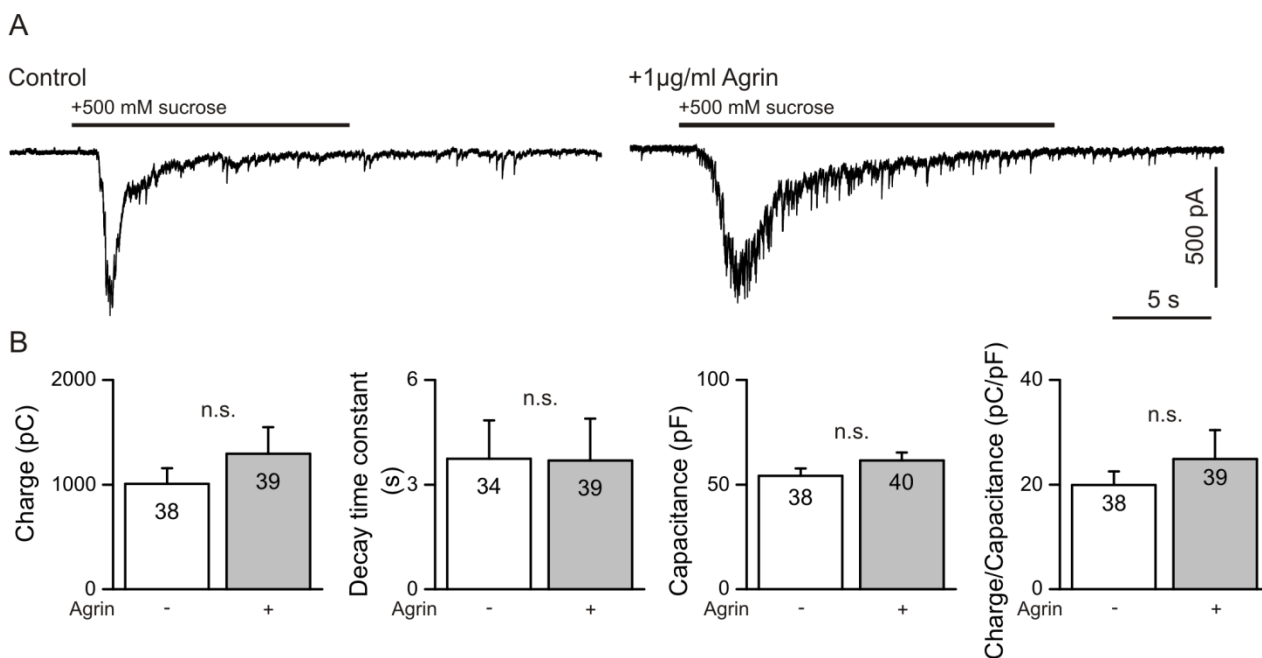


Figure 45: Evoked IPSCs in monolayer neuron cultures are unchanged after treatment with 100 ng/ml neuronal agrin. Stimulation with a monopolar electrode (red) (A) led to robust responses in the postsynaptic neuron that was patched (green) and recorded (B). All investigated cells showed paired-pulse depression (B). The amplitudes of the evoked IPSCs were not changed by agrin application (C) as well as the decay time constants (D). No differences in their paired-pulse ratios were observed after agrin incubation (E). Sometimes autaptic connections were detected. By stimulating the neuron with the patch pipette (green) IPSCs could be evoked (F and G). No changes after agrin incubation were observed for autaptic connections in amplitude (H) and decay time constant (I) of the aIPSC. The paired-pulse ratio was also unaffected by agrin treatment (J). Stimulus artifacts in B and G have been removed. All data were subjected to Mann-Whitney rank sum tests or t-tests resulting in  $p$ -values  $>0.05$ . Numbers in columns C to E and H to J represent the number of investigated individual cells. Bar plots represent mean values + SEM. eIPSCs and aIPSCs were recorded in the presence of 20  $\mu$ M DNQX and 100  $\mu$ M APV at a holding potential of -70 mV.

### 3.2.6 The readily releasable synaptic vesicle pool of cortical neurons in monolayer cultures is not influenced by agrin incubation

As the agrin-mediated effect was not caused by changes in neurotransmitter release and the number of inhibitory synapses the size of the readily releasable vesicle pool was analyzed using high osmolarity sucrose stimulation and a higher concentration of neuronal agrin. Local superfusion with EC solution supplemented with 500 mM sucrose led to a current responses induced by the release of neurotransmitter from presynaptic terminals that could be recorded from a postsynaptic neuron in voltage clamp mode (Figure 46A). Current responses of cells that had been treated with 1 $\mu$ g/ml agrin for three to five hours and untreated control neurons did not differ in their charge ( $1295.4 \pm 252.2$  vs.  $993.2 \pm 148.2$  pC;  $p=0.682$ ; Figure 46B) and decay time constant ( $3.69 \pm 1.2$  vs.  $3.73 \pm 1.1$  ms;  $p=0.188$ ; Figure 46B). The capacitance of the cells was also not altered ( $61.5 \pm 3.8$  vs.  $54.1 \pm 3.6$  pF;  $p=0.130$ ; Figure 46B) as was the ratio of the charge and capacitance ( $24.9 \pm 5.5$  vs.  $19.7 \pm 2.6$  pF/pC;  $p=0.867$ ; Figure 46B).

These results indicate that the readily releasable vesicle pool was not affected by agrin treatment.



**Figure 46: Analysis of the readily releasable vesicle pool after agrin treatment.** Control or agrin-treated neurons that were stimulated by local superfusion with high osmolarity sucrose containing EC solution elicited current responses in the presence of APV, DNQX and TTX at a holding potential of -70 mV (A). The charge of these responses as well as the decay kinetic was not influenced by incubation for three to five hours with 1 $\mu$ g/ml neuronal agrin. Cell capacitance and charge/capacitance ratios were not influenced by agrin-treatment either. All data were subjected to Mann-Whitney rank sum tests yielding p-values of >0.05. Numbers in columns in B represent investigated individual cells. Bar plots represent mean values + SEM.

### 3.2.7 Passive and active cell properties of cortical neurons remain unchanged after agrin treatment

It is plausible that incubation experiments with recombinant proteins could influence the passive and active membrane properties of cultured neurons by various mechanisms. Since the synaptic modifications by treatment with neuronal agrin were of interest here, it was important to test if agrin would induce changes in the cells input resistance, indicative of changes of the membrane's "tightness" or influence the cells capacitance, causing the neuron e.g. to swell or increase in size. The input resistance of neurons cultured for 6-8 days *in vitro* after treatment with 100 ng/ agrin for three to five hours was recorded in the presence of 20  $\mu$ M DNQX, 100  $\mu$ M APV and 1  $\mu$ M TTX in the bath solution to block AMPA/kainate, NMDA receptors and action potentials and compared to untreated cells. Application of agrin did not change the input resistance of the agrin-treated neurons ( $1019.2 \pm 75.6$  vs.  $978.1 \pm 74.2$  M $\Omega$ ;  $p=0.496$ ; Figure 47A). The cell capacitance was also not influenced by agrin ( $49.2 \pm 1.6$  vs.  $48.2 \pm 1.8$  pF;  $p=0.595$ ; Figure 47B). As a further means to investigate the passive membrane properties of the neurons the specific membrane resistance of untreated cells was compared to agrin-treated ones yielding no changes induced by the incubation ( $49.1 \pm 3.7$  vs.  $44.2 \pm 3.4$  k $\Omega$ \*cm $^2$ ;  $p=0.302$ ; Figure 47C).

In conclusion agrin did not affect the cells passive properties in a way that was measurable with electrophysiological means.

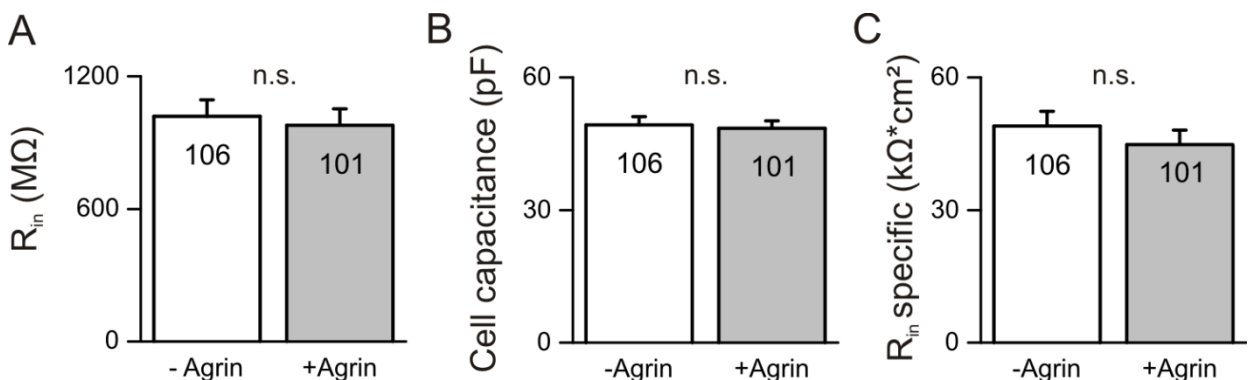


Figure 47: Agrin induces no change in passive membrane properties. Neurons cultured for 6-8 days and incubated with 100 ng/ml neuronal agrin did not exhibit changes in their passive membrane properties. All parameters investigated were not influenced by agrin treatment. The  $R_{in}$  (A), cell capacitance (B) and  $R_{in}$  specific (C) values were compared with untreated control neurons and tested with a Mann-Whitney rank sum test yielding  $p$ -values  $>0.05$ . Numbers in columns in A to C represent investigated cells. Bar plots represent mean values + SEM.

Next the voltage-gated  $K^+$  currents of the investigated neurons were compared. Note that the analysis of voltage-gated  $Na^+$  currents was not possible in these experiments due to the presence of TTX in the extracellular solution. Untreated as well as neurons treated with agrin were subjected to a voltage clamp protocol to induce potassium-driven current responses (Figure 48A and B). Maximal current amplitudes were compared and showed no difference between untreated control and agrin-treated neurons ( $2079.2 \pm 104.3$  vs.  $2271.3 \pm 111.5$  pA;  $p=0.073$ ; Figure 48C) as did their respective current densities ( $44.9 \pm 2.3$  vs.  $55.1 \pm 3.4$  pA/pF;  $p=0.081$ ; Figure 48C). These data suggest that agrin incubation is not causing changes in voltage-gated  $K^+$  current properties.

In conclusion treatment with neuronal agrin did not induce changes in neither the passive membrane properties nor the active voltage-gated  $K^+$  current properties in cortical neurons.

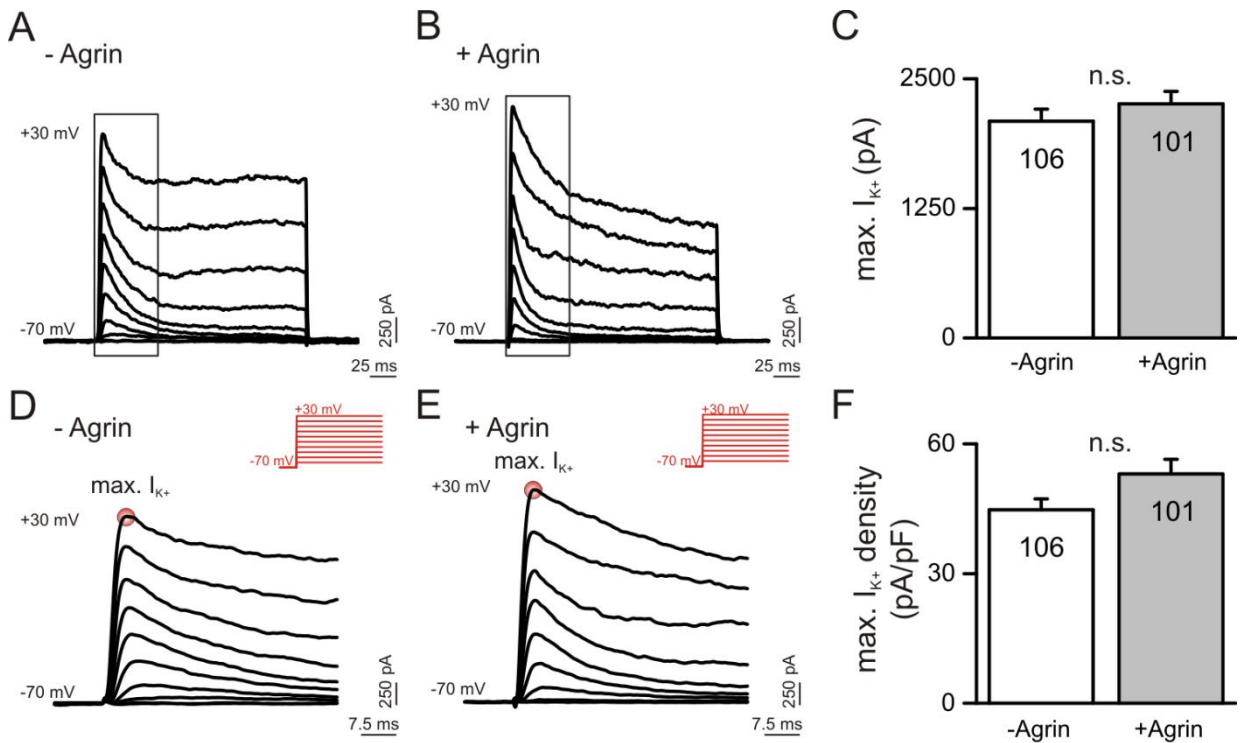


Figure 48: The properties of  $K^+$  currents are unaffected by agrin treatment. Voltage-gated  $K^+$  currents have been analyzed by voltage clamp protocols (see insets in red in D and E) to show that treatment with 100 ng/ml agrin for three to five hours did not change their properties. The membrane potential was successively depolarized by 10 mV increments and the current responses recorded from agrin-treated and untreated control neurons (A and D, B and E). The current traces framed by boxes in A and B have been magnified in D and E to illustrate where the maximal current was measured from. The maximal current amplitudes (C) and densities (D) in both conditions were of similar values and not significantly changed by agrin application. Significance was tested with Mann-Whitney rank sum test. Numbers in columns in C and F represent the number of investigated cells. Bar plots represent mean values + SEM.

### 3.2.8 Agrin does not influence synaptic transmission of cortical neurons of agrin-deficient animals

Since in all wild type neurons endogenous agrin was still present the analysis of agrin-deficient neurons was an important issue that needed to be addressed. Agrin-deficient cultures were investigated using the same methods as for wild type cultures.

Cells prepared from agrin-deficient and agrin wild type embryos showed no differences in their passive and active membrane properties at DIV6-8 when they were treated with 100 ng/ml neuronal agrin for three to five hours or left untreated (data not shown). The analysis of mIPSCs showed that there still was an increase in mIPSC frequency in agrin wild type neurons however this was not statistically significant in this series of cultures ( $0.306 \pm 0.06$  vs.  $0.539 \pm 0.17$  Hz;  $p=0.782$ ; Figure 49A and B). Agrin-deficient neurons were able to form inhibitory synapses and displayed no changes in their mIPSC frequency after agrin incubation ( $0.221 \pm 0.05$  vs.  $0.164 \pm 0.03$  Hz;  $p=0.232$ ; Figure 49B and D). Other parameters of the miniature postsynaptic currents (amplitude, decay time and rise time constant) were not different between genotypes and unaffected by agrin treatment (Figure 49C, E and F).

Excitatory synaptic transmission was also investigated. Herefore the same electrophysiological procedures were applied as for the analysis of mIPSCs only changing the blockers in the EC solution. In general cortical neurons of agrin-deficient mice were also capable of forming excitatory synapses at DIV13-15 in monolayer cultures as can be seen by the appearance of mEPSCs in the voltage clamp traces of these cells (Figure 49J). Incubation with neuronal agrin led to a decrease in the frequency of these mEPSCs in agrin wild type neurons but not to a significant extent ( $1.597 \pm 0.521$  vs.  $0.620 \pm 0.181$  Hz;  $p=0.469$ ; Figure 49G). The mEPSC frequency of agrin-treated and untreated agrin-deficient neurons was not influenced by the addition of agrin to the culture medium ( $0.905 \pm 0.264$  vs.  $1.224 \pm 0.384$  Hz;  $p=0.968$ ; Figure 49G, H and J). The other properties of the miniature postsynaptic currents were also unaffected by agrin treatment and did not differ between the genotypes (Figure 49I, K and L).

These results implicate that synaptogenesis in monolayer cultures of agrin-deficient cortical neurons seems to be unaffected and not responsive to treatment with neuronal agrin.

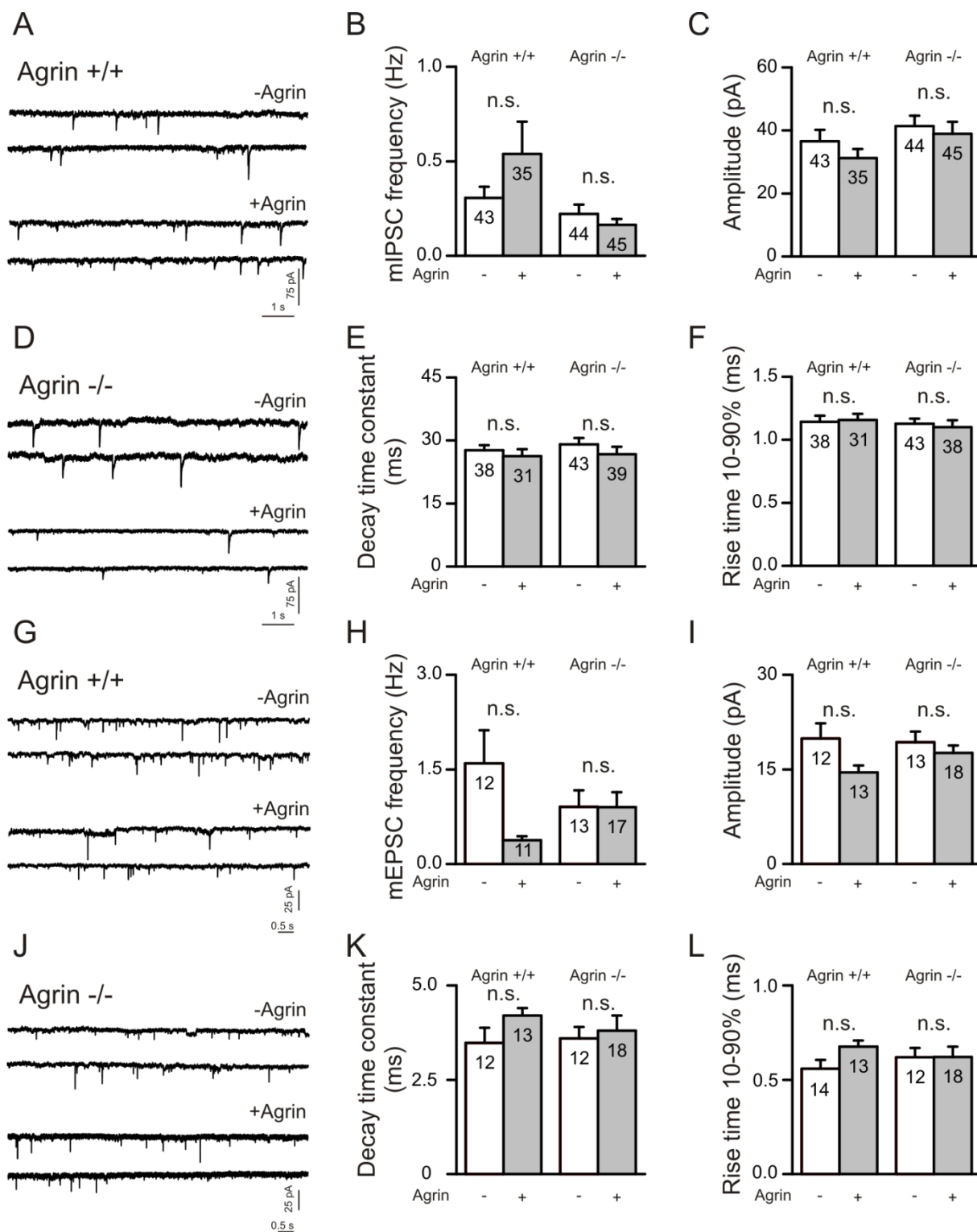
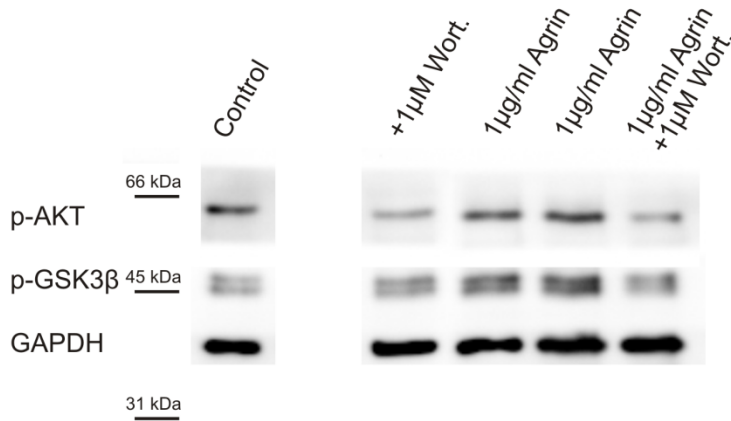


**Figure 49: Analysis of the synaptic activity of agrin mutant neurons in monolayer cultures.** Treatment with neuronal agrin (100 ng/ml, 3-5h) increased mIPSC frequency in agrin +/+ neurons (DIV6-8) but not significantly, while not inducing any changes in the mIPSC frequency of agrin -/- neurons (A,B and D). mIPSC amplitudes were not affected by agrin treatment in +/+ and -/- neurons (B). Decay time constants of both genotypes were unaffected by agrin treatment as well (E). The rise time kinetic of the neurons was unchanged by agrin treatment in both genotypes (F). mEPSC frequency was also not influenced by agrin in agrin +/+ and -/- neurons (G,H and J). mEPSC amplitudes of DIV14 were not affected by agrin treatment in +/+ and -/- neurons (I). Decay time constants of both genotypes were unaffected by agrin treatment as well (K). The rise time of the investigated neurons was unchanged by agrin treatment in both genotypes (L). Statistical analysis was done using Mann-Whitney rank sum tests yielding p-values >0.05. Numbers in columns in B, C, E, F, H, I, K and L represent investigated individual cells. Wild type (+/+) and agrin-deficient (-/-) neurons were prepared from pregnant heterozygous mothers at E15. mIPSCs were recorded in the presence of 20  $\mu$ M DNQX, 100  $\mu$ M APV and 1  $\mu$ M TTX. mEPSCs were recorded in the presence of 20  $\mu$ M bicuculline and 1  $\mu$ M TTX. Bar plots represent mean values + SEM.

### **3.2.9 PI3K is stimulated in cortical neurons by agrin incubation**

PI3K is a prominent kinase involved in a diverse set of functions in the nervous system (Brennan-Minnella et al., 2013; Cosker and Eickholt, 2007; Man et al., 2003) and in the formation of the neuromuscular junction (Schmidt et al., 2012). Since Schmidt et al. had shown that PI3K is stimulated by agrin in experiments using cultured myotubes it was tempting to perform similar experiments with cultured neurons. After stimulation for 10 min with 1, 5 or 10 µg/ml neuronal agrin, 1 µM PI3K blocker wortmannin or a combination of agrin and wortmannin, cells were harvested and their protein lysate used for western blot experiments. Phosphorylation of AKT and GSK3β was increased in agrin-treated cells (pAKT: 234.1 %; pGSK3β: 160.4 % [1 µg/ml Agrin]; p<0.001; Figure 50A and B) whereas treatment with wortmannin led to a significant decrease in their phosphorylation levels compared to untreated cells (pAKT: 49.6%; pGSK3β: 66.0%; p<0.001). This effect was not seen in cells that were treated with high concentrations of agrin (10 µg/ml) where the intensity of the bands was below the level of untreated control cells.

A



B

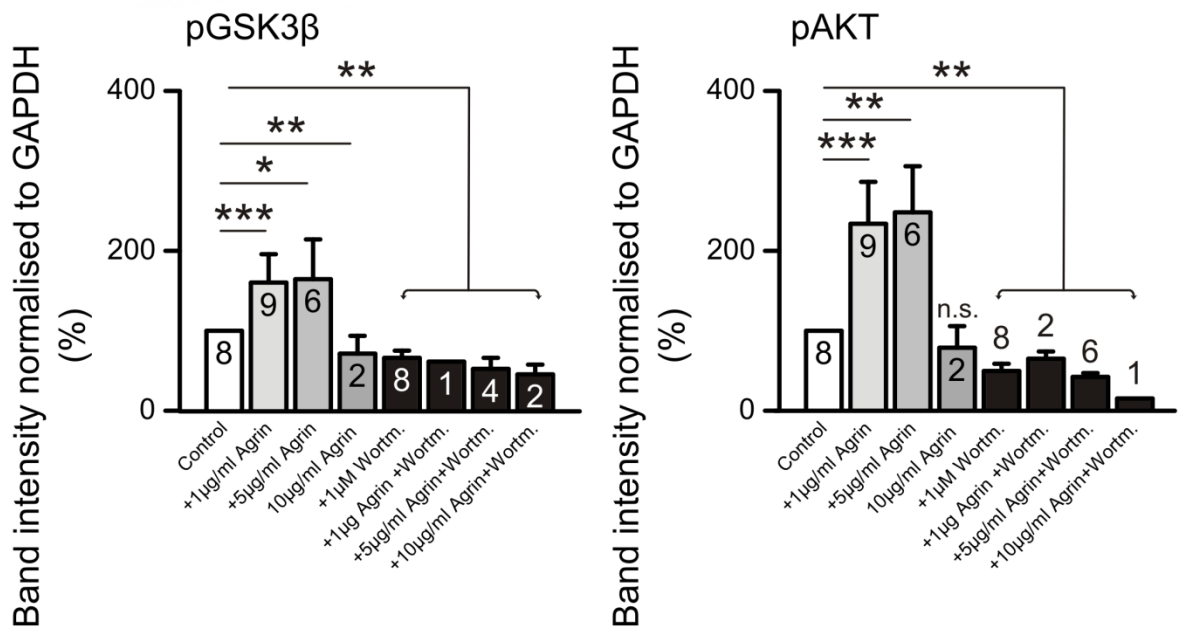
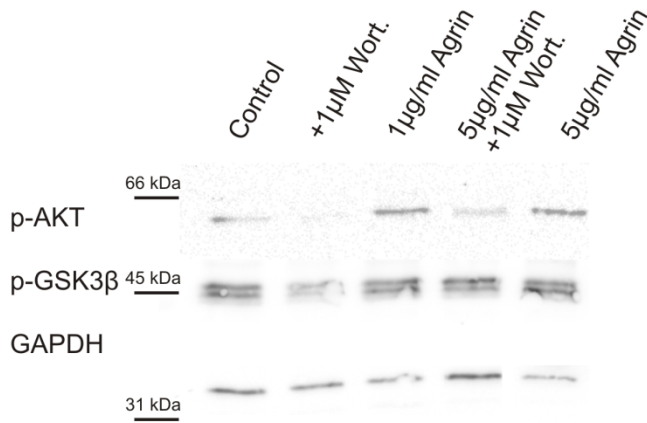


Figure 50: Western blot of PI3K downstream targets show a increase in phosphorylation after 10 min agrin incubation. Agrin stimulation for 10 min led to a strong increase in pAKT and pGSK3β in western blots (A). Higher agrin concentrations as 5μg/ml did not induces a significant change in pAKT and pGSK3β levels (B). Application of wortmannin significantly reduced the amount of pGSK3β and pAKT below control levels. Statistical analysis was done with Mann-Whitney rank sum tests. Numbers in columns in B represent individual experiments. Bar plots represent mean values + SEM.

After changing the incubation time from 10 to 30 min a less pronounced effect of PI3K stimulation was seen. AKT and GSK3β phosphorylation levels were still significantly up regulated by treatment with 1μg/ml neuronal agrin compared to untreated cells (pAKT: 168.6 %; pGSK3β: 123.8 % [1 μg/ml Agrin]; p=0.016) and wortmannin again blocked the phosphorylation of the two proteins (pAKT: 50.6 %; pGSK3β: 29.0 % [1 μg/ml Agrin]; p=0.016 and 0.008; Figure 51A and B).

A



B

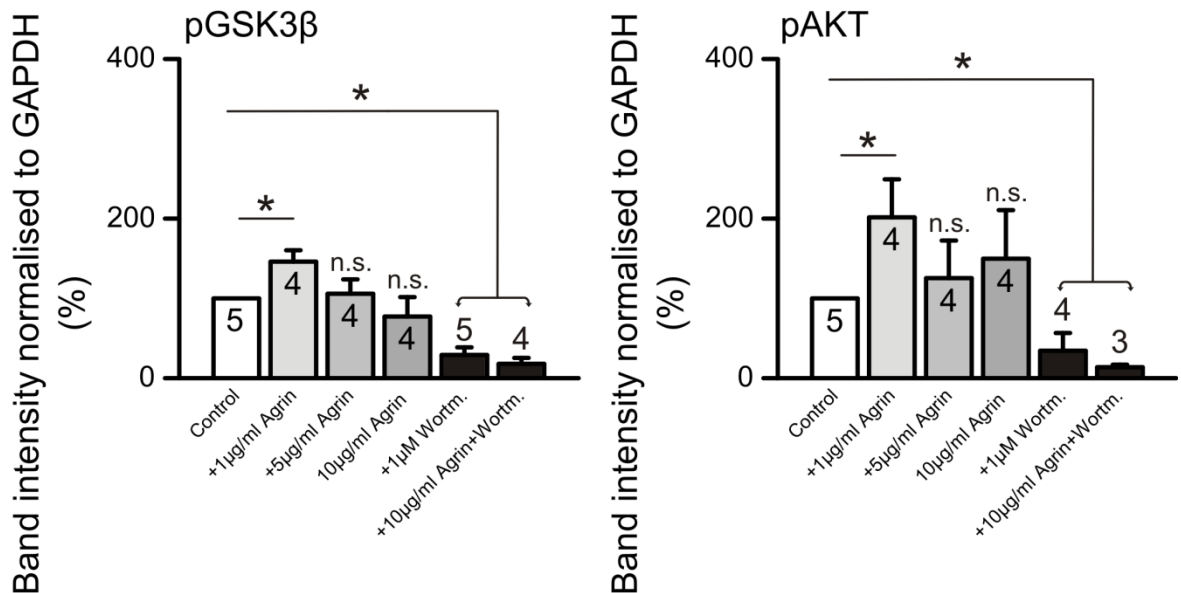
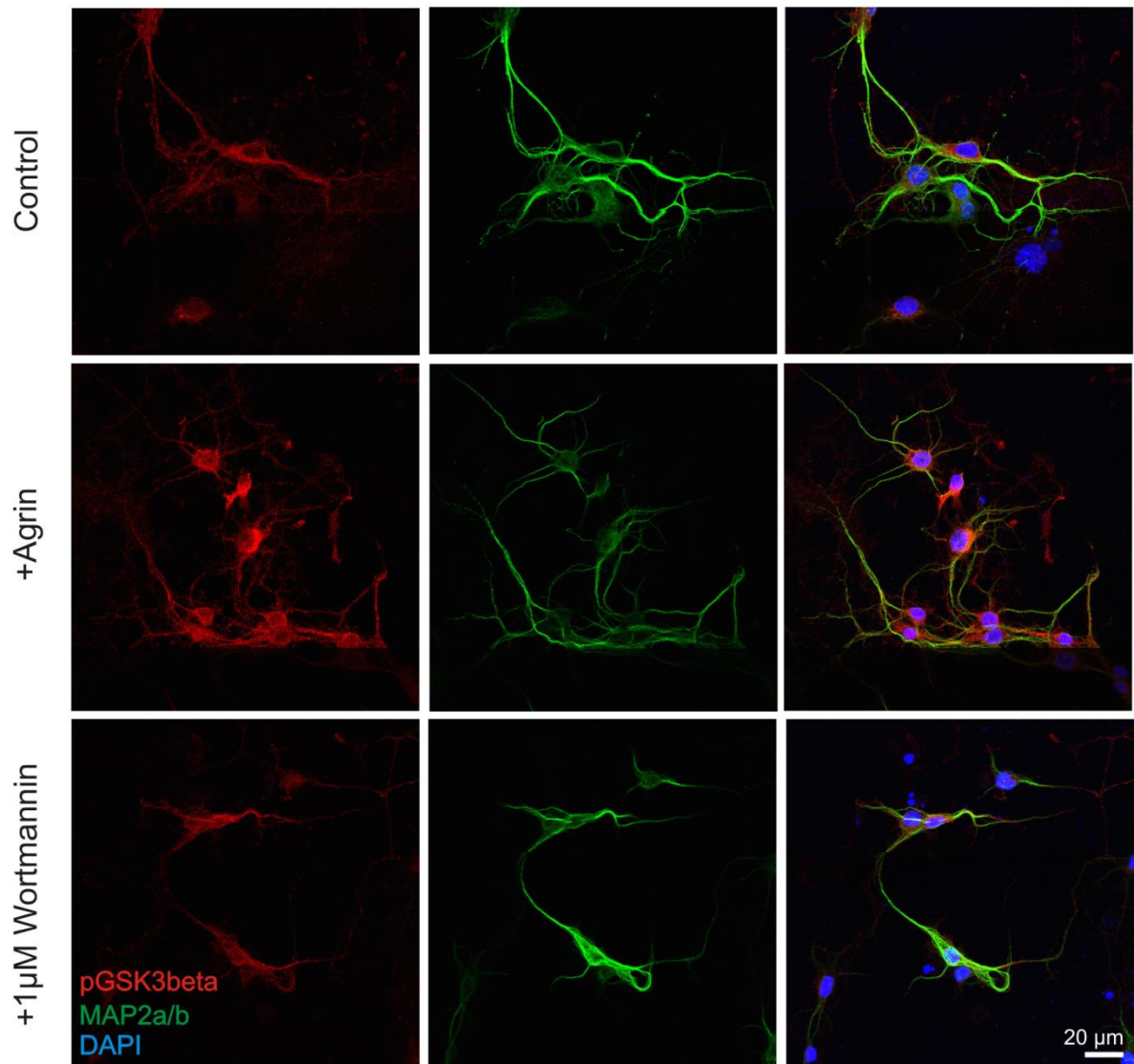


Figure 51: Western blot of PI3K downstream targets show an increase in phosphorylation after 30 min agrin incubation. Agrin stimulation for 30 min led to an increase in pAKT and pGSK3β (A). Higher agrin concentrations as 1μg/ml did not induce a significant change in pAKT and pGSK3β levels (B). Application of wortmannin reduced the amount of pGSK3β and pAKT below control levels. Statistical analysis was done with Mann-Whitney rank sum tests. Numbers in columns in B represent individual experiments. Bar plots represent mean values + SEM.

The effect on the phosphorylation status of the PI3K downstream target GSK3β was also analyzed by using immunocytochemistry. Incubation with 1 μg/ml neuronal agrin for 3-5 hours led to an increase in the fluorescence of pGSK3β in the soma of the neurons (114 % of control value; unadjusted  $p=0.0005$ ). By applying 1 μM wortmannin to the cultures the phosphorylation status of GSK3β was reduced below control values (72 % of control value; unadjusted  $p < 0.0001$ ).

These data provide evidence for the involvement of PI3K activation by agrin incubation.

A



B



Figure 52: Agrin activates PI3K in monolayer cultured neurons. Antibodies against MAP2a/b as a marker for neurons and pGSK3β as a readout for PI3K activity were used in this experiment. Stimulation with agrin led to an increase in pGSK3β fluorescence indicating an activation of PI3K (A and B). Wortmannin treatment reduced fluorescence of pGSK3β significantly below the control levels (A and B). p-values were determined with a One way ANOVA test using the multiple comparisons method after Holm-Sidak. Numbers in columns in B represent individual cells analyzed. Bar plots represent mean values + SEM.

### 3.2.10 LRP4 mRNA expression is increased in agrin-deficient cortical neurons

Known and putative agrin binding partners were screened by quantitative real time PCR to test for changes of the mRNA expression level of any of these proteins in agrin mutant E15 cortices. Agrin mRNA was not detectable in agrin mutant cortices (Figure 53A and B). The expression of LRP4, the agrin binding partner at the NMJ, showed a 1.35 fold expression increase in mRNA in agrin mutants compared to wild type tissues of littermates (Figure 53B). The expression pattern of other possible binding partners of agrin was not significantly changed in controls and agrin mutant embryos leading to the conclusion that LRP4 seems to be of importance in the cortices of embryonic agrin-deficient mice.

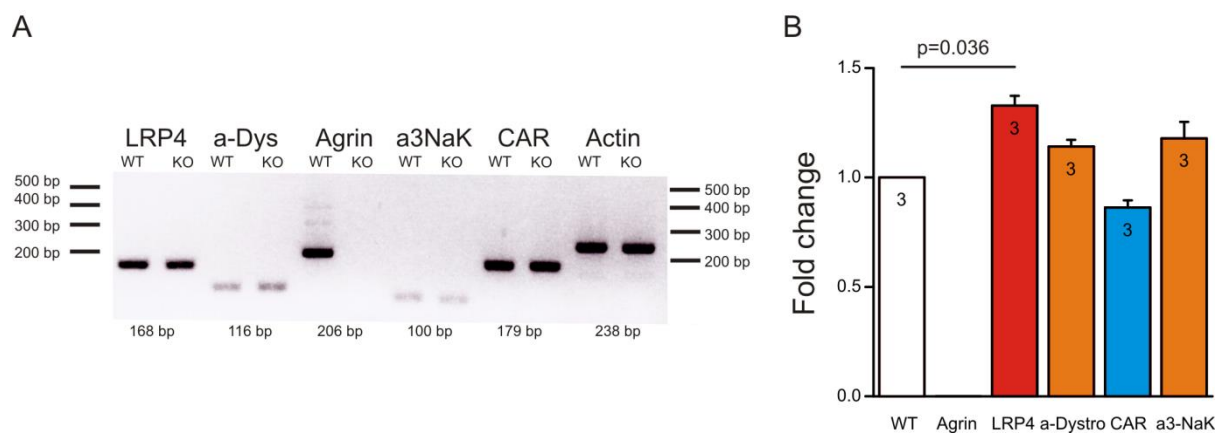
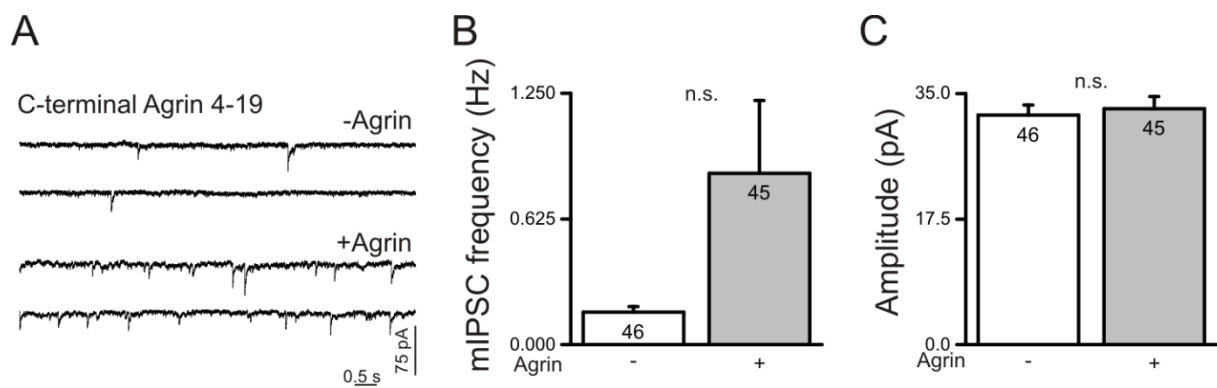


Figure 53: qRT-PCR analysis of agrin mutant embryos shows increased LRP4 mRNA expression. A 3% agarose gel was used to validate the respective sizes of the PCR products from a qRT-PCR run (A). Note the absence of transcription products in agrin KO animals. LRP4 expression was up regulated in agrin KO E15 cortices (B). A t-test was used to determine the p-value. The data was taken from three different preparations. Numbers in the columns in B represent the number of individual preparations. Bar plots represent mean values + SEM.

### 3.2.11 Incubation with a 95 kDa C-terminal agrin fragment does not change the mIPSC frequency of cortical neurons

The C-terminal fragments of agrin have been used by other investigators and have been linked to agrin function at the NMJ (Ferns et al., 1993; Gautam et al., 1996). Therefore a 95 kDa C-terminal fragment of agrin was used to investigate its effect on the mIPSC frequency of neurons in monolayer cultures. After treatment for three to five hours an increase in mIPSC frequency ( $0.161 \pm 0.028$  vs.  $0.852 \pm 0.362$  Hz;  $p=0.533$ ) could be seen but due to high variation in the mIPSC frequencies of the recorded cells statistical analysis did not reveal a significant difference compared to untreated neurons (Figure 54A and B). The amplitudes of the events were also not influenced by the treatment with this agrin fragment ( $32.0 \pm 1.4$  vs.  $32.9 \pm 1.7$  pA;  $p=0.707$ ; Figure 54C). The lack of an agrin response is surprising and will be discussed further in chapter 4.



**Figure 54: Effect on mIPSC frequency after incubation with 95 kDa C-terminal agrin.** Voltage clamp traces recorded in the presence of TTX, DNQX and APV at  $V_h = -70$  mV show an insignificant increased mIPSC frequency in agrin-treated cells (A). 1  $\mu$ g/ml agrin 4-19 increased the frequency of mIPSCs but not to a significant level (B). The amplitudes were almost similar in untreated and agrin-incubated neurons (C). Significance was tested using Mann-Whitney rank sum tests yielding p-values  $>0.05$ . Numbers in columns in B and C represent investigated individual cells. Bar plots represent mean values + SEM.

## 4. Discussion

Agrin is a well described proteoglycan known for its importance as a synaptic organizer at the neuromuscular junction however its function and binding partners in the central nervous system remain elusive. This study aimed at unraveling the role of agrin during synaptogenesis of cortical neurons in microisland and conventional monolayer cultures.

Different modes of action have been linked to agrin in the CNS. It has been implicated to be important in e.g. filopodia outgrowth (Annie et al., 2006; Matsumoto-Miyai et al., 2009; McCroskery et al., 2009), induction of c-FOS (Hilgenberg et al., 2002; Kim et al., 2003) and p-CREB (Ji et al., 1998). Its strong expression in the CNS (Burgess et al., 2000; Hoch et al., 1993; Koulen et al., 1999; Stone and Nikolics, 1995) and effects on synaptogenesis (Böse et al., 2000; Ferreira, 1999; Ksiazek et al., 2007) suggests a significant role for agrin in its development.

A mainly electrophysiological approach was pursued to investigate the effect of neuronal soluble agrin on cortical neurons of E15 embryos in monolayer and microisland cultures by adding recombinant agrin to the culture medium. Passive and active membrane properties as well as synaptic transmission were analyzed and compared between agrin-treated and untreated control cells to characterize agrin's effect on these neurons. Agrin- and LRP4-deficient neurons were treated with agrin as well to find out if endogenous agrin and LRP4, the agrin receptor at the NMJ, are required for the agrin-mediated effects during synapse development of cultured neurons.

### 4.1 Comparison of neurons in monolayer or microisland culture shows similar maturation of their active and passive membrane properties as well as synaptic properties

Since two different cell culture approaches were used in this study it is of importance to compare these characteristics of neurons cultured in those two systems. The passive and active membrane properties of the cultured neurons exhibited similar developmental processes in both cell culture types. All cells showed a decrease in input resistance ( $R_{in}$ ) and an increase in their membrane capacitance ( $C_m$ ) (Figure 16 and 38) from DIV6-8 to DIV13-15 which is in accordance with published results for hippocampal neurons (Yang et al., 1993) indicating maturational processes in these neurons over time. The amplitude of voltage-gated  $K^+$  currents increased as did the frequency of mEPSCs and mIPSCs with prolonged

culturing periods (Figure 17, 18, 38 and 39). This indicates a comparable development of these properties in the cultivated neurons that is similar as described for cultured neurons elsewhere (Barish, 1986). The properties of mEPSCs (decay, rise-time, amplitude and frequency) were similar in both culture systems and were comparable to results found in other studies (Mennerick et al., 1995; Wilcox et al., 1994) for hippocampal neurons. These data highlight that in both culture systems the neurons undergo similar developmental and maturational changes affecting their passive and active properties as well as their synaptogenesis.

## **4.2 Agrin induces excitatory synapses in microisland cultures of single neurons**

This chapter will focus on the agrin-induced effect, that is the induction of excitatory synapses, on cortical neurons cultured on astrocyte-containing microislands. The microisland culture system has the beneficial effects that solitary neurons form autapses, which are synapses onto the neuron itself, and the lack of network activity influencing synaptogenesis. Excitatory cells are more numerous and can be easily distinguished from inhibitory neurons in this system and it enables the analysis of the synaptic properties of solitary neurons.

Since less than 40% of the neurons cultivated on microislands were synaptically active at DIV5-6, older neurons from DIV13-15 were chosen for agrin-related experiments. These cells already had established synapses but they are still not fully matured (Figure 18) as the synaptic density has been shown to increase in cultured neurons between DIV15 and 21 (McCroskery et al., 2009).

### **4.2.1 Differences between GABAergic and glutamatergic neurons**

Microisland cultures provided the means to investigate the differences not only between inhibitory/GABAergic and excitatory/glutamatergic synaptic transmission but also the differences in the passive and active properties of these two types of neurons. Analysis of the morphology revealed that excitatory/glutamatergic neurons were characterized by a larger somatic diameter as their inhibitory/GABAergic counterparts and were mostly oval in shape while excitatory cells tended to have round somata (Figure 19 and 20). This was also corroborated by electrophysiological measurements reflecting a larger membrane capacitance and a smaller input resistance in excitatory compared to inhibitory cells. Miniature excitatory postsynaptic currents in these cells were defined by small amplitudes

and fast decay times whereas the mIPSCs showed large amplitudes and had slow decay kinetics (Figure 21). The analysis of voltage-gated currents showed distinct differences between the two types of neurons. Excitatory cells had larger Na<sup>+</sup> current amplitudes compared to inhibitory cells but similar current densities (Figure 20). The amplitudes for K<sup>+</sup> currents in both cell types were equal but the current density in inhibitory cells was increased compared to excitatory cells. This finding supports the idea that more K<sup>+</sup> channels per membrane area are present in the membrane of these neurons. All these data suggest that excitatory and inhibitory neurons show distinct differences in their membrane and intrinsic properties stressing the fact that these two neuronal cell types are very different from each other.

#### **4.2.2 mEPSC frequency in microisland cultures is increased by agrin treatment**

After incubation with neuronal agrin miniature postsynaptic currents were investigated. Neurons at DIV13-15 showed a strong agrin-mediated effect on the frequency and amplitude of mEPSCs but not mIPSCs (Figure 21). This indicates that mainly excitatory synapses/neurons seem to be affected by addition of agrin. Agrin has been previously shown to have an influence on excitatory synapses in CNS neurons (Böse et al., 2000; Hilgenberg et al., 2002; Ksiazek et al., 2007) corroborating the result seen in the microisland cultures used in this study. This increase in mEPSC frequency is an indication towards a change in either the presynaptic release of neurotransmitter or the number of excitatory synapses. Since decay times of the mEPSCs are not changed but their amplitude increased significantly after agrin treatment this alteration could be regulated by modifying the quantity of excitatory postsynaptic receptors (Turrigiano et al., 1998).

#### **4.2.3 Agrin incubation increases the number of excitatory synapses and clusters AMPAR at the synaptic site**

The second possible cause for the increased mEPSC frequency after agrin incubation is an increase in the number of excitatory synapses. Immunocytochemistry verified that after a three to five hour treatment with neuronal agrin indeed more excitatory synapses, revealed by co-localization of PSD95 and VGlut1+2, were visible on single excitatory neurons (Figure 22) explaining the increase in mEPSC frequency. The reason for larger amplitudes of the mEPSCs was also investigated. Staining of postsynaptic AMPAR and presynaptic VGlut1+2 showed that in agrin-treated cells AMPAR clustered around the synaptic site leading to an increased area of co-localization with VGlut1+2 (Figure 23). The data indicates that the

addition of agrin to the culture medium led to a remodeling of the postsynapse by insertion or relocation of AMPAR to the synaptic site. This clarifies the increase in mEPSC amplitude without changes in the decay kinetics of these events while also giving an explanation to the increase in the amplitude of the aEPSCs during paired-pulse experiments. Similar increases in the amplitude of AMPAR-mediated mEPSC have been described in synaptic scaling events where AMPAR are inserted at the synaptic site after blocking synaptic transmission (Ibata et al., 2008; Turrigiano et al., 1998; Wierenga et al., 2005). The lack of changes in the decay kinetics of mEPSCs after agrin treatment may indicate a lack of alteration of the subunit composition of the AMPAR (Geiger et al., 1995).

#### **4.2.4 Presynaptic release is unaffected by agrin-treatment in microisland cultures**

Presynaptic release of excitatory neurotransmitters was also investigated as a possible cause for the increased mEPSC frequency. Since single neurons grown on microislands form autaptic connections, which are self-innervating, monoaxonal connections, no external stimulation with a monopolar electrode was needed to induce aEPSCs or aIPSCs (Rost et al., 2010). Single neurons displayed a robust paired-pulse depression (PPD) in all cases investigated, indicating a high probability of neurotransmitter release. Incubation with neuronal agrin for three to five hours did not influence the paired-pulse ratio (PPR) but changes in the amplitude of the first current response were visible for aEPSCs after agrin incubation further strengthening the notion of changes at the postsynaptic site (Wierenga et al., 2005). The decay time constant of the first current response of the aEPSC was also unaffected by agrin treatment indicating no modification of the postsynaptic receptor subunit composition (Turrigiano et al., 1998). Using the quantal size of the previously analyzed mEPSCs the quantal content was determined and yielded an increase in agrin-treated neurons compared to untreated excitatory cells (Figure 24). More vesicles seem to be released on the first stimulation pulse in agrin-treated excitatory neurons as compared to untreated cells. The increase in quantal content can also be explained by an increased number of synapses or differences in postsynaptic receptor density (Kerchner and Nicoll, 2008) which is more likely the cause here. High-frequency stimulation protocols did not show a difference in the depletion of the vesicle pool between treated and untreated cells. This indicates that agrin does not exert an effect on short-term synaptic plasticity. Changes of the postsynaptic site are apparent that can be explained by the insertion of more AMPAR receptors at the synaptic site and/or a general increase of excitatory synapses, similar to

synaptic up scaling of AMPAR-mediated mEPSCs after TTX treatment or AMPAR blockade (Ibata et al., 2008; Jakawich et al., 2010).

Inhibitory synaptic current responses were never affected by agrin incubation and showed no changes in their paired-pulse ratio, amplitude, decay kinetics and quantal content (Figure 25). Also high frequency stimulation did not unravel differences in the depletion of the vesicle pool in agrin-treated and untreated control cells. These results demonstrate that in single inhibitory neurons incubation with neuronal agrin does not lead to changes in the presynaptic release apparatus. The data suggests that agrin-mediated effects in single cortical neurons might be restricted to excitatory synapses/neurons.

#### **4.2.5 LRP4 and endogenous agrin are essential for the agrin-mediated increase of mEPSCs**

Agrin and its binding partner LRP4 are essential for the development and maintenance of the NMJ. Since LRP4 has not been thoroughly described in the CNS at first the expression of this receptor in cortices of wild type animals was investigated. Strong expression of LRP4 in embryonic and young postnatal mice and a decrease in mature stages was observed in western blots indicating a role for LRP4 in the development and maturation of the cerebral cortex.

Using astrocyte microislands from LRP4-deficient embryos, cortical neurons, also harvested from LRP4-deficient embryos, were investigated by whole cell patch clamp experiments. In a first step the passive membrane properties of these cells were compared to wild type neurons from C57BL/6N animals. LRP4 neurons showed significant differences in their input resistance, membrane capacitance and somatic diameter compared to wild type cells indicating a faster development of these properties (Figure 30). The maximal K<sup>+</sup> current amplitudes were significantly higher which is also in accordance to the other observations. This shift in development also explains the moderate but significant increase in mEPSC frequency in LRP4-deficient neurons compared to wild type neurons since mPSC frequency rises with prolonged days *in vitro* (Mozhayeva et al., 2002) . Incubation with neuronal agrin did not increase mEPSC frequency and amplitudes in LRP4-deficient neurons corroborating the notion that agrin signaling is dependent on LRP4 as a cofactor/-receptor at excitatory cortical synapses (Figure 31). The fact that LRP4 interacts biochemically with the PDZ domains of PSD95 and SAP97 further stresses the validity of the here acquired data and the

authors argument that also an interaction with AMPAR and NMDAR may be possible (Tian et al., 2006). As  $\alpha$ SAP97 has been shown to regulate synaptic pools of AMPAR (Li et al., 2011) this interaction may be a cause of increased AMPAR-mediated synaptic transmission as seen in wild type neurons after agrin incubation. A very recent paper on LRP4 in the hippocampus highlighted its importance for learning (Gomez et al., 2014). Mice with rescued LRP4 expression in muscle displayed cognitive defects and showed a decreased frequency in mEPSCs of CA1 pyramidal neurons and a reduction in spine density on their apical dendrites (Gomez et al., 2014). Although this effect was not seen in the microisland experiments with LRP4-deficient neurons, maybe due to differences in the preparations, it is obvious that LRP4 is of great importance for the synaptic development in the CNS.

The same electrophysiological set of experiments that was used for LRP4-deficient neurons was also conducted on agrin-deficient neurons. The passive properties of agrin-deficient neurons were not different from wild type cells from C57BL/6N animals. Only the  $K^+$  current related properties were decreased in agrin-deficient cells (Figure 32). The frequency of mEPSCs was reduced compared to wild type cells and only after agrin-treatment increased back to the level of untreated control neurons from wild type C57BL/6N animals (Figure 33). The increase in mEPSC frequency after agrin treatment was not significant and thus seems to be also dependent on endogenous agrin to be adequately induced.

In conclusion agrin and LRP4 are important for synaptogenesis but not essential since neurons lacking either of the proteins were still capable of forming functional synapses.

#### **4.2.6 Agrin induces PI3K signaling in single neurons**

PI3K activation by agrin stimulation was investigated by using immunocytochemistry of GSK3 $\beta$  to monitor phosphorylation of this PI3K target in single cortical neurons since western blots of single cells were impossible to realize. GSK3 $\beta$  functions as read-out for the activity PI3K. Its involvement in synaptic processes has been previously shown as it forms complexes with AMPAR stressing the importance of PI3K signaling in LTP (Peineau et al., 2007). After incubation with neuronal agrin, the cells showed a stronger fluorescence of the phosphorylated form of the PI3K downstream target GSK3 $\beta$  compared to untreated control cells and neurons with blocked PI3K only had residual fluorescence comparable to background levels (Figure 35). These results suggest that PI3K is activated by agrin. To further strengthen the assumption that PI3K signaling is needed for the agrin-mediated

increase in mEPSCs frequency a physiological approach was employed using selective blockers of PI3K. As a first step the effects of PI3K blockers on basal synaptic transmission were tested. Incubation for three to five hours with the specific PI3K blocker wortmannin did not reduce the basal level of mEPSCs compared to untreated control cells and did also not affect the amplitudes of these events. LY294002 on the other hand did lower the mEPSCs frequency significantly below the level of untreated control cells indicating a presynaptic effect on the spontaneous fusion of synaptic vesicles without affecting the amplitude of the mEPSCs. Treatment with 50  $\mu$ M LY294002 may be interfering with the processes necessary for the fusion or docking of synaptic vesicles e.g. by preventing priming of vesicles via synaptotagmin (Schiavo et al., 1997). Application of either blocker together with neuronal agrin did not increase mEPSC frequency showing that PI3K signaling is essential for the remodeling of already established synapses or the induction of new excitatory synapses (Figure 36). PI3K has been shown to be associated with AMPAR receptors (Man et al., 2003), is implicated in the induction of LTP (Opazo et al., 2003; Sanna et al., 2002) and has also been shown to be needed for the insertion of AMPAR during LTP of mEPSCs (Baxter and Wyllie, 2006; Man et al., 2003) resulting in an increase of the mEPSC amplitude. This increase in mEPSC amplitude and frequency was achieved by stimulating NMDAR with glycine (Man et al., 2003). Since NMDAR are blocked under the conditions used in this study the agrin-induced mechanism needs to be NMDAR-independent. Baxter and Wyllie (2006) discuss a possible calcium-dependent way that leads to PI3K activation and AMPAR insertion that is not being NMDAR-driven. Agrin-signaling has also been linked to increases in intracellular calcium (Hilgenberg and Smith, 2004) as has been the activation of PI3K after reelin stimulation, which increases intracellular calcium as well (Bal et al., 2013). Thus intracellular increases in calcium might further explain the agrin-induced effects.

The insertion of AMPAR to the synaptic site is mainly regulated by the interaction of stargazin and PSD95 (Chen et al., 2000; Schnell et al., 2002). This may indicate that these molecules would be also needed in agrin-mediated processes where AMPARs are shuttled to the synaptic site leading to an increase in mEPSC amplitude.

Application of rapamycin, a blocker of mTOR, prevented effectively the increase in mEPSC frequency by agrin making the involvement of mTOR in agrin-mediated signaling very likely. As it has been shown for PI3K also mTOR has a relevance for shaping dendritic morphology

in neurons (Kumar et al., 2005; Urbanska et al., 2012) and could thus be an important factor for agrin-related signaling.

Taking all these findings into account agrin signaling is activating PI3K/mTOR, maybe through increases in intracellular calcium leading eventually to an insertion of AMPAR into the synaptic site membrane and the induction of new synapses.

#### **4.2.7 Agrin incubation does not influence voltage-gated Ca<sup>2+</sup> currents**

Agrin has been previously shown to be able to induce an increase in voltage-gated Ca<sup>2+</sup> currents in myotubes, an increase in intracellular Ca<sup>2+</sup> concentration in cortical neurons and PI3K to mediate voltage-gated Ca<sup>2+</sup> channel translocation to the membrane of COS7 cells and DRG neurons (Bandi et al., 2008; Hilgenberg et al., 2002; Viard et al., 2004). Pharmacological isolation of Ca<sup>2+</sup> currents in microisland cultures of cortical neurons and comparison of untreated control cells with agrin-incubated cells indicated no difference in the density of the voltage-gated Ca<sup>2+</sup> currents (Figure 37). The changes seen in myotubes could not be recapitulated in this experiment set showing that agrin has no effect on the density of Ca<sup>2+</sup> currents in neurons. PI3K also does not seem to be affecting the translocation of Ca<sup>2+</sup> channels, as described in DRGs by Viard et al., 2004, in cultured cortical neurons even though the kinase is activated in neurons after the addition of agrin. Since agrin has been shown to increase intracellular calcium concentrations in neurons (Hilgenberg and Smith, 2004) one could argue that this effect must be immediate and cannot be seen after three to five hours of incubation. Thus agrin may activate VGCC only shortly after application.

#### **4.2.8 A proposed model for agrin-mediated signaling in single excitatory neurons**

The increase in mEPSC frequency, amplitude and excitatory synapse number after incubation with soluble neuronal agrin has been demonstrated to depend to some extent on the interaction of endogenous agrin, LRP4 and the activation of the PI3K/mTOR pathway. Here, I propose a mechanism in which soluble agrin might enhance agrin-mediated signaling at excitatory synapses (Figure 55).

Adding soluble neuronal agrin to the cultured neurons seems to increase existing agrin-mediated signaling dependent on the interaction of LRP4 and agrin (Figure 55A). Since it was already shown that MuSK is also expressed in the brain (Ksiazek et al., 2007) it cannot be ruled out that this kinase plays an integral part in agrin-mediated signaling in the CNS and may be activating PI3K/mTOR. Increases in intracellular calcium, coming from VGCC and

internal stores, have also been attributed to the stimulation with agrin in neurons (Hilgenberg and Smith, 2004). This increase in calcium could activate AMPAR-associated PI3K (Man et al., 2003) leading to the protein synthesis of novel AMPARs, the induction of new synapses and also preventing lateral diffusion of these receptors (Borgdorff and Choquet, 2002). This increase must stem from an immediate reaction to agrin stimulation because VGCC expression was not altered by agrin. Interaction between LRP4, PSD95 and SAP97 via their PDZ domains might help to stabilize AMPARs at the synaptic site (Tian et al., 2006). Blocking PI3K/mTOR signaling with wortmannin, LY294002 or rapamycin abolishes the agrin-mediated effect on the frequency of mEPSCs and may prevent the synthesis/insertion of AMPAR at newly generated synaptic sites (Figure 55B). A genetic knock out of components of the agrin receptor complex (Agrin, LRP4 and presumably MuSK) also prevents agrin-mediated signaling in excitatory cortical neurons abolishing the increase in mEPSC frequency (Figure 55C and D). This model is further strengthened by the observation that agrin-deficient mice rescued by transgenic expression of agrin in motor neurons show a selective reduction of excitatory synaptic transmission (Ksiazek et al., 2007). Furthermore, LRP4-deficient mice, rescued from perinatal death by transgenic LRP4 expression in muscle, show severe learning deficits and reduced excitatory synaptic transmission (Gomez et al., 2014). These findings clearly demonstrate the importance of agrin/LRP4 signaling for synaptic development.

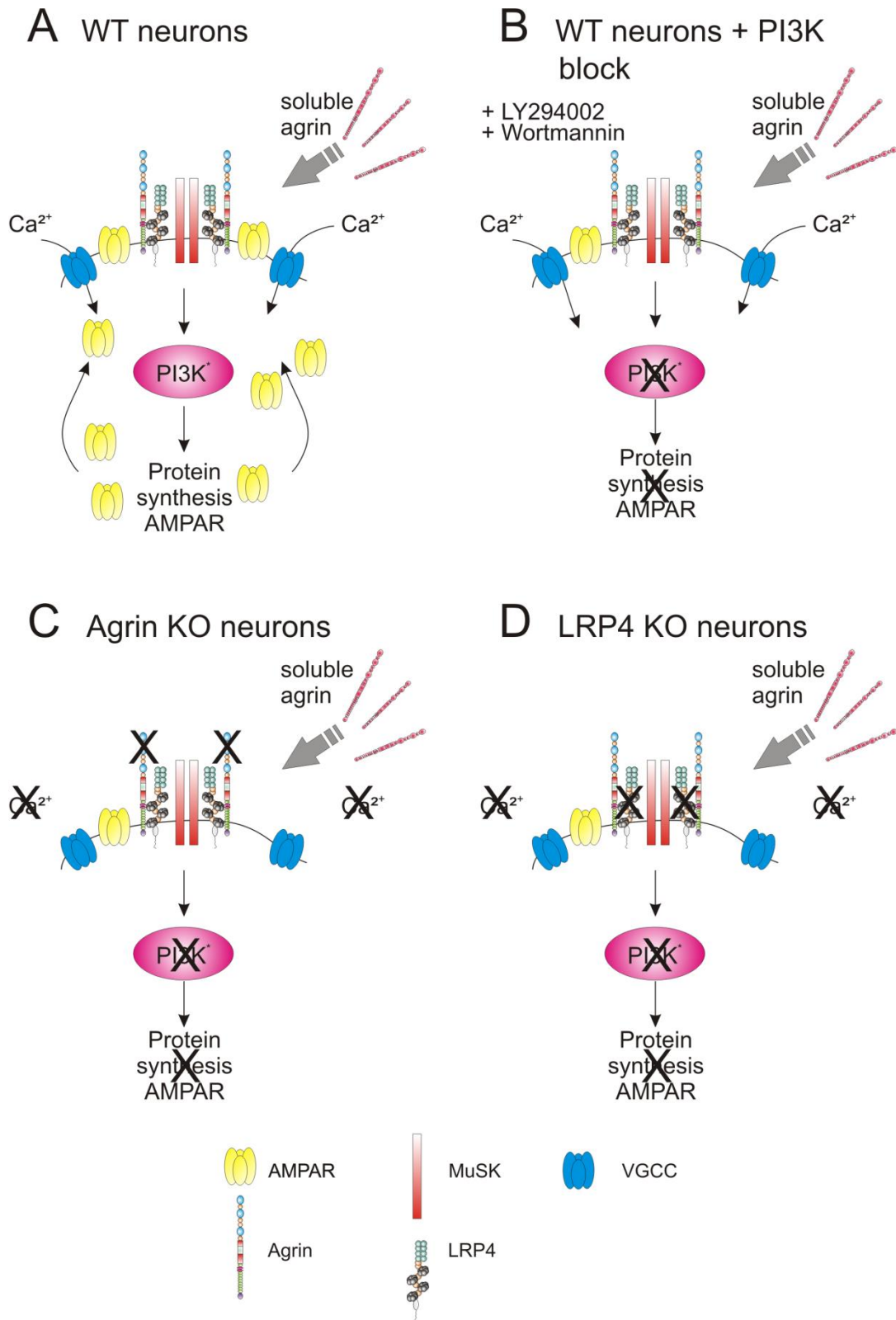


Figure 55: A proposed model for agrin-mediated signaling at excitatory synapses of single neurons. (A) Adding soluble neuronal agrin to the culture medium stimulates agrin-signaling by interaction with LRP4/Agrin probably by activating MuSK. Calcium entry through VGCC and from intracellular stores and agrin signaling activate PI3K leading in turn to protein synthesis, insertion and immobilization of AMPAR at the synaptic site and the induction of new synapses. (B) Blocking PI3K with wortmannin or LY294002 stops the signaling of PI3K and also stops the insertion of AMPAR and induction of new synapses. (C) Knock out of agrin also inhibits PI3K activation as does the knock out of LRP4 (D).

### 4.3 Agrin increases the mIPSC frequency in monolayer cultures of cortical neurons

This part of the discussion will focus on the agrin-mediated effects on monolayer cultures of cortical neurons.

#### 4.3.1 mIPSC frequency in monolayer cultures is increased by agrin treatment

Since miniature postsynaptic currents represent currents induced by spontaneous fusions of single vesicles they are a good tool to investigate synaptic properties through electrophysiological means. In monolayer cultures different cell types are present. GABAergic as well as glutamatergic neurons form vast networks of synaptic contacts with one another. Under these conditions a specific effect on inhibitory synaptic transmission in neurons that were cultured for 6-8 days *in vitro* was found. Neurons incubated for three to five hours with neuronal agrin showed an increase in their mIPSC frequency (Figure 39). This effect was not evident in cells that were cultivated for 13-15 days *in vitro* indicating a specific time window for the induction of the changes seen here (Figure 39). It also seemed to be specific for the type of synapse since only inhibitory postsynaptic currents were affected indicating specificity for an agrin interaction at inhibitory synapses. One could think of a synapse specificity for agrin as has been described for  $\alpha$ -dystroglycan with GABAergic synapses (Pribrag et al., 2014) or NL-2 inducing inhibitory synapses (Chih et al., 2005). The change in mIPSC frequency was time-dependent (Figure 42) and was not apparent after just one hour of treatment indicating that there are processes activated that require time for e.g. protein synthesis. Increasing the agrin concentration from 0.5  $\mu\text{g/ml}$  to 1  $\mu\text{g/ml}$  did not further increase the frequency of mIPSCs (Figure 43) indicating that there is a saturation of the agrin response as has been shown for the clustering of AChR at the NMJ (Ferns et al., 1993; Gesemann et al., 1995; Nitkin et al., 1987; Reist et al., 1992). At a concentration between 0.5 to 1  $\mu\text{g/ml}$  the increase in mIPSC frequency is maximal. Surprisingly the use of a 95 kDa C-terminal agrin fragment containing four amino acid inserts at the A and 19 at the B splice site did not induce a significant change in mIPSC frequency in neurons at DIV6-8 (Figure 54) even though this isoform had been previously shown to have the same synapse inducing and stabilizing powers at the NMJ as full-length agrin (Campagna and Fallon, 2006; Gesemann et al., 1995). It could be possible that in the case of the central synapse other agrin domains at the more N-terminal region are required for the effect seen here, as has been described for the induction of filopodia. Here the seventh follistatin-like domain is

necessary to induce filopodia-like processes in neurons and non-neuronal cells (Porten et al., 2010).

#### **4.3.2 The increase in mIPSC frequency is not caused by an increase in the number of inhibitory synapses**

A possible cause for the increase in the frequency of miniature postsynaptic currents is often associated with an increase in the number of synapses or dendritic spines (Tyler and Pozzomiller, 2001). By employing immunocytochemistry co-localization of pre- and postsynaptic proteins (VGAT and gephyrin) for inhibitory synapses was examined. Surprisingly no difference in the number of co-localized puncta was apparent after three to five hours of agrin incubation between untreated and agrin-treated neurons at DIV6-8 (Figure 44). The lack of the increase in synapse number is not a result that negates the other effects seen for agrin-treated cells since one could also expect an increase in miniature postsynaptic current frequency caused by presynaptic changes influencing the release of neurotransmitters.

#### **4.3.3 The presynaptic release is unaffected by treatment with neuronal agrin**

The analysis of the presynaptic release properties of neurons is an important method to investigate changes at the presynaptic site (see Regehr, 2012 for a review of these mechanisms). Changes in the release machinery could also explain the effect on the mIPSC frequency in agrin-treated cells. All cells investigated showed a prominent paired-pulse depression (PPD) indicating a high release probability of synaptic vesicles that has been described at many vertebrate synapses (Debanne et al., 1996; Scheuss et al., 2002; Wilcox and Dichter, 1994) and was also seen in neurons of microisland cultures. This PPD was not modified by agrin incubation. The paired-pulse ratio (PPR) was also not affected and stayed on almost the same level as in untreated neurons indicating no change at the presynaptic transmitter release behavior (Figure 45). Since single neurons on microislands behaved similar to neurons in monolayer cultures it seems plausible that inhibitory presynaptic release is indeed not influenced by agrin incubation.

#### **4.3.4 The readily releasable pool (RRP) is unaffected by agrin treatment**

The readily releasable vesicle pool is defined as a subset of vesicles that are tethered to the active zone's membrane and are ready for immediate release. When cells are stimulated with high osmolality sucrose this pool will be rapidly depleted and the current response can be used to determine the charge of the response thus giving insights on the size of the RRP

(Rosenmund and Stevens, 1996; Stevens and Tsujimoto, 1995). Since the PPR and the number of synapses were unaffected by agrin treatment the RRP was considered to be influenced by agrin incubation. A larger pool of docked vesicles being ready for immediate release would be a way to explain the changes in the mIPSC frequency seen after agrin treatment since the possibility for spontaneous vesicle fusions would be much higher as in neurons with a normal sized RRP. A high amount (1 µg/ml) of neuronal agrin was used to yield maximal effects. The data obtained in this set of experiments did not show changes in the size of the RRP after treatment with neuronal agrin compared to untreated neurons though, leaving no explanation for the agrin induced effect on the mIPSC frequency in monolayer cortical cultures (Figure 46).

#### **4.3.5 Agrin-deficient neurons do not react to external agrin stimuli and express more LRP4 mRNA**

The lack of an agrin-mediated increase in mEPSC or mIPSC frequency in agrin-deficient neurons has been demonstrated in voltage clamp experiments (Figure 49). This leads to the following assumption. It could be possible that endogenous agrin is essential for the effect on mIPSC frequency of neurons in monolayer cultures to be elicited. Agrin may not be the essential for synaptogenesis, since synapses also form in agrin mutant neurons, but may play an important part in it. A biochemical study has shown that a short version of agrin is indeed capable of dimerization as well as oligomerization (Patel et al., 2011) making the assumption of an agrin-agrin interaction feasible.

Quantitative real-time PCR of agrin-deficient E15 cortical tissues showed a slight increase in LRP4 expression (Figure 53). A possible way to explain this result may be that the neuronal network could be trying to compensate for the lack of agrin-mediated signaling by up regulating the expression of LRP4 mRNA thus trying to strengthen the signaling cascade again. A similar mechanism has been described for synaptic scaling of excitatory synapses after TTX treatment (Ibata et al., 2008; Wierenga et al., 2005). Again, these data seem to further corroborate the interaction of agrin and LRP4 in the CNS.

#### **4.3.6 Agrin induces PI3K signaling in neurons of monolayer cultures**

Since it had been shown that agrin is able to induce PI3K signaling in myotubes (Schmidt et al., 2012) it was of interest to find out if this also was true for cultured neurons. After stimulation with neuronal agrin and harvesting of the cells one could see a robust

stimulation of the phosphorylation of PI3K downstream targets GSK3 $\beta$  and AKT in western blots (Figure 50 and 51) and in immunocytochemical staining of pGSK3 $\beta$  (Figure 52) activation of PI3K by agrin incubation in cortical neurons was observed. The results obtained here were similar to the ICC experiments in microisland cultures (Figure 35) which further corroborates PI3K's involvement in agrin-mediated signaling.

The fact that different publications show that PI3K signaling is important for neurite outgrowth, dendritic morphology and is implicated in LTP (Cosker and Eickholt, 2007; Man et al., 2003; Sánchez et al., 2004) also makes PI3K a possible candidate for agrin-mediated signaling in neurons of the CNS.

#### **4.4 Agrin incubation is not affecting input resistance, cell capacitance and voltage-gated K<sup>+</sup> currents**

The treatment with neuronal agrin did not influence the passive properties of neurons in monolayer as well as in microisland cultures (Figure 26, 47 and 48). The input resistance and membrane capacitance of agrin-treated neurons were comparable to untreated control cells. Only in microisland cultures a small increase in the membrane capacitance of agrin-treated cells was apparent (Figure 26). This increase was not seen when the specific membrane resistance was computed, indicating that the neuron's size is not affected by agrin treatment. Analysis of the K<sup>+</sup> current properties shows similar current responses in untreated and agrin-incubated neurons highlighting the fact that there is no obvious effect on this kind of conductance through agrin (Figure 26 and 48). Current-voltage-plots of these K<sup>+</sup> currents were almost identical indicating no changes of the K<sup>+</sup> conductance through agrin treatment.

#### **4.5 Differences between monolayer and microisland cultures of cortical neurons**

Though monolayer and microisland cortical cell cultures shared some of their properties (e.g. development of passive and active membrane properties) there were some differences in the agrin-related experiments. It was evident that agrin mainly influenced the frequency of mIPSC in monolayer cultures whereas it was exclusively having significant effects on the frequency of mEPSC in microisland cultures. A possible explanation might be the reason that during development of monolayer cultures neurons are constantly in contact with a multitude of other neurons. Throughout their development there may be processes at work

that balance inhibition and excitation in a way that masks agrin-mediated effects on excitatory synapses making them not as prominent as in single excitatory neurons where network activity is absent. Although neurons in monolayer culture exhibited miniature postsynaptic currents at early stages of development (starting at DIV4, personal observation) less than half of the single neurons at DIV5-6 grown on microislands were synaptically active indicating a slower synaptic maturation in microisland cultured neurons because of a lack of possible synaptic partners in close vicinity. The data showing that GABAergic synapses in single inhibitory neurons are not affected by agrin-treatment could be due to the fact that GABAergic synapses appear earlier in development (around DIV4) meaning that the single neurons on microislands were already beyond their agrin-sensitive stage as neurons in monolayer cultures also do not respond to agrin at DIV13-15.

In general, single neurons cultured on microislands of astrocytes are valuable tools for the investigation of synaptogenesis and maintenance due to the fact that only mono-axonal stimulation determines the synaptic vesicle release in paired-pulse experiments and only one type of synapse (inhibitory or excitatory) is present when only one neuron is located on an island. Monolayer cultures on the other hand form very dense and extensive networks so one can never know how many axons/cells will be stimulated by using extracellular electrodes or how many synaptic contacts from different cells arrive at the cell patched.

#### **4.6 Homophilic agrin interactions**

The ability of agrin to bind to itself has been discussed as a possible mechanism for the agrin-induced effect on miniature postsynaptic current frequency. To test this interaction a biochemical approach was undertaken using ELISA. Unlabeled agrin was immobilized and incubated with biotinylated agrin using streptavidin coupled to HRP for detection. This colorimetric assay did not indicate significant binding of agrin to agrin since BSA-coated wells showed stronger absorbance as the ones incubated with agrin solution (Figure 34). This does not mean that there is indeed no interaction between agrin molecules since the assay is a very reductionist approach. Agrin molecules could be already aggregated to one another before the incubation with agrin-biotin so that a possible binding would be impossible to achieve or biotinylation could cause conformational changes obstructing binding sites. In conclusion this assay may not be suitable to detect an agrin-agrin interaction.

## 4.7 Outlook

Further studies will focus on the importance of LRP4 at the central synapse. Co-localization studies with synaptic proteins will shed further light into the expression of LRP4 in the central nervous system. A possible explanation for the effect on excitatory synapses in single neurons would be a restriction of LRP4 expression to only excitatory synapses. A tamoxifen-inducible LRP4 overexpression mutant mouse line using CaMKII to drive the overexpression, generated in the lab of Stephan Kröger, could be used to unravel agrin's interaction with LRP4 in the CNS by using brain slices of these animals. Incubation with neuronal agrin might induce even stronger synaptic changes in these animals and due to the type of preparation the cortical architecture would remain mostly intact which is preferable from cell cultures. Since MuSK is also expressed in the brain (Ksiazek et al., 2007) transgenic knock out mice will be used to analyze the synaptic properties of cortical neurons from these animals and their reaction to the stimulation with neuronal agrin will be investigated by patch clamp experiments using microisland cultures. Although MuSK is an integral part of the agrin signaling machinery at the NMJ it is currently unknown whether agrin might influence the mEPSC frequency/synaptogenesis of MuSK-deficient neurons. As for LRP4, the expression of MuSK at central synapses will be examined by immunocytochemistry with antibodies generated in rabbits against a recombinant purified MuSK protein. Co-localization with other synaptic markers will be employed to find out whether MuSK is only located to a subset of synapses or ubiquitously expressed. Concerning the PI3K signaling experiments also LRP4 and agrin-deficient neurons have to be investigated and the responsiveness of PI3K to agrin-induced stimuli needs to be assessed. One would suspect no difference in PI3K signaling even after agrin incubation in these neurons if LRP4 and agrin are indeed necessary for the activation of PI3K. These data would corroborate the already performed electrophysiological experiments on wild type neurons. With the aid of recombinant agrin the necessity of the neuronal splice site insert will be investigated. Therefore a full-length agrin variant devoid of any amino acid inserts has already been purified from HEK293 cells and will be tested as well as another commercially available C-terminal 44 kDa agrin fragment (Hettwer et al., 2014) in microisland cultures of cortical neurons.

## 4.8 Conclusions

In this study mainly electrophysiological approaches were undertaken to identify a role for the synaptic organizer agrin at the central synapse of cultured cortical neurons. Cortical neurons from wild type E15 embryos were incubated with soluble agrin for three to five hours and their passive and active membrane properties as well as their synaptic properties investigated. Two culture systems were chosen, single neurons cultivated on microislands of astrocytes and conventional monolayer cultures. Only single excitatory neurons were affected by agrin incubation in microisland cultures and revealed an increased mEPSC frequency and amplitude. The increase in mEPSC frequency was not due to changes in presynaptic neurotransmitter release but caused by an increase in the number of excitatory synapses. The larger amplitude of the mEPSCs was associated with an increased area and incidence of AMPAR clusters in agrin-treated cells. Analysis of LRP4- and agrin-deficient cells in the microisland culture system revealed a lack of responsiveness to extracellular applied agrin indicating a dependency on these molecules for agrin signaling. Western blots and ICC revealed that PI3K is activated by agrin incubation and blocking PI3K with wortmannin and LY294002 in single excitatory neurons stopped the agrin-mediated changes in mEPSC frequency and amplitude indicating an involvement of PI3K in agrin-mediated signaling in cortical neurons. Since PI3K has been linked to LTP and AMPAR trafficking this corroborates the results obtained in this study.

Neurons grown in conventional monolayer cultures reacted in a different way to the addition of neuronal agrin. These cells displayed an increase in mIPSC frequency that was time and concentration dependent. However this finding could neither be supported by an increase in inhibitory synapse number nor by an increase in neurotransmitter release. Agrin-deficient neurons also did not react to agrin treatment. The involvement of PI3K in agrin-signaling could be demonstrated in western blots and ICC.

Since monolayer cultures build vast neuronal networks the lack of an explanation for the mIPSC increase after agrin incubation could be caused by network activity overshadowing the agrin-mediated effect.

## 5. Summary

The proteoglycan agrin is an integral part and of utmost importance in the development and maintenance of the neuromuscular junction of vertebrates. Even though it is expressed at developmental stages in the central nervous system its role in synaptogenesis is currently unknown. By employing the whole cell patch clamp technique agrin's effect on the synaptogenesis of cortical neurons in microisland and conventional monolayer cultures was investigated in this thesis. In microisland cultures of single cortical neurons excitatory and inhibitory neurons could be investigated separately. Incubation with soluble agrin for three to five hours led to a robust increase in mEPSC frequency and amplitude in these cultures. Neurotransmitter release and the number of excitatory synapses were investigated. The paired-pulse ratios of agrin-treated cells remained unchanged but the current amplitudes were larger after agrin incubation. Studies on the co-localization of VGlut1+2 and PSD95 showed that treatment with soluble agrin increased the number of co-localized puncta. Stainings with antibodies against AMPAR revealed a larger area of AMPAR clusters and more AMPAR/VGlut1+2 co-localized puncta in agrin-treated cells opposed to VGlut1+2 positive areas. This observation explains the increase in mEPSC amplitude and frequency by an increased number of AMPAR-containing excitatory synapses. Endogenous agrin and the presence of the agrin receptor LRP4 are necessary to induce the increase in mEPSC frequency since LRP4- and agrin-deficient neurons were unable to react to agrin treatment demonstrating the importance of these proteins. The mechanism behind this increase was shown to be related to PI3K/mTOR signaling. Incubation with neuronal agrin led to increased phosphorylation of GSK3 $\beta$  in immunostainings of single cortical neurons and blocking PI3K/mTOR with wortmannin, LY293002 or rapamycin abolished agrin-mediated effects on the increase of the mEPSC frequency. The data suggest that agrin might influence synaptogenesis in cortical neurons by activating PI3K/mTOR signaling leading to the formation of new excitatory synapses.

In contrast to microisland cultures conventional monolayer cultures of neurons showed an increase in the frequency of mIPSCs after treatment with soluble agrin for three to five hours. This effect was time and concentration dependent. However changes in the release probability of neurotransmitters and changes in the number of inhibitory synapses were not discovered. Paired-pulse ratios were unaffected by agrin treatment as well as the number of inhibitory synapses. The analysis of agrin-deficient neurons showed no increase in mIPSC

frequency after agrin treatment suggesting that endogenous agrin important for proper signal transduction.

In summary microisland cultures are a suitable tool to investigate synaptogenesis with electrophysiological and immunocytochemical methods. Using this experimental approach, this study demonstrated that agrin is important during synaptogenesis or synapse maintenance in cortical neurons but not essential.

## 6. Zusammenfassung

Das Proteoglykan Agrin ist ein integraler Bestandteil von äußerster Wichtigkeit bei der Entwicklung und Aufrechterhaltung der neuromuskulären Endplatte von Vertebraten. Obwohl es auch während der Entwicklung des zentralen Nervensystems exprimiert wird, ist seine Rolle in der Synaptogenese noch ungeklärt. Mit Hilfe der whole-cell Patch-Clamp-Technik wurde die Wirkung von Agrin bei der Synaptogenese von kortikalen Neuronen in microisland und konventionellen Kulturen in dieser Arbeit untersucht. In microisland Kulturen konnten einzelne exzitatorische sowie inhibitorische Neurone getrennt voneinander untersucht werden. Inkubation mit löslichem Agrin führte in diesen Kulturen zu einem robusten Anstieg der mEPSC Frequenz und ihrer Amplitude. Die Neurotransmitterausschüttung und die Anzahl der exzitatorischen Synapsen wurde untersucht. Das Paired-pulse-Verhältnis blieb unverändert verglichen mit unbehandelten Kontrollneuronen aber die Stromamplituden waren größer nach der Inkubation mit Agrin. Kolokalisationsstudien von Vglut1+2 und PSD95 zeigten einen Anstieg der kolokalisierten Puncta nach der Behandlung mit löslichem Agrin. Färbungen mit Antikörpern gerichtet gegen AMPAR offenbarten eine größere Fläche von AMPAR-Anhäufungen gegenüberliegend von VGlut1+2 positiven Arealen sowie mehr kolokalisierte AMPAR/VGlut1+2 puncta in Agrin-behandelten Zellen. Diese Beobachtung erklärt den Anstieg der mEPSC Frequenz und Amplitude durch eine erhöhte Anzahl an AMPAR-enthaltenden exzitatorischen Synapsen. Endogenes Agrin und das Vorhandensein des Agrinrezeptors LRP4 sind notwendig, um den Anstieg der mEPSC-Frequenz zu induzieren, da LRP4- und agrindefiziente Neurone nicht in der Lage waren auf die Agrinbehandlung zu reagieren, was die Wichtigkeit dieser Proteine unterstreicht. Der Mechanismus der hinter diesem Anstieg liegt ist verbunden mit dem PI3K/mTOR Signalweg. Die Inkubation mit löslichem Agrin führte zu einer erhöhten Phosphorylierung von GSK3 $\beta$  in Immunfärbungen von einzelnen kortikalen Neuronen und die Blockade von PI3K/mTOR mit Wortmannin, LY294002 oder Rapamycin hob den Agrin-vermittelten Effekt auf die Zunahme der mEPSC Frequenz auf. Diese Daten lassen vermuten, dass Agrin einen Einfluss auf die Synaptogenese in kortikalen Neuronen durch die Aktivierung des PI3K/mTOR Signalwegs ausübt und zur Bildung neuer exzitatorischer Synapsen führt.

Im Unterschied zu microisland Kulturen zeigten konventionelle einschichtige Neuronenkulturen einen Anstieg in der Frequenz von mIPSCs nach einer drei bis fünf

stündigen Behandlung mit löslichem Agrin. Dieser Effekt war zeit- und konzentrationsabhängig. Allerdings wurden weder Veränderungen im Verhalten bei der Neurotransmitterausschüttung noch in der Anzahl von inhibitorischen Synapsen entdeckt. Das Paired-pulse-Verhältnis blieb unverändert durch die Agrinbehandlung genau wie die Anzahl der inhibitorischen Synapsen. Die Analyse von agrin-defizienten Neuronen zeigte keinen Anstieg der mIPSC-Frequenz nach Agrinbehandlung was dafür spricht, dass endogenes Agrin wichtig für eine exakte Signaltransduktion ist.

Zusammenfassend lässt sich feststellen, dass microisland Kulturen ein geeignetes System darstellen, um Synaptogenese mit elektrophysiologischen und immunocytochemischen Methoden zu untersuchen. In dieser Arbeit konnte mit diesem Versuchsansatz gezeigt werden, dass Agrin die Bildung oder Stabilität von Synapsen in kortikalen Neuronen fördern kann, aber nicht essentiell ist.

## 7. Abbreviations list

µm	Micron
µM	Micromolar
4-AP	4-Aminopyridine
A	Ampere
AChR	Acetylcholine receptor
aEPSC	Autaptic excitatory postsynaptic current
aIPSC	Autaptic inhibitory postsynaptic current
AKT	Protein kinase B (PKB)
ALS	Amyotrophic lateral sclerosis
AMPA	α-amino-3-hydroxy-5-methyl-4-isoxazolepropionic acid receptor
AP	Action potential
APS	Ammonium persulphate
APV	2R-amino-5-phosphonovaleric acid
BDNF	Brain-derived neurotrophic factor
bp	Base pairs
BSA	Bovine serum albumin
C	Coulomb
CAR	Coxsackievirus and adenovirus receptor
cDNA	Complementary DNA
CF	Cytosolic fraction
CHAPS	3-[(3-Cholamidopropyl)dimethylammonio]-1-propanesulfonate
C <sub>m</sub>	Membrane capacitance
CNS	Central nervous system
CsCl	Cesium chloride
CsOH	Cesium hydroxide
Da	Dalton
DAPI	4',6-diamidino-2-phenylindole
DDT	Dichlorodiphenyltrichloroethane
DEA	Diethanolamine
DEPC	Diethylpyrocarbonate
DGC	Dystrophin-associated glycoprotein complex
DIV	Days <i>in vitro</i>
DMEM	Dulbecco's modified Eagle's medium
DMSO	Dimethyl sulfoxide
DNA	Deoxyribonucleic acid
DNQX	6,7-dinitroquinoxaline-2,3-dione
E15	Embryonic day 15
EC	Extracellular solution
ECM	Extracellular matrix
EDTA	Ethylenediaminetetraacetic acid
eEPSC	Evoked excitatory postsynaptic current
EGTA	Ethylene glycol tetraacetic acid
eIPSC	Evoked inhibitory postsynaptic current
ELISA	Enzyme-linked immunosorbent assay
EtBr	Ethidium bromide
F	Farrad
GABA	γ-aminobutyric acid
GAPDH	Glyceraldehyde 3-phosphate dehydrogenase

GFAP	Glial fibrillary acidic protein
GP	Guinea pig
GSK3 $\beta$	Glycogen synthase kinase 3 beta
h	Hour(s)
HBSS	Hank's balanced salt solution
HCl	Hydrochloric acid
HEK	Human embryonic kidney cells
HEPES	4-(2-hydroxyethyl)-1-piperazineethanesulfonic acid
HRP	Horseradish peroxidase
I	Current
IC	Intracellular solution
ICC	Immunocytochemistry
$I_{max}$	Maximal current amplitude
ISI	Interstimulus interval
IV plot	Current/voltage plot
kb	Kilo base
KCl	Potassium chloride
KO	Knock out
KOH	Potassium hydroxide
LRP4	Low-density lipoprotein receptor-related protein 4
LTP	Long-term potentiation
m	Milli
M	Mega or molar
MAP2	Microtubule-associated protein 2
mEPSC	Excitatory miniature postsynaptic current
MF	Membrane fraction
MG	Myasthenia gravis
min	Minute
mIPSC	Inhibitory miniature postsynaptic current
mRNA	Messenger RNA
ms	Millisecond(s)
mTOR	Mammalian target of rapamycin
MuSK	Muscle-specific kinase
n	Nano
NaCl	Sodium chloride
NaOH	Sodium hydroxide
NCAM	Neural Cell Adhesion Molecule
NGF	Nerve growth factor
NKA	Sodium, potassium ATPase
NMDAR	N-methyl-D-aspartate receptor
NMJ	Neuromuscular junction
n.s.	Not significant
NTP	Nucleoside triphosphate
p	Pico
P0	Postnatal day 0
PBS	Phosphate-buffered saline
PFA	Paraformaldehyde
PI3K	Phosphatidylinositol-4,5-bisphosphate 3-kinase
PMSF	Phenylmethanesulfonylfluoride
PPD	Paired-pulse depression
PPR	Paired-pulse ratio

P/S	Penicillin/streptomycin
PSD95	Postsynaptic density protein 95
qRT-PCR	Quantitative real-time PCR
Rb	Rabbit
RGC	Retinal ganglion cell
R <sub>in</sub>	Input resistance
RNA	Ribonucleic acid
RNAi	RNA interference
ROI	Region of interest
RRP	Readily releasable pool
R <sub>s</sub>	Series resistance
R <sub>spec</sub>	Specific membrane resistance
RT	Room temperature
SAP97	Synapse-associated protein 97
SDS	Sodium dodecyl sulfate
SEM	Standard error of the mean
TAE	Tris base, acetic acid and EDTA
TEA-Cl	Tetraethylammonium chloride
TEMED	Tetramethylethylenediamine
TTX	Tetrodotoxin
U	Voltage
V	Volt
VF	View field
VGAT	Vesicular inhibitory amino acid transporters
VGCC	Voltage-gated calcium channel
VGlut	Vesicular glutamate transporter
V <sub>h</sub>	Holding potential
WB	Western blot
WT	Wild type
α3NKA	Alpha 3 subunit of sodium/potassium ATPase
Ω	Ohm

## 8. Reference list

- Annie, M., Bittcher, G., Ramseger, R., Löschinger, J., Wöll, S., Porten, E., Abraham, C., Rüegg, M.A., and Kröger, S. (2006). Clustering transmembrane-agrin induces filopodia-like processes on axons and dendrites. *Mol. Cell. Neurosci.* *31*, 515–524.
- Apel, E.D., Glass, D.J., Moscoso, L.M., Yancopoulos, G.D., and Sanes, J.R. (1997). Rapsyn is required for MuSK signaling and recruits synaptic components to a MuSK-containing scaffold. *Neuron* *18*, 623–635.
- Bal, M., Leitz, J., Reese, A.L., Ramirez, D.M.O., Durakoglugil, M., Herz, J., Monteggia, L.M., and Kavalali, E.T. (2013). Reelin mobilizes a VAMP7-dependent synaptic vesicle pool and selectively augments spontaneous neurotransmission. *Neuron* *80*, 934–946.
- Bandi, E., Jevsek, M., Mars, T., Jurdana, M., Formaggio, E., Sciancalepore, M., Fumagalli, G., Grubic, Z., Ruzzier, F., and Lorenzon, P. (2008). Neural agrin controls maturation of the excitation-contraction coupling mechanism in human myotubes developing in vitro. *Am. J. Physiol. Cell Physiol.* *294*, C66–73.
- Barik, A., Zhang, B., Sohal, G.S., Xiong, W.-C., and Mei, L. (2014). Crosstalk between Agrin and Wnt signaling pathways in development of vertebrate neuromuscular junction. *Dev. Neurobiol.* *74*, 828–838.
- Barish, M.E. (1986). Differentiation of voltage-gated potassium current and modulation of excitability in cultured amphibian spinal neurones. *J. Physiol.* *375*, 229–250.
- Baxter, A.W., and Wyllie, D.J.A. (2006). Phosphatidylinositol 3 kinase activation and AMPA receptor subunit trafficking underlie the potentiation of miniature EPSC amplitudes triggered by the activation of L-type calcium channels. *J. Neurosci.* *26*, 5456–5469.
- Borgdorff, A.J., and Choquet, D. (2002). Regulation of AMPA receptor lateral movements. *Nature* *417*, 649–653.
- Böse, C.M., Qiu, D., Bergamaschi, A., Gravante, B., Bossi, M., Villa, A., Rupp, F., and Malgaroli, A. (2000). Agrin controls synaptic differentiation in hippocampal neurons. *J. Neurosci.* *20*, 9086–9095.
- Brennan-Minnella, A.M., Shen, Y., El-Benna, J., and Swanson, R.A. (2013). Phosphoinositide 3-kinase couples NMDA receptors to superoxide release in excitotoxic neuronal death. *Cell Death Dis.* *4*, 1–9.
- Brümmendorf, T., Kenwrick, S., and Rathjen, F.G. (1998). Neural cell recognition molecule L1: from cell biology to human hereditary brain malformations. *Curr. Opin. Neurobiol.* *8*, 87–97.
- Burgess, R.W., Skarnes, W.C., and Sanes, J.R. (2000). Agrin Isoforms with Distinct Amino Termini : Differential Expression , Localization , and Function. *J. Cell Biol.* *151*, 41–52.
- Campagna, J.A., and Fallon, J. (2006). Lipid rafts are involved in C95 (4,8) agrin fragment-induced acetylcholine receptor clustering. *Neuroscience* *138*, 123–132.

- Caspar, D.L.D., Goodenough, D.A., Makowski, L.E.E., and Phillips, W.C. (1977). GAP JUNCTION STRUCTURES I. Correlated Electron Microscopy and X-Ray Diffraction. *J. Cell Biol.* 74, 605–628.
- Chen, L., Chetkovich, D.M., Petralia, R.S., Sweeney, N.T., Kawasaki, Y., Wenthold, R.J., Bredt, D.S., and Nicoll, R.A. (2000). Stargazin regulates synaptic targeting of AMPA receptors by two distinct mechanisms. *Nature* 408, 936–943.
- Chih, B., Engelman, H., and Scheiffele, P. (2005). Control of excitatory and inhibitory synapse formation by neuroligins. *Science* 307, 1324–1328.
- Cosker, K.E., and Eickholt, B.J. (2007). Phosphoinositide 3-kinase signalling events controlling axonal morphogenesis. *Biochem. Soc. Trans.* 35, 207–210.
- Daniels, M.P. (2012). The role of agrin in synaptic development, plasticity and signaling in the central nervous system. *Neurochem. Int.* 61, 848–853.
- Debanne, D., Guerineau, N.C., Giihwiler, B.H., and Thompson, S.M. (1996). Paired-pulse facilitation and depression at unitary synapses in rat hippocampus : quantal fluctuation affects subsequent release. *J. Physiol.* 491, 163–176.
- DeChiara, T.M., Bowen, D.C., Valenzuela, D.M., Simmons, M. V, Poueymirou, W.T., Thomas, S., Kinetz, E., Compton, D.L., Rojas, E., Park, J.S., et al. (1996). The receptor tyrosine kinase MuSK is required for neuromuscular junction formation in vivo. *Cell* 85, 501–512.
- Denzer, A.J., Brandenberger, R., Gesemann, M., Chiquet, M., and Rugg, M.A. (1997). Agrin Binds to the Nerve–Muscle Basal Lamina via Laminin. *J. Cell Biol.* 137, 671–683.
- Essrich, C., Lorez, M., Benson, J.A., Fritschy, J.-M., and Lüscher, B. (1998). Postsynaptic clustering of major GABA A receptor subtypes requires the  $\gamma$  2 subunit and gephyrin. *Nat. Neurosci.* 1, 563–571.
- Ferns, M.J., Campanelli, J.T., Hoch, W., Scheller, R.H., and Hall, Z. (1993). The ability of agrin to cluster AChRs depends on alternative splicing and on cell surface proteoglycans. *Neuron* 11, 491–502.
- Ferreira, A. (1999). Abnormal synapse formation in agrin-depleted hippocampal neurons. *J. Cell Sci.* 112, 4729–4738.
- Friedman, H. V, Bresler, T., Garner, C.C., and Ziv, N.E. (2000). Assembly of new individual excitatory synapses: time course and temporal order of synaptic molecule recruitment. *Neuron* 27, 57–69.
- Fukuda, T., and Kosaka, T. (2000). Gap junctions linking the dendritic network of GABAergic interneurons in the hippocampus. *J. Neurosci.* 20, 1519–1528.
- Gautam, M., Noakes, P.G., Mudd, J., Nichol, M., Chu, G.C., Sanes, J.R., and Merlie, J.P. (1995). Failure of postsynaptic specialization to develop at neuromuscular junctions of rapsyn-deficient mice. *Lett. to Nat. Vol.* 377, 232–236.

- Gautam, M., Noakes, P.G., Moscoso, L., Rupp, F., Scheller, R.H., Merlie, J.P., and Sanes, J.R. (1996). Defective Neuromuscular Synaptogenesis in Agrin-Deficient Mutant Mice. *Cell* *85*, 525–535.
- Geiger, J.R.P., Melcher, T., Koh, D.S., Sakmann, B., Seeburg, P.H., Jonas, P., and Monyer, H. (1995). Relative Abundance of Subunit mRNAs Determines Gating and Ca<sup>2+</sup> Permeability of AMPA Receptors in Principal Neurons and Interneurons in Rat CNS. *Neuron* *15*, 193–204.
- Gesemann, M., Denzer, A.J., and Ruegg, M.A. (1995). Acetylcholine receptor-aggregating activity of agrin isoforms and mapping of the active site. *J. Cell Biol.* *128*, 625–636.
- Glass, D.J., Bowen, D.C., Stitt, T.N., Radziejewski, C., Bruno, J., Ryan, T.E., Gies, D.R., Shah, S., Mattsson, K., Burden, S.J., et al. (1996). Agrin acts via a MuSK receptor complex. *Cell* *85*, 513–523.
- Godfrey, E.W., Nitkin, R.M., Wallace, B.G., Rubin, L.L., and McMahan, U.J. (1984). Components of Torpedo electric organ and muscle that cause aggregation of acetylcholine receptors on cultured muscle cells. *J. Cell Biol.* *99*, 615–627.
- Gomez, A.M., Froemke, R.C., and Burden, S.J. (2014). Synaptic Plasticity and Cognitive Function Are Disrupted in the Absence of Lrp4. *Elife*.
- Hamzei-Sichani, F., Kamasawa, N., Janssen, W.G.M., Yasumura, T., Davidson, K.G. V, Hof, P.R., Wearne, S.L., Stewart, M.G., Young, S.R., Whittington, M.A., et al. (2007). Gap junctions on hippocampal mossy fiber axons demonstrated by thin-section electron microscopy and freeze fracture replica immunogold labeling. *Proc. Natl. Acad. Sci. U. S. A.* *104*, 12548–12553.
- Hettwer, S., Lin, S., Kucsera, S., Haubitz, M., Oliveri, F., Fariello, R.G., Ruegg, M.A., and Vrijbloed, J.W. (2014). Injection of a soluble fragment of neural agrin (NT-1654) considerably improves the muscle pathology caused by the disassembly of the neuromuscular junction. *PLoS One* *9*, e88739.
- Hilgenberg, L.G.W., and Smith, M.A. (2004). Agrin signaling in cortical neurons is mediated by a tyrosine kinase-dependent increase in intracellular Ca<sup>2+</sup> that engages both CaMKII and MAPK signal pathways. *J. Neurobiol.* *61*, 289–300.
- Hilgenberg, L.G., Hoover, C.L., and Smith, M.A. (1999). Evidence of an agrin receptor in cortical neurons. *J. Neurosci.* *19*, 7384–7393.
- Hilgenberg, L.G.W., Ho, K.D., Lee, D., O’Dowd, D.K., and Smith, M.A. (2002). Agrin regulates neuronal responses to excitatory neurotransmitters in vitro and in vivo. *Mol. Cell. Neurosci.* *19*, 97–110.
- Hilgenberg, L.G.W., Su, H., Gu, H., O’Dowd, D.K., and Smith, M.A. (2006). Alpha<sub>3</sub>Na<sup>+</sup>/K<sup>+</sup>-ATPase is a neuronal receptor for agrin. *Cell* *125*, 359–369.
- Hoch, W., Ferns, M., Campanelli, J.T., Hall, Z.W., and Scheller, R.H. (1993). Developmental regulation of highly active alternatively spliced forms of agrin. *Neuron* *11*, 479–490.

- Hu, X., and Dahl, G. (1999). Exchange of conductance and gating properties between gap junction hemichannels. *FEBS Lett.* *451*, 113–117.
- Ibata, K., Sun, Q., and Turrigiano, G.G. (2008). Rapid synaptic scaling induced by changes in postsynaptic firing. *Neuron* *57*, 819–826.
- Ippolito, D.M., and Eroglu, C. (2010). Quantifying synapses: an immunocytochemistry-based assay to quantify synapse number. *J. Vis. Exp.* 1–10.
- Jakawich, S.K., Nasser, H.B., Strong, M.J., McCartney, A.J., Perez, A.S., Rakesh, N., Carruthers, C.J.L., and Sutton, M. a (2010). Local presynaptic activity gates homeostatic changes in presynaptic function driven by dendritic BDNF synthesis. *Neuron* *68*, 1143–1158.
- Ji, R., Bose, C.M., Lesuisse, C., Qiu, D., Huang, J.C., Zhang, Q., and Rupp, F. (1998). Specific Agrin Isoforms Induce cAMP Response Element Binding Protein Phosphorylation in Hippocampal Neurons. *J. Neurosci.* *18*, 9695–9702.
- Kang, Y., Zhang, X., Dobie, F., Wu, H., and Craig, A.M. (2008). Induction of GABAergic postsynaptic differentiation by alpha-neurexins. *J. Biol. Chem.* *283*, 2323–2334.
- Kerchner, G.A., and Nicoll, R.A. (2008). Silent synapses and the emergence of a postsynaptic mechanism for LTP. *Nat. Rev. Neurosci.* *9*, 813–825.
- Kim, M.J., Cotman, S.L., Halfter, W., and Cole, G.J. (2003). The heparan sulfate proteoglycan agrin modulates neurite outgrowth mediated by FGF-2. *J. Neurobiol.* *55*, 261–277.
- Kim, N., Stiegler, A.L., Cameron, T.O., Hallock, P.T., Gomez, A.M., Huang, J.H., Hubbard, S.R., Dustin, M.L., and Burden, S.J. (2008). Lrp4 is a receptor for Agrin and forms a complex with MuSK. *Cell* *135*, 334–342.
- Kins, S., Betz, H., and Kirsch, J. (2000). Collybistin , a newly identified brain- specific GEF , induces submembrane clustering of gephyrin. *Nat. Neurosci.* *3*, 22–29.
- Körber, C., Richter, A., Kaiser, M., Schlicksupp, A., Mükusch, S., Kuner, T., Kirsch, J., and Kuhse, J. (2012). Effects of distinct collybistin isoforms on the formation of GABAergic synapses in hippocampal neurons. *Mol. Cell. Neurosci.* *50*, 250–259.
- Koulén, P., Honig, L.S., Fletcher, E.L., and Kröger, S. (1999). Expression, distribution and ultrastructural localization of the synapse-organizing molecule agrin in the mature avian retina. *Eur. J. Neurosci.* *11*, 4188–4196.
- Kröger, S., and Mann, S. (1996). Biochemical and functional characterization of basal lamina-bound agrin in the chick central nervous system. *Eur. J. Neurosci.* *8*, 500–509.
- Kröger, S., Horton, S.E., and Honig, L.S. (1996). The Developing Avian Retina Expresses Agrin Isoforms during Synaptogenesis. *J. Neurobiol.* *29*, 165–182.

Ksiazek, I., Burkhardt, C., Lin, S., Seddik, R., Maj, M., Bezakova, G., Jucker, M., Arber, S., Caroni, P., Sanes, J.R., et al. (2007). Synapse loss in cortex of agrin-deficient mice after genetic rescue of perinatal death. *J. Neurosci.* *27*, 7183–7195.

Kumar, V., Zhang, M.-X., Swank, M.W., Kunz, J., and Wu, G.-Y. (2005). Regulation of dendritic morphogenesis by Ras-PI3K-Akt-mTOR and Ras-MAPK signaling pathways. *J. Neurosci.* *25*, 11288–11299.

Kuzirian, M.S., and Paradis, S. (2011). Emerging themes in GABAergic synapse development. *Prog. Neurobiol.* *95*, 68–87.

Li, D., Specht, C.G., Waites, C.L., Butler-Munro, C., Leal-Ortiz, S., Foote, J.W., Genoux, D., Garner, C.C., and Montgomery, J.M. (2011). SAP97 directs NMDA receptor spine targeting and synaptic plasticity. *J. Physiol.* *589*, 4491–4510.

Li, Z., Massengill, J.L., O’Dowd, D.K., and Smith, M. a (1997). Agrin gene expression in mouse somatosensory cortical neurons during development in vivo and in cell culture. *Neuroscience* *79*, 191–201.

Li, Z., Hilgenberg, L.G., O’Dowd, D.K., and Smith, M.A. (1999). Formation of functional synaptic connections between cultured cortical neurons from agrin-deficient mice. *J. Neurobiol.* *39*, 547–557.

Lin, W., Burgess, R.W., Dominguez, B., Pfaff, S.L., Sanes, J.R., and Lee, K.F. (2001). Distinct roles of nerve and muscle in postsynaptic differentiation of the neuromuscular synapse. *Nature* *410*, 1057–1064.

López-Muñoz, F., Boya, J., and Alamo, C. (2006). Neuron theory, the cornerstone of neuroscience, on the centenary of the Nobel Prize award to Santiago Ramón y Cajal. *Brain Res. Bull.* *70*, 391–405.

Makowski, L.E.E., Caspar, D.L.D., and Phillips, W.C. (1977). GAP JUNCTION STRUCTURES II . Analysis of the X-Ray Diffraction Data. *J. Cell Biol.* *74*, 629–645.

Man, H.-Y., Wang, Q., Lu, W.-Y., Ju, W., Ahmadian, G., Liu, L., D’Souza, S., Wong, T.P., Taghibiglou, C., Lu, J., et al. (2003). Activation of PI3-kinase is required for AMPA receptor insertion during LTP of mEPSCs in cultured hippocampal neurons. *Neuron* *38*, 611–624.

Mann, S., and Kröger, S. (1996). Formation of Synaptic Specializations in the Inner Plexiform Layer of the Developing Chick Retina. *Mol. Cell. Neurosci.* *8*, 1–13.

Matsumoto-Miyai, K., Sokolowska, E., Zurlinden, A., Gee, C.E., Lüscher, D., Hettwer, S., Wölfel, J., Ladner, A.P., Ster, J., Gerber, U., et al. (2009). Coincident pre- and postsynaptic activation induces dendritic filopodia via neurotrypsin-dependent agrin cleavage. *Cell* *136*, 1161–1171.

McCroskery, S., Bailey, A., Lin, L., and Daniels, M.P. (2009). Transmembrane agrin regulates dendritic filopodia and synapse formation in mature hippocampal neuron cultures. *Neuroscience* *163*, 168–179.

Mennerick, S., Que, J., Benz, A., and Zorumski, C.F. (1995). Passive and synaptic properties of hippocampal neurons grown in microcultures and in mass cultures. *J. Neurophysiol.* *73*, 320–332.

Mozhayeva, M.G., Sara, Y., Liu, X., and Kavalali, E.T. (2002). Development of Vesicle Pools during Maturation of Hippocampal Synapses. *J. Neurosci.* *22*, 654–665.

Nguyen, T., and Sudhof, T.C. (1997). Binding Properties of Neuroligin 1 and Neurexin 1 Reveal Function as Heterophilic Cell Adhesion Molecules. *J. Biol. Chem.* *272*, 26032–26039.

Nitkin, R., Smith, M., and Magill, C. (1987). Identification of agrin, a synaptic organizing protein from Torpedo electric organ. *J. Cell Biol.* *105*, 2471–2478.

O'Connor, L.T., Lauterborn, J.C., Gall, C.M., and Smith, M. a (1994). Localization and alternative splicing of agrin mRNA in adult rat brain: transcripts encoding isoforms that aggregate acetylcholine receptors are not restricted to cholinergic regions. *J. Neurosci.* *14*, 1141–1152.

Ohkawara, B., Cabrera-Serrano, M., Nakata, T., Milone, M., Asai, N., Ito, K., Ito, M., Masuda, A., Ito, Y., Engel, A.G., et al. (2014). LRP4 third  $\beta$ -propeller domain mutations cause novel congenital myasthenia by compromising agrin-mediated MuSK signaling in a position-specific manner. *Hum. Mol. Genet.* *23*, 1856–1868.

Opazo, P., Watabe, A.M., Grant, S.G.N., and Dell, T.J.O. (2003). Phosphatidylinositol 3-Kinase Regulates the Induction of Long-Term Potentiation through Extracellular Signal-Related Kinase-Independent Mechanisms. *J. Neurosci.* *23*, 3679–3688.

Patel, T.R., Besong, T.M.D., Patel, N., Meier, M., Harding, S.E., and Winzor, D.J. (2011). Evidence for Self-Association of a Miniaturized Version of Agrin from Hydrodynamic and Small-Angle X-ray Scattering Measurements. *J Phys Chem B.* *115(38)*, 11286–11293.

Peineau, S., Taghibiglou, C., Bradley, C., Wong, T.P., Liu, L., Lu, J., Lo, E., Wu, D., Saule, E., Bouschet, T., et al. (2007). LTP inhibits LTD in the hippocampus via regulation of GSK3 $\beta$ . *Neuron* *53*, 703–717.

Perkins, G.A., Goodenough, D.A., and Sosinsky, G.E. (1998). Formation of the Gap Junction Intercellular Channel Requires a 30 Rotation For Interdigitating Two Apposing Connexons. *J.Mol.Biol.* *277*, 171–177.

Porten, E., Seliger, B., Schneider, V.A., Wöll, S., Stangel, D., Ramseger, R., and Kröger, S. (2010). The process-inducing activity of transmembrane agrin requires follistatin-like domains. *J. Biol. Chem.* *285*, 3114–3125.

Poulopoulos, A., Aramuni, G., Meyer, G., Soykan, T., Hoon, M., Papadopoulos, T., Zhang, M., Paarmann, I., Fuchs, C., Harvey, K., et al. (2009). Neuroligin 2 drives postsynaptic assembly at perisomatic inhibitory synapses through gephyrin and collybistin. *Neuron* *63*, 628–642.

- Pribrag, H., Peng, H., Shah, W.A., Stellwagen, D., and Carbonetto, S. (2014). Dystroglycan mediates homeostatic synaptic plasticity at GABAergic synapses. *Proc. Natl. Acad. Sci. U. S. A.* *111*, 6810–6815.
- Punga, A.R., and Ruegg, M.A. (2012). Signaling and aging at the neuromuscular synapse: lessons learnt from neuromuscular diseases. *Curr. Opin. Pharmacol.* *12*, 340–346.
- Regehr, W.G. (2012). Short-term presynaptic plasticity. *Cold Spring Harb. Perspect. Biol.* *4*, a005702.
- Reist, E.N., Werle, J.M., and McMahan, U.J. (1992). Agrin Released by Motor Neurons Induces the Aggregation of Acetylcholine Receptors at Neuromuscular Junctions. *Neuron* *8*, 865–868.
- Robertis, E.D.P., and Bennett, H.S. (1955). Some Features of the submicroscopic Morphology of Synapses in Frog and Earthworm. *J. Biophys. Biochem. Cytol.* *1*, 47–58.
- Rosenmund, C., and Stevens, C.F. (1996). Definition of the readily releasable pool of vesicles at hippocampal synapses. *Neuron* *16*, 1197–1207.
- Rost, B.R., Breustedt, J., Schoenherr, A., Grosse, G., Ahnert-Hilger, G., and Schmitz, D. (2010). Autaptic cultures of single hippocampal granule cells of mice and rats. *Eur. J. Neurosci.* *32*, 939–947.
- Ruegg, M.A., and Bixby, J.L. (1998). Agrin orchestrates synaptic differentiation at the vertebrate neuromuscular junction. *Trends Neurosci.* *21*, 22–27.
- Ruegg, M.A., Tsim, K.W., Horton, S.E., Kröger, S., Escher, G., Gensch, E.M., and McMahan, U.J. (1992). The agrin gene codes for a family of basal lamina proteins that differ in function and distribution. *Neuron* *8*, 691–699.
- Sabo, S.L., Gomes, R.A., and McAllister, A.K. (2006). Formation of presynaptic terminals at predefined sites along axons. *J. Neurosci.* *26*, 10813–10825.
- Sánchez, S., Jiménez, C., Carrera, a. , Diaz-Nido, J., Avila, J., and Wandosell, F. (2004). A cAMP-activated pathway, including PKA and PI3K, regulates neuronal differentiation. *Neurochem. Int.* *44*, 231–242.
- Sanes, J.R., and Lichtman, J.W. (1999). DEVELOPMENT OF THE VERTEBRATE NEUROMUSCULAR JUNCTION. *Annu. Rev. Neurosci.* *22*, 389–442.
- Sanna, P.P., Cammalleri, M., Berton, F., Simpson, C., Lutjens, R., Bloom, F.E., and Francesconi, W. (2002). Phosphatidylinositol 3-Kinase Is Required for the Expression But Not for the Induction or the Maintenance of Long-Term Potentiation in the Hippocampal CA1 Region. *J. Neurosci.* *22*, 3359–3365.
- Sara, Y., Biederer, T., Atasoy, D., Chubykin, A., Mozhayeva, M.G., Südhof, T.C., and Kavalali, E.T. (2005). Selective capability of SynCAM and neuroligin for functional synapse assembly. *J. Neurosci.* *25*, 260–270.

- Scheiffele, P., Fan, J., Choih, J., Fetter, R., and Serafini, T. (2000). Neuroligin Expressed in Nonneuronal Cells Triggers Presynaptic Development in Contacting Axons. *Cell* *101*, 657–669.
- Scheuss, V., Schneggenburger, R., and Neher, E. (2002). Separation of Presynaptic and Postsynaptic Contributions to Depression by Covariance Analysis of Successive EPSCs at the Calyx of Held Synapse. *J. Neurosci.* *22*, 728–739.
- Schiavo, G., Gu, Q., Prestwich, G.D., So, T.H., and Rothman, J.E. (1997). Calcium-dependent switching of the specificity of phosphoinositide binding to synaptotagmin. *PNAS* *94*, 13327–13332.
- Schmidt, N., Basu, S., Sladeczek, S., Gatti, S., van Haren, J., Treves, S., Pielage, J., Galjart, N., and Brenner, H.R. (2012). Agrin regulates CLASP2-mediated capture of microtubules at the neuromuscular junction synaptic membrane. *J. Cell Biol.* *198*, 421–437.
- Schnell, E., Sizemore, M., Karimzadegan, S., Chen, L., Brecht, D.S., and Nicoll, R.A. (2002). Direct interactions between PSD-95 and stargazin control synaptic AMPA receptor number. *PNAS* *99*, 13902–13907.
- Serpinskaya, A.S., Feng, G., Sanes, J.R., and Craig, A.M. (1999). Synapse formation by hippocampal neurons from agrin-deficient mice. *Dev. Biol.* *205*, 65–78.
- Shen, C., Lu, Y., Zhang, B., Figueiredo, D., Bean, J., Jung, J., Wu, H., Barik, A., Yin, D., Xiong, W., et al. (2013). Antibodies against low-density lipoprotein receptor – related protein 4 induce myasthenia gravis. *J. Clin. Invest.* *123*, 5190–5202.
- Song, J.-Y., Ichtchenko, K., Südhof, T.C., and Brose, N. (1999). Neuroligin 1 is a postsynaptic cell-adhesion molecule of excitatory synapses. *PNAS* *96*, 1100–1105.
- Stevens, C.F., and Tsujimoto, T. (1995). Estimates for the pool size of releasable quanta at a single central synapse and for the time required to refill the pool. *J. Neurosci.* *15*, 846–849.
- Stone, D.M., and Nikolics, K. (1995). Tissue- and age-specific expression patterns of alternatively spliced agrin mRNA transcripts in embryonic rat suggest novel developmental roles. *J. Neurosci.* *15*, 6767–6778.
- Sugiyama, J., Bowen, C., and Hall, Z.W. (1994). Dystroglycan Binds Nerve and Muscle Agrin. *Neuron* *13*, 103–115.
- Tian, Q.-B., Suzuki, T., Yamauchi, T., Sakagami, H., Yoshimura, Y., Miyazawa, S., Nakayama, K., Saitoh, F., Zhang, J.-P., Lu, Y., et al. (2006). Interaction of LDL receptor-related protein 4 (LRP4) with postsynaptic scaffold proteins via its C-terminal PDZ domain-binding motif, and its regulation by Ca/calmodulin-dependent protein kinase II. *Eur. J. Neurosci.* *23*, 2864–2876.
- Tsim, K.W., Ruegg, M.A., Escher, G., Kröger, S., and McMahan, U.J. (1992). cDNA that encodes active agrin. *Neuron* *8*, 677–689.

- Turrigiano, G.G., Leslie, K.R., Desai, N.S., Rutherford, L.C., and Nelson, S.B. (1998). Activity-dependent scaling of quantal amplitude in neocortical neurons. *Lett. to Nat.* *391*, 892–896.
- Tyler, W.J., and Pozzo-miller, L.D. (2001). BDNF Enhances Quantal Neurotransmitter Release and Increases Hippocampal Excitatory Synapses. *21*, 4249–4258.
- Tzartos, J.S., Zisimopoulou, P., Rentzos, M., Karandreas, N., Zouvelou, V., Evangelakou, P., Tsonis, A., Thomaidis, T., Lauria, G., Andreetta, F., et al. (2014). LRP4 antibodies in serum and CSF from amyotrophic lateral sclerosis patients. *Ann. Clin. Transl. Neurol.* *1*, 80–87.
- Urbanska, M., Gozdz, A., Swiech, L.J., and Jaworski, J. (2012). Mammalian target of rapamycin complex 1 (mTORC1) and 2 (mTORC2) control the dendritic arbor morphology of hippocampal neurons. *J. Biol. Chem.* *287*, 30240–30256.
- Viard, P., Butcher, A.J., Halet, G., Davies, A., Nürnberg, B., Heblich, F., and Dolphin, A.C. (2004). PI3K promotes voltage-dependent calcium channel trafficking to the plasma membrane. *Nat. Neurosci.* *7*, 939–946.
- Walsh, F.S., and Doherty, P. (1997). Neural cell adhesion molecules of the immunoglobulin superfamily: role in axon growth and guidance. *Annu. Rev. Cell Dev. Biol.* *13*, 425–456.
- Weatherbee, S.D., Anderson, K. V, and Niswander, L. a (2006). LDL-receptor-related protein 4 is crucial for formation of the neuromuscular junction. *Development* *133*, 4993–5000.
- Wierenga, C.J., Ibata, K., and Turrigiano, G.G. (2005). Postsynaptic expression of homeostatic plasticity at neocortical synapses. *J. Neurosci.* *25*, 2895–2905.
- Wilcox, K.S., and Dichter, M.A. (1994). Paired Pulse Depression in Cultured Hippocampal Neurons Is Due to a Presynaptic Mechanism Independent of GABA<sub>A</sub> Autoreceptor Activation. *J. Neurosci.* *14*(3), 1775–1788.
- Wilcox, K.S., Buchhalter, J., and Dichter, M.A. (1994). Properties of Inhibitory and Excitatory Synapses Between Hippocampal Neurons in Very Low Density Cultures. *Synapse* *18*, 128–151.
- Wu, H., Lu, Y., Shen, C., Patel, N., Gan, L., Xiong, W.C., and Mei, L. (2012). Distinct roles of muscle and motoneuron LRP4 in neuromuscular junction formation. *Neuron* *75*, 94–107.
- Yang, J., Thio, L.L., Clifford, D.B., and Zorumski, C.F. (1993). Electrophysiological properties of identified postnatal rat hippocampal pyramidal neurons in primary culture. *Dev. Brain Res.* *71*, 19–26.
- Zhang, B., Luo, S., Wang, Q., Suzuki, T., Xiong, W.C., and Mei, L. (2008). LRP4 serves as a coreceptor of agrin. *Neuron* *60*, 285–297.
- Zhang, B., Shen, C., Bealmear, B., Ragheb, S., Xiong, W.-C., Lewis, R. a, Lisak, R.P., and Mei, L. (2014). Autoantibodies to agrin in myasthenia gravis patients. *PLoS One* *9*, e91816.

## 9. Acknowledgements

I want to express my gratitude towards Prof. Dr. Fritz G. Rathjen for giving me the opportunity to work in his lab and his support throughout this project.

Prof. Dr. Gary Lewin I want to thank for agreeing to be the second reviewer of this thesis.

I also want to express my gratitude towards Prof. Dr. Rosenmund and his team for the possibility to obtain the pre-coated microisland coverslips. It was crucial for the success of this project.

Very special thanks to Dr. René Jüttner for all his support and fruitful ideas during my time at the MDC. You were always open for discussions and more than once helped me in times of need. Thanks also for making me run every year in the Firmenlauf 😊.

For providing the agrin mice and stably transfected HEK cells I want to express my gratitude to Prof. Dr. Markus Rugg.

For giving me a mating trio of LRP4 mice and for help with their genotyping I want to thank Dr. Annette Hammes-Lewin & Fabian Paul.

Prof. Dr. Jochen Meier and Dr. Aline Winkelmann from the MDC I want to thank for providing the VGlut1+2 antibodies used in this work.

To all the people in the Rathjen lab ... you hold a special place in my heart, especially my fellow PhD companions, Hanna, Philip, Gohar, Claudia and Alexandre. Thanks for being such good friends, for always being there in times of trouble and uplifting my bad moods. Also I want to thank my friends from outside my own lab: Dámaris for all the great talks about movies and books and in general for being a great friend (you are truly one of a kind), Kate for always forcing me to have fun, Christina for those blood-soaked evenings of horror in the cinema (that was always a great diversion) and Andreas for all the support and guidance throughout the years.

Also I want to thank my family for their loving support.

To all the people I forgot to thank ... please have mercy with an old man trapped in a young man's body.

## 10. Curriculum vitae

For privacy reasons the curriculum vitae is not included in the online version of this dissertation.

*Posters and conferences:*

Posters:

1. Marc Lohse, Axel Nagel, Alex Finck, Anika Jöcker, Heiko Schoof, Detlev Groth, Dörte Lodka, Malgorzata Ryngajllo, **Florian Hetsch**, Alisdair R. Fernie, Mark Stitt, Björn Usadel

**GABI Mercator: Sorting plant proteins into pathways and processes using a manual curation database underlying an automatic classification process.** 3rd International Biocuration Conference, Berlin, April 16-19 2009

2. Andreas Abraham, **Florian Hetsch**, Rudolf A. Deisz, Marianne Vater

**Intrinsic properties of supragranular pyramidal neurons and interneurons in the auditory cortex of mice.** The 10th Biannual Meeting of the German Society for Cognitive Science KogWis2010, Potsdam, October 3-6 2010

3. Andreas Abraham, Hartmut Niekisch, **Florian Hetsch**, Marianne Vater

**Layer-specific intrinsic properties of pyramidal neurons and interneurons in the auditory cortex of mice.** Ninth Göttingen Meeting of the German Neuroscience Society, Göttingen, May 23-27 2011

4. Andreas Abraham, Marlen Dierich, Hartmut Niekisch, **Florian Hetsch**

**Maturation of intrinsic properties of pyramidal neurons and fast-spiking interneurons in the auditory cortex of mice.** Proceedings of the 5<sup>th</sup> International Conference on Auditory Cortex, Magdeburg, September 13-17, 2014

5. **Florian Hetsch**, René Jüttner, Fritz G. Rathjen

**Agrin increases the number of excitatory synapses via LRP4 and PI3K activation.** Collaborative Research Center 665 International Symposium – Developmental Disturbances in the Nervous System, Schorfheide, 18-20 September 2014

Attended conferences:

1. European Synapse Summer School 2013, Bordeaux France, 9-27 September 2013
2. Collaborative Research Center 665 International Symposium – Developmental Disturbances in the Nervous System, Schorfheide, 18-20 September 2014

## **11. Eidesstattliche Erklärung**

Hiermit erkläre ich, Florian Jan Alexander Hetsch, geboren am 11.10.1983, in Berlin, dass die von mir vorgelegte Dissertation von mir selbstständig angefertigt wurde. Verwendete Hilfsmittel und Hilfen wurden vollständig angegeben.

Diese Dissertation wurde noch keiner anderen Fakultät oder Universität zur Prüfung vorgelegt. Die diesem Promotionsverfahren zu Grunde liegende Promotionsordnung habe ich zur Kenntnis genommen.

Berlin, den \_\_\_\_\_ 2015

---

Florian Jan Alexander Hetsch